eRHIC Design Wikibook

(collection of eRHIC Accelerator Wiki pages, 02/11/13)

Contributors:

Sergey Belomestnykh[1,2], Ilan Ben-Zvi[1,2], Michael M. Blaskiewicz[1], Kevin A. Brown[1], Jean Clifford Brutus[1], Andrey Elizarov[1,2], Alexei Fedotov[1], Pei Kuan Feng[1], David Gassner[1], Harald Hahn[1], Yue Hao[1,2], Ping He[1], Lawrence T. Hoff[1], William Jackson[1], Animesh Jain[1], Yichao Jing[1], Dmitry Kayran[1], Robert Lambiase[1], Vladimir N. Litvinenko[1,2], Chuyu Liu[1], Yun Luo[1], Michael Mapes[1], George Mahler[1], Gary McIntyre[1], Wuzheng Meng[1], Michiko Minty[1], Robert Michnoff[1], Brett Parker[1], Alexander Pendzick[1], Alexander Pikin[1], Igor Pinayev[1], Vadim Ptitsyn[1], Triveni Rao[1],Eric Riehn[1], Thomas Roser[1], Jon Sandberg[1], John Skaritka[1], Brian Sheehy[1], Kevin Smith[1], Steven Tepikian[1], Oleg Tchoubar[1], Yatming Than[1], Charles Theisen[1], Dejan Trbojevic[1], Evgeni Tsentalovich[3], Nicholaos Tsoupas[1,2], Joseph Tuozzolo[1], Gang Wang[1], Qiong Wu[1], Wencan Xu[1], Alex Zaltsman[1], Wu Zhang[1], Anatoly Zelenski[1]

1 Brookhaven National Laboratory, Upton, NY 11973
2 Department of Physics and Astronomy, Stony Brook University, Stony Brook, 11784
3 MIT-Bates, Middleton, MA 01949

1 Overview 5
Accelerator Concept and Staging 5
Accelerator Concept *5*
Staging *6*
Beam Parameters and Luminosities 7
Energy ranges *7*
Limiting factors *7*
Main Beam Parameters *8*
Luminosities at different energies *9*
Luminosities Sharing with multiple detectors *10*
2 Electron Accelerator 11
Design Concept Overview 11
Beam Parameters 12
Layout Figures 12
Time Structure 14
Frequency Matching *15*
Bunch pattern *18*
Injector System 20
Polarized Electron Source *22*
10 MeV Injector *28*
Beam dump *30*
Lattice 31
Arc Lattice *32*
Splitters/Combiners *37*
By-pass lines *40*
Main Linacs *43*
Path lengthening for frequency matching *44*
Small path length and R_{56} adjustment *46*
Superconducting RF 51
Main Linacs *54*
Energy Loss Compensator *57*
Crab Cavity Design *57*
Beam Dynamics 61
Energy Loss and Energy Spread *61*
Transverse Emittance *70*
Beam Disruption and Mismatching *71*
Ion Trapping in Linac *75*
Single Pass Beam Break Up *77*
Beam Loss 78
Touschek Effect and IBS *78*
Beam-Gas Scattering *80*
Beam Polarization 82
Longitudinal orientation in collision point *82*
Systems 84
Cryogenics *84*
Magnets *87*
Beam Chamber and Vacuum System *91*
Beam Instrumentation *93*

Abort System *98*

3 Ion Beam **102**

Beam Parameters and Upgrades Overview 102

Overview *102*

Beam Parameters *103*

Coherent Electron Cooling 104

Beam Dynamics 105

Coherent Instabilities *105*

Beam-Beam Effects *109*

Number of bunches 117

Resistive Wall Heating 118

4 Interaction Region **120**

Overview 120

Detector Integration *122*

Hadron IR Beamline 123

Hadron Lattice *123*

Chromatic Correction *123*

Hadron Magnet Parameters *125*

Electron Line 126

Layout and parameters *126*

Integration with detector components *127*

Synchrotron Radiation 128

Crab-Crossing 131

Hadron beam *131*

Electron beam *132*

Magnet Design 133

Combined function magnet *133*

Spin Rotators 135

1 Overview

Accelerator Concept and Staging

Accelerator Concept

The future electron-ion collider (EIC) is based on the existing Relativistic Heavy Ion Collider (RHIC) hadron facility, with two intersecting superconducting rings, each 3.8 km in circumference. We plan adding a polarized electron-beam with energy tunable within the 5-30-GeV range to collide with variety of species in the existing RHIC-accelerator complex, from polarized protons with a top energy of 250 GeV, to heavy fully striped ions with energies up to 100 GeV/u. Using the present significant margin of the RHIC superconducting magnets, we may be able to increase the maximum beam energy by 10 to 25 percent; correspondingly, this would bring the energy's reach to 325 GeV and 130 GeV/u. The design is based on one of the RHIC's hadron rings and a multi-pass energy-recovery linac (ERL). Using the ERL as the electron accelerator assures high luminosity in the 10^{33}-10^{34} cm^{-2} sec^{-1} range, and for the natural staging of eRHIC, with the ERL located inside the RHIC tunnel.

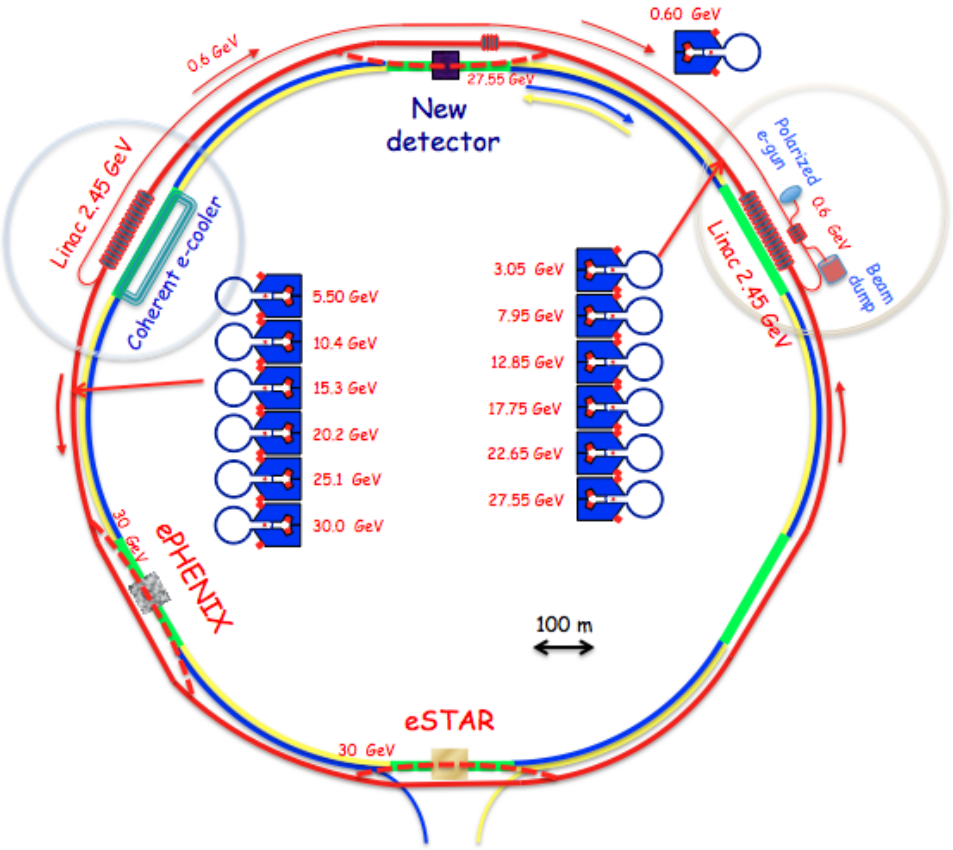

Figure 1.1: eRHIC Accelerator Layout

Main layout features:

- Injection complex, which includes the polarized beam injector and 600 MeV pre-accelerator ERL is located near IR2
- Acceleration of the electrons (up to 30 GeV max) is done by the energy recovery linacs (ERLs) placed in IR2 and IR10.
- In full staged design the collisions can be done in 3 interaction regions. On first stage the collisions are arranged only in ePHENIX detector in IR8.
- Each electron bunch passes each of main linacs 12 times: 6 times in accelerating phase, gaining energy, and 6 times in decelerating phase, giving the energy back to RF cavities.

We considered several IR designs for eRHIC. The latest one, with a 10 mrad crossing angle and β^*=5cm, takes advantage of newly commissioned Nb_3Sn quadrupoles.

The current eRHIC design focuses on electron-hadron collisions. If justified by the EIC physics, we will add a 30-GeV polarized positron ring with full energy-injection from eRHIC ERL. This addition to the eRHIC facility provide for positron-hadron collisions, but at a significantly lower luminosity than those attainable in the electron-hadron mode.

As a novel high-luminosity EIC, eRHIC faces many technical challenges, such as generating 50 mA of polarized electron current. eRHIC also will employ coherent electron cooling (CeC) for the hadron beams. Staff at BNL, JLab, and MIT is pursuing vigorously an R&D program for addressing these challenges.

Staging

First stage should provide the electron energy at least 5 GeV.

Main scenario:

- The six-pass magnetic system with small-gap magnets will be installed already on the first stage.
- The length of each of the main linacs on the first stage is 40m to provide the acceleration on 6 accelerating passes to 5 GeV.
- On further stages the each linac length is gradually increased (from the center to both sides) to 200m to reach 26.5 GeV energy.
- On last stage, 30 GeV will be achieved by increasing the energy gain from 18 MeV to 20.4 MeV per cavity.
- Pre-accelerator linac length is also increased from 10 m on first stage to 60 m in full staged design.

Staging scenario variations:

1. To minimize the first stage machine cost, only two recirculation passes are placed in the RHIC tunnel, while four, lower energy, recirculation passes are placed locally, around the injector area. Only one 830 MeV main linac is used on the first stage.
2. On first stage, in order to accelerate to 5 GeV use 3-4 recirculation passes in the tunnel (instead of 6) and the length of each main linac of 60m. On further stages increase each linac length and add 2-3 more recirculation passes.

3. The full staged design has 6 recirculation passes but only 4 of them will be used to accelerate the beam up to 20 GeV energy. 5th and 6th passes are only used for the acceleration beyond 20 GeV. Additional electron transport lines have to be added to connect the 4th and 6th pass (which going through the experimental detector) in this case.

- Staging also includes the upgrade of RHIC cryo plant.
- Major ion ring upgrades: Coherent Electron Cooling and the increased number of bunches, are assumed to be ready already for the first stage.

Beam Parameters and Luminosities

Energy ranges

Electrons : from 5 to 30 GeV

Heavy ions (Au): from 50 to 100 GeV per nucleon; (with possible extension up to 130 GeV per nucleon)

Protons: from 100 to 250 GeV ; (with possible extensions: down to 50 GeV and up to 325 GeV)

'*C.M. energy ranges*:

from 44.7 to 173.2 GeV for polarized e-p ; (possible extended range: 31.6-197.5 GeV)

from 31.6 to 109.5 GeV for electron heavy-ion-collisions; (with possible extension up to 125 GeV)

Limiting factors

Several physics and practical considerations influenced our choice of beam parameters for eRHIC. Some of these limitations, such as the intensity of the hadron beam , the space charge and beam-beam tune shift limits for hadrons, come from experimental observations at RHIC or other hadron colliders. Some of them, for example $\beta^* = 5$ cm for hadrons, are at the limits of current accelerator technology, while others are derived either from practical- or cost-considerations.

For example, from considering the operational costs, we limit the electron beam's power loss for synchrotron radiation to about 8 MW, corresponding to a 50 mA beam current at 20 GeV. Above 20 GeV, the electron beam's current will decrease in inverse proportion to the fourth power of energy, and will be restricted to about 10 mA at energy of 30 GeV. It means that the luminosity of eRHIC operating with 30 GeV electrons will be a1/5th of that with 20 GeV.

Since the ERL provides fresh electron bunch at every collision, the electron beam can be strongly abused, i.e., it can heavily distorted during collision. The only known effect that might cause a serious problem is the so-called kink instability. The ways of suppressing it within range of parameters accessible by eRHIC is well understood.

Assumed limits and parameters:

1. Beam-intensity limits: For protons: $4 \cdot 10^{11}$
   For Au ions: $3 \cdot 10^{9}$
   Electron-beam current: 50 mA
2. Minimum $\beta^* = 5$ cm for all species.
3. Space-charge tune shift for hadrons is compensated by electron column
4. Maximum proton (ion) beam-beam parameter: 0.015
5. Coherent e-cooling will cool and maintain the hadron beam at
   a. Hadron beam 95% normalized emittance: 1.2 mm mrad
   b. RMS bunch length 5 cm
6. Synchrotron radiation's intensity limit is defined at 10 MW
7. Collision repetition-rate : 14 MHz

Main Beam Parameters

eRHIC beam parameters for collision of 10 GeV electrons with different ion species:

	e	p	$^{2}He^{3}$	$^{79}Au^{197}$
Energy, GeV	10	250	167	100
CM energy, GeV		100	82	63
Number of bunches/distance between bunches	71 nsec	166	166	166
Bunch intensity (nucleons)		$4 \cdot 10^{11}$	$6 \cdot 10^{11}$	$6 \cdot 10^{11}$
Bunch charge, nC	3.54	64	64	39
Beam current, A	0.05	0.83	0.83	0.5
Normalized emittance of hadrons 95% , mm mrad		1.1	1.1	1.1
Normalized emittance of electrons, rms, mm mrad		13	25	33
Polarization, %	80	70	70	none
RMS bunch length, cm	0.2	5	5	5
β^*,cm	5	5	5	5
Luminosity per nucleon, $10^{34}cm^{-2}s^{-1}$		2.7	0.9	1.6

The luminosity in the table accounts for both the hourglass and the e-pinch effects

Luminosities at different energies

The limitations on luminosity resulting from various considerations are involved. The main trend is that eRHIC's luminosity does not depend on the electron beam's energy (below 15 GeV), and reaches its maximum at the hadron beam's highest energy.

The contour plots of eRHIC luminosity with stage I beam parameters as a function of the electron- and proton-energies (top), and the c.m. energy and the ratio of the e-beam's and the proton beam's energies (bottom). The box in top plot shows the reach of energy stage I .

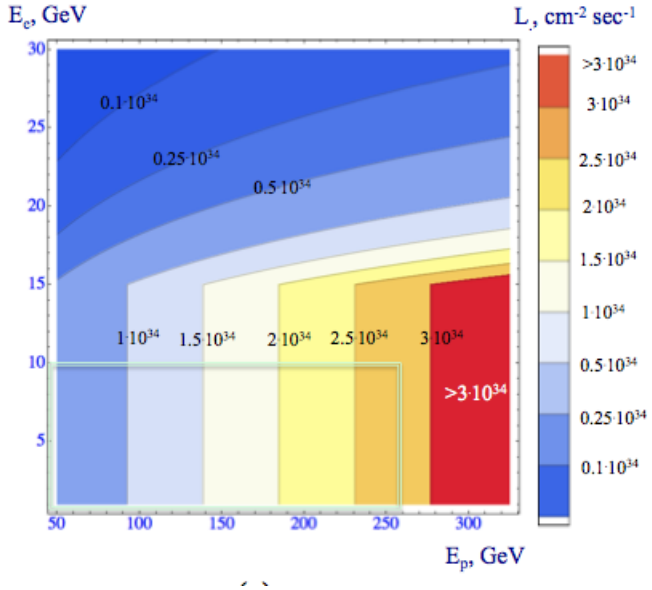

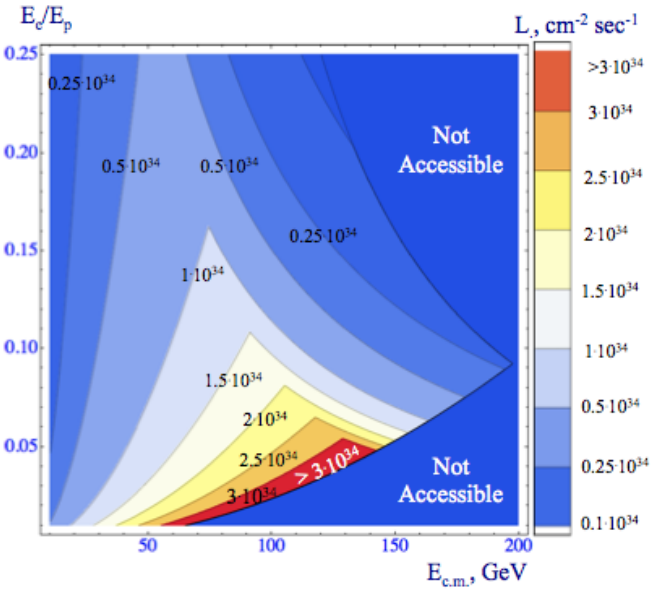

Luminosities Sharing with multiple detectors

Since the circumference of the electron recirculating passes is larger than the hadron ring circumference, the collisions can not be arranged simultaneously in all detectors. If the hadron and electron beam collide in the center of one of possible detectors the beam crossing point at another detectors is shifted by the distance ranging from one to three meters, depending on the detector locations. Because of the 10 mrad IR crossing angle the beams are already well separated in those shifted crossing points and do not produce collisions.

With the multiple detectors the luminosity sharing will be accomplished by alternating collisions in different detectors. This will be realized by varying the longitudinal phase of the electron beam with respect to the hadrons to switch between collisions in different detectors. The proper longitudinal phase variation of the electron beam can provide any wanted pattern of the luminosity sharing. That is, one detector can be given more average luminosity than others if wanted.

2 Electron Accelerator

Design Concept Overview

The features of the electron component placement in the RHIC tunnel:

- Injector is placed inside wide straight section in IR2 region.
- Recirculating passes are placed in the outer part of the RHIC tunnel
- Main ERLs are placed in inner part of IR2 and IR10 straight sections of the RHIC tunnel
- Spreader and combiners are installed between the main ERLs and recirculating passes. Those components also provide the electron line passages from the inner to outer part of the RHIC tunnel above the RHIC ion magnet lines.
- In the experimental straight section the top energy line goes above ion magnet cryostats to get right in between the ion magnet lines, coming to the interaction point. The magnet lines for other electron energies by-pass the experimental detector, making ~5m excursion from the detector center.
- When the STAR detector is not used (on the first stage), the all electron passes, including the top energy, by-pass the detector, making ~4.5m excursion.

The complete sequence of the electron accelerator components is described in the White Paper: Electron beam path in eRHIC.

Beam Parameters

Electron beam parameter ranges:

Electron, for polarized e-p	**max**	**Energy, GeV**	**min**	**Energy,GeV**
Bunch intensity, 10^{11}	0.22	$E_e \leq 20$	0.044	$E_e=30$
Bunch charge, nC	3.5	$E_e \leq 20$	0.69	$E_e=30$
Beam current, mA	50	$E_e \leq 20$	9.9	$E_e=30$
Rms normalized emittance, 1e-6 m	198	$E_p=50$ $E_e=30$	5.1	$E_p=325$ $E_e=5$
Rms emittance, 1e-9 m	3.4	$E_p=50$	0.52	$E_p=325$
Disruption parameter	142	$E_p=250$ $E_e=5$	0.19	$E_p=50$ $E_e=30$
Beam size at IP, mum	13	$E_p=50$	5.1	$E_p=325$
Angular spread at IP, murad	260	$E_p=50$	102	$E_p=325$
rms bunch length, cm	0.2		0.2	
Peak current, A	212	$E_e \leq 20$	42	$E_e=30$

Layout Figures

The main ERL placed in the straight section of IR2 is shown here:

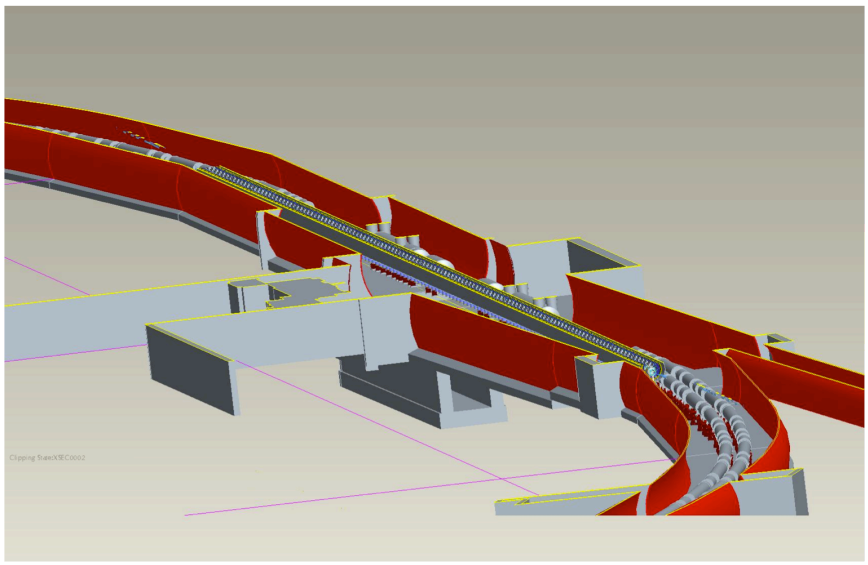

The end of main ERL and the splitter magnets crossing over the RHIC ion magnet cryostats from inner to outer part of the tunnel:

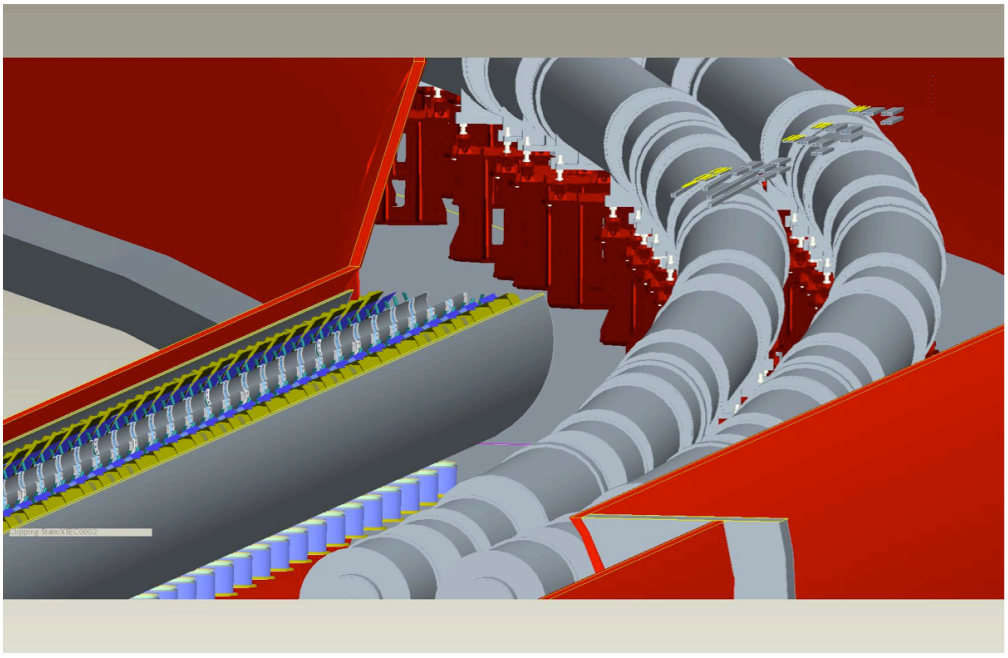

The example of 5 recirculating arcs vertically placed under each other:

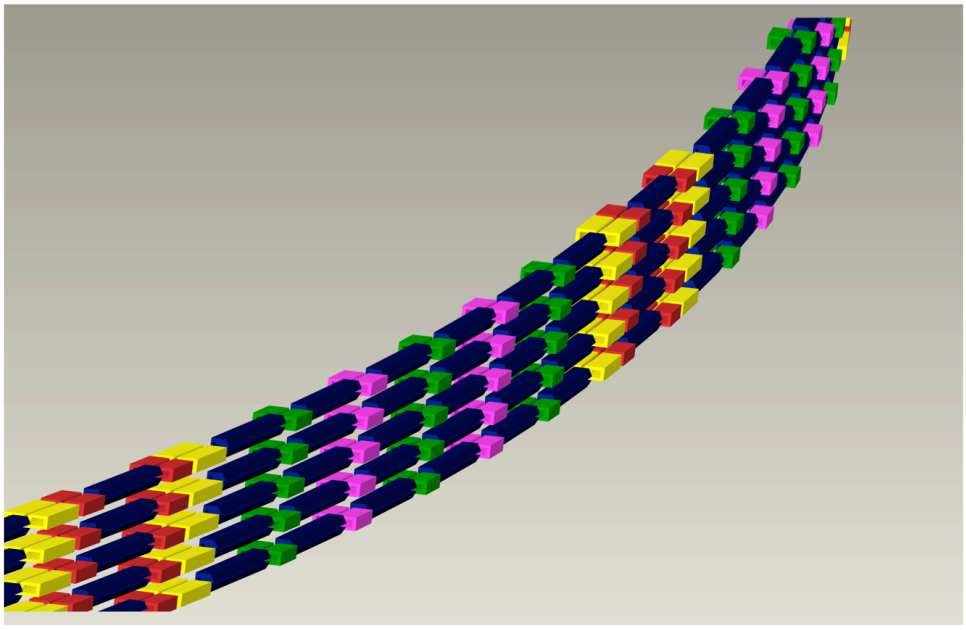

Time Structure

- The time structure of the electron beam is defined by the condition for the electron bunch frequency (f_be) to match the proton bunch frequency (f_bp) at the collision points (f_be = f_bp). Therefore, in the highest energy arc, as well as in the electron gun and in the 10 MeV pre-accelerator the electron current has bunches following with the repetition rate f_bp. This is the CW bunch structure without any gaps or the subdivisions on bunch trains.
- Since the proton (ion) revolution frequency, and, therefore, the proton (ion) bunch frequency f_bp considerably depend on the proton (ion) energy, the electron bunch frequency and the linac RF frequency depend on the proton (ion) beam energy.
- In recirculating arcs with beam energies other than top electron energy and in the 600 MeV pre-accelerator ERL, the two electron currents, corresponding to accelerating and decelerating beams, are superimposed, each of the beam current with the bunch frequency f_bp. Correspondingly, in each of the main linacs the beam time structure is superposition of 12 beam currents (each with the bunch frequency f_bp), from six accelerating and six decelerating beams. The bunch patterns in the recirculating arcs and the main and 600 MeV linacs are defined by the path length of the recirculating arcs.

proton E,Gev	325
proton gamma	346.38
proton beta	0.999995833
proton revolution frequency, kHz	78.196169
proton bunch rep rate, MHz	14.075310
electron revolution frequency, kHz	77.988200
electron bunch rep rate, MHz	14.075310
electron bunch to RF harmonic	50
electron RF frequency, MHz	703.7655188
electron RF harmonic	9024
electron circumference, m	3844.075
proton circumference, m	3833.835

Frequency Matching

Since the protons (or ions) in eRHIC are not yet ultra-relativistic, the revolution frequency of the hadron beam, and, therefore, the bunch repetition rate depends noticeably on the hadron energy. This variation of the bunch repetition rate has to be matched with the electron beam, which is ultra-relativistic.

Parameter summary table:

	matching protons		**matching Au ions**	
proton (ion) E,Gev	325	100	130	53
proton (ion) gamma	346.4	106.6	139.6	56.9
proton (ion) beta	0.999995	0.999955	0.999974	0.999845
proton (ion) revol. frequency, kHz	78.1961	78.1930	78.1944	78.1844
proton (ion) bunch rep rate, MHz	14.0753	14.0747	14.0750	14.0732
electron revolution frequency, kHz	77.9882	77.9850	77.9865	77.9851
electron bunch rep rate, MHz	14.0753	14.0747	14.0750	14.0732
electron RF frequency, MHz	703.7655	703.7374	703.7503	703.6598
electron RF harmonic	9024	9024	9024	9023
electron circumference, m	3844.075	3844.228	3844.157	3844.226
proton circumference, m	3833.835			

To match the energy-dependent proton bunch repetition frequency, following aspects has to be accommodated in the electron accelerator design:

- The RF frequency of the 704 MHz cavities (in all linacs) has to be varied with the proton energy.

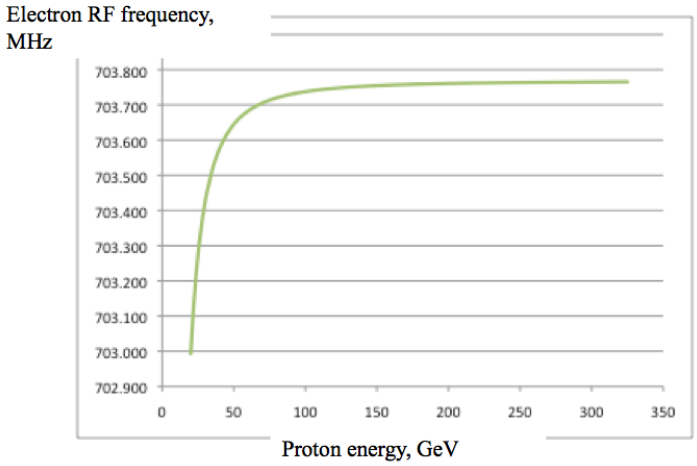

Requirement on cavity detuning: Δf_{rf}(53 GeV – 325 GeV) = -105.7 kHz

The RF frequency of additional cavities (higher harmonics cavities for the energy loss/spread compensation, crab cavities) have to be correspondingly varied too.

- The bunch frequency at the electron gun has to be varied with the proton energy. That concerns the driving laser control.

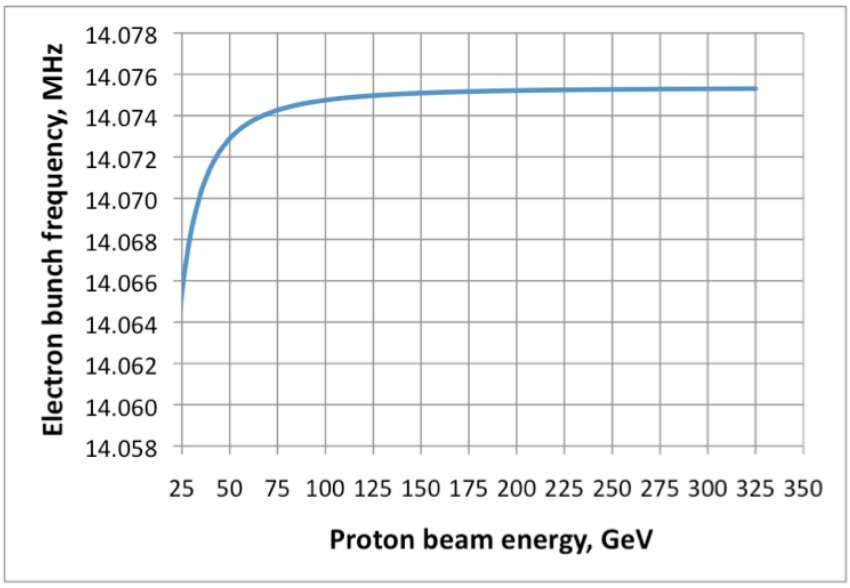

Δf_b(53 GeV – 325 GeV) = -2.1 kHz

- The combination of the electron arc circumference path lengthening and RF harmonic (the ratio of the RF frequency to the revolution frequency) switching can be used to provide matched electron bunch frequency. Presently, we plan to have the path lengthening variation of ~15cm maximum. This will allow to do the frequency matching in the proton energy range from 100 to 325 GeV, with electron RF harmonic constant at 9024. Switching of the RF harmonic to 9023 allows to work with proton energies in the range from 53 to 61 GeV, and with even lower RF harmonics the some ranges of lower proton energies can be accessible.

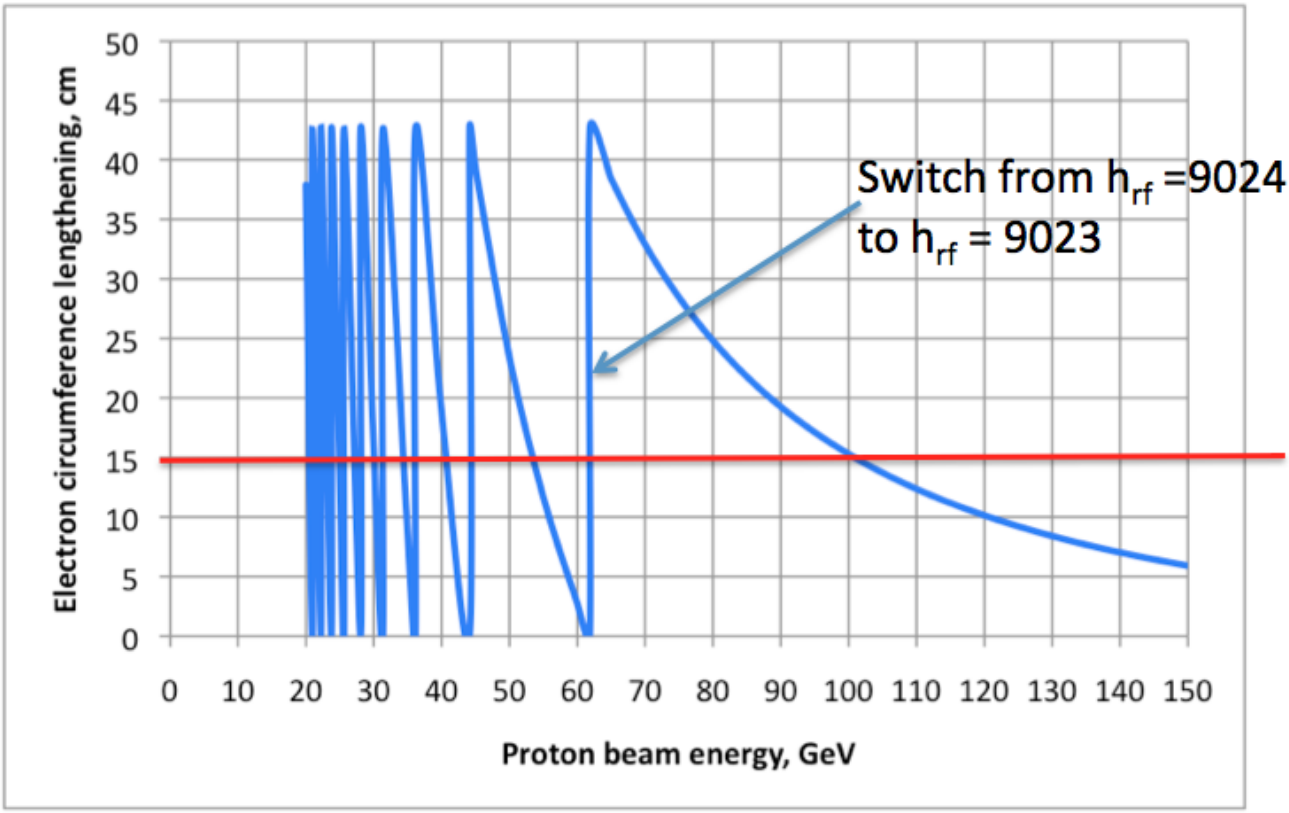

The design of path lengthening insertion has been developed.

Bunch pattern

The factors defining the bunch pattern observed at various accelerator locations are the bunch repetition frequency and the path length of the recirculating passes, which can be related with and described by the RF harmonic number.

Top energy recirculating arc

Since the electron beam passes the top energy arc just once, the bunch pattern consists of the equally spaced bunches with the bunch repetition frequency of f_be = 14.0753 MHz (at proton beam energy of 325 GeV). For variation of f_be with the proton energy see Frequency Matching.

The beam lines connecting the main ERLs and the pre-accelerator ERL, 10 MeV injector line and beam dump line

The bunch pattern in these beam lines is the same as in the top energy recirculating arc, that is defined only by the bunch repetition frequency.

Main linacs

In each of the main linacs the bunch pattern is formed by the superposition of 12 beam currents (each with the bunch frequency f_be) from six accelerating and six decelerating beams. The considerations of RF control and the ion accumulation effect call for the bunch patterns where the bunches are grouped together as opposed to the bunches more or less equally spaced. By selecting the RF harmonic equal to 9024, and making the top energy arc by ~2.35 m longer than the other recirculating arcs, one comes to the bunch pattern shown in the figure for the IR2 linac:

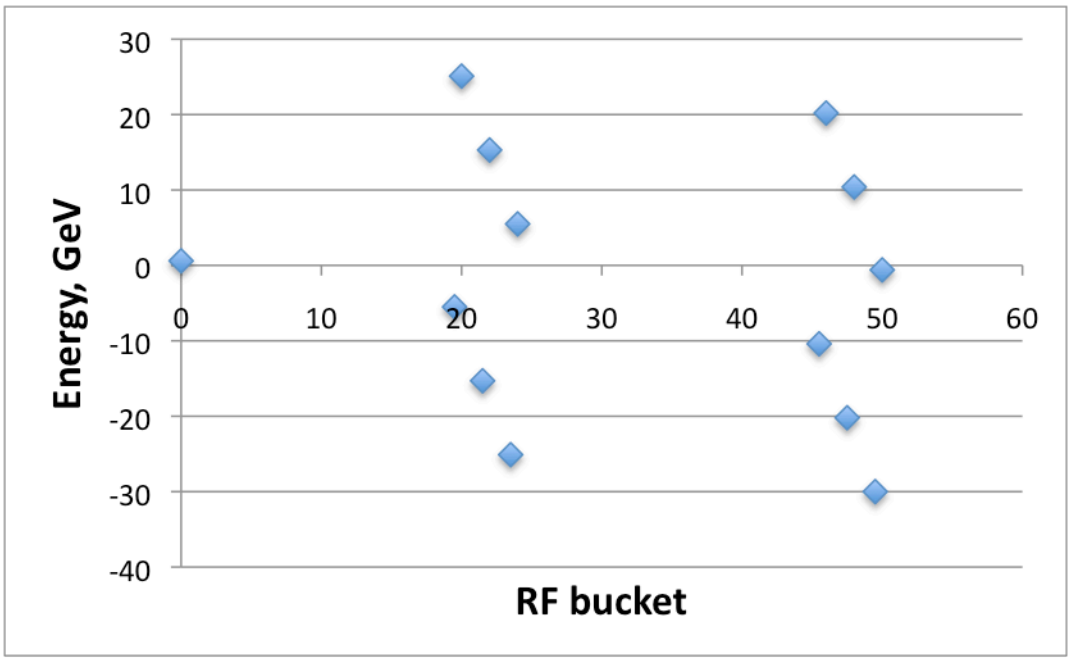

Here the

Energy, GeV	Bucket number
0.6	0
5.5	24
10.4	48
15.3	22
20.2	46
25.1	20
-30	49.5
-25.1	23.5
-20.2	47.5
-15.3	21.5
-10.4	45.5
-5.5	19.5
-0.6	50

Injector System

- The injector system includes:
- 250-300 keV high average current polarized electron source
- 10 MeV injector, which includes bunch compression system
- 600 MeV pre-accelerator energy recovery linac, consisting from 704 MHz cavities
- 0.5 MW beam dump
- Beam lines interconnecting the system components and two beam lines connecting the injector system to the 600 MeV recirculating pass and to the main ERL.

- The main components of the injector system are presented in this scheme:

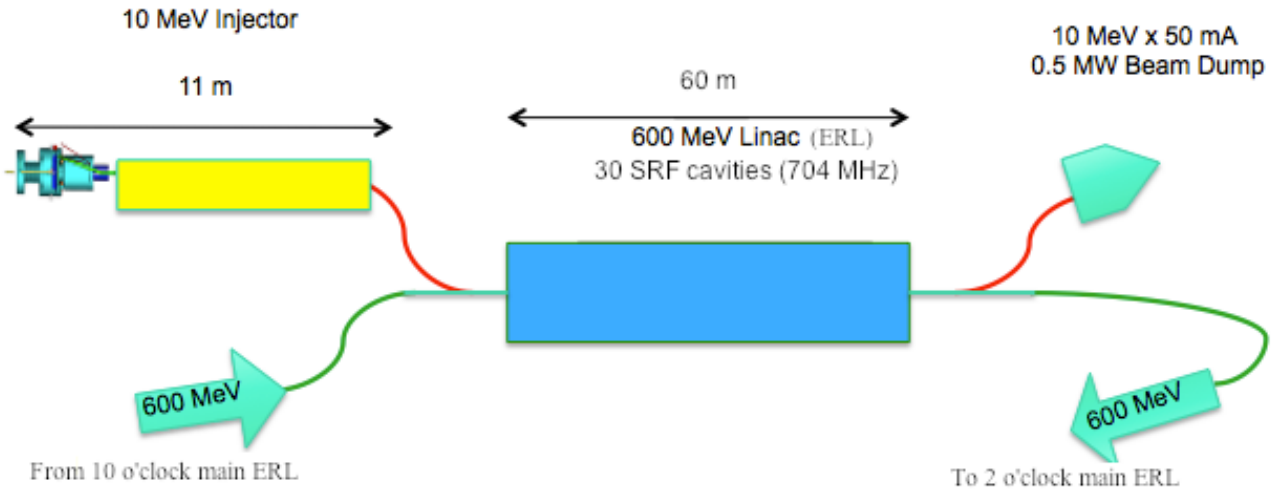

- The injector system can be put in the RHIC IR2 tunnel, using the advantage of the large tunnel width on one side from the IR2 center:

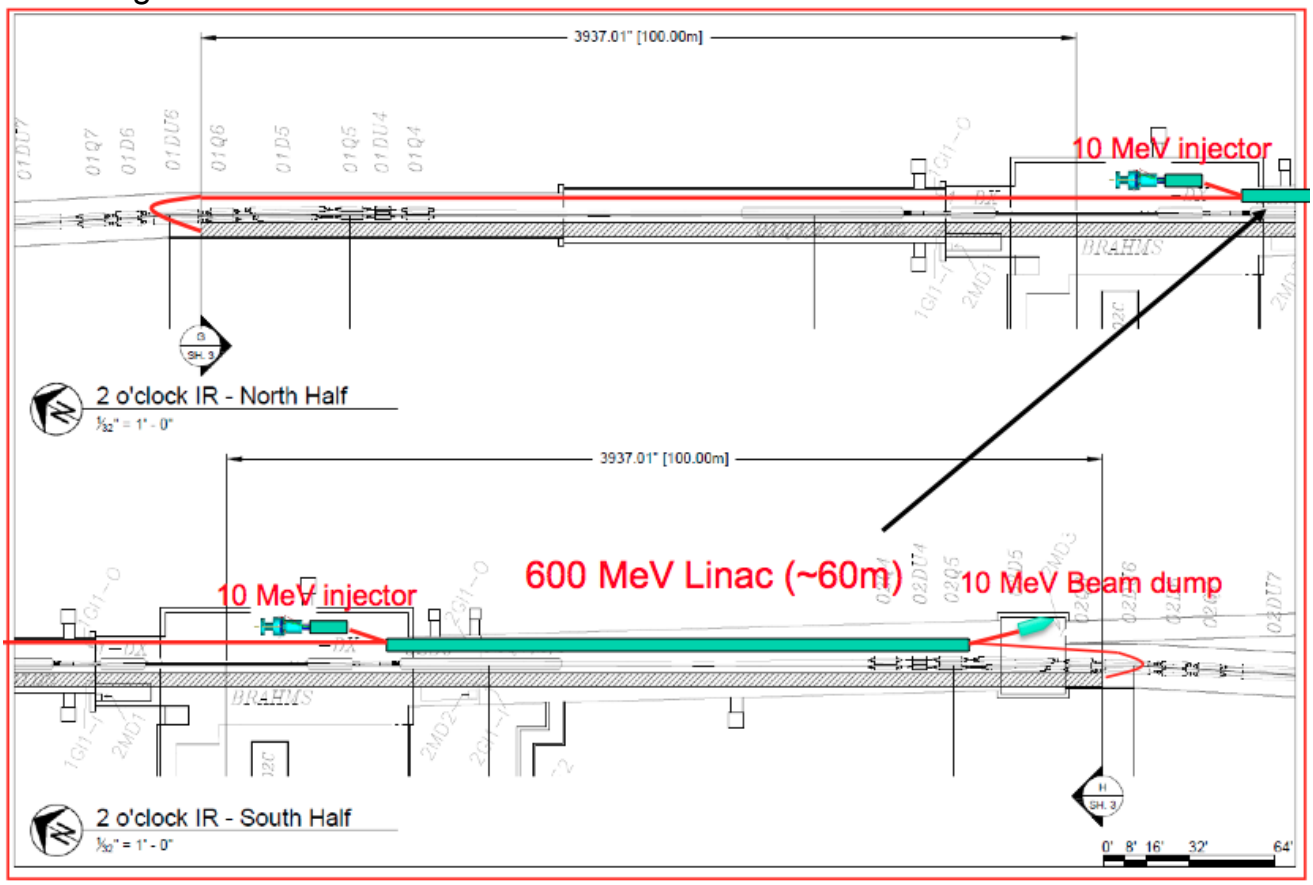

More details on the eRHIC Injector can be found in White Paper: Electron Injector.

Polarized Electron Source

The following are the requirements on the polarized electron source for eRHIC:

- The average current up to 50 mA
- Bunch charge up to 3.6 nC
- Bunch repetition frequency: 14.075 MHz (has to be variable at least by 2.1 kHz)
- Fast switching of the polarization sign
- Normalized transverse emittance: from 5 to 200 mm*mrad

The polarized electron source is one of major R&D items in the present eRHIC design, since the required average current is an order of the magnitude higher than the presently demonstrated. Two alternative design development have been pursued on the R&D path: Gatling gun design and large cathode gun design.

Gatling gun

The principle of the Gatling gun design can be seen in the Figure 1. The Gatling gun is a multipole cathode gun where the bunches originating from different cathodes are merged into one sequence using the electro-magnetic combiner. This leads to multiplying the gun output beam current.

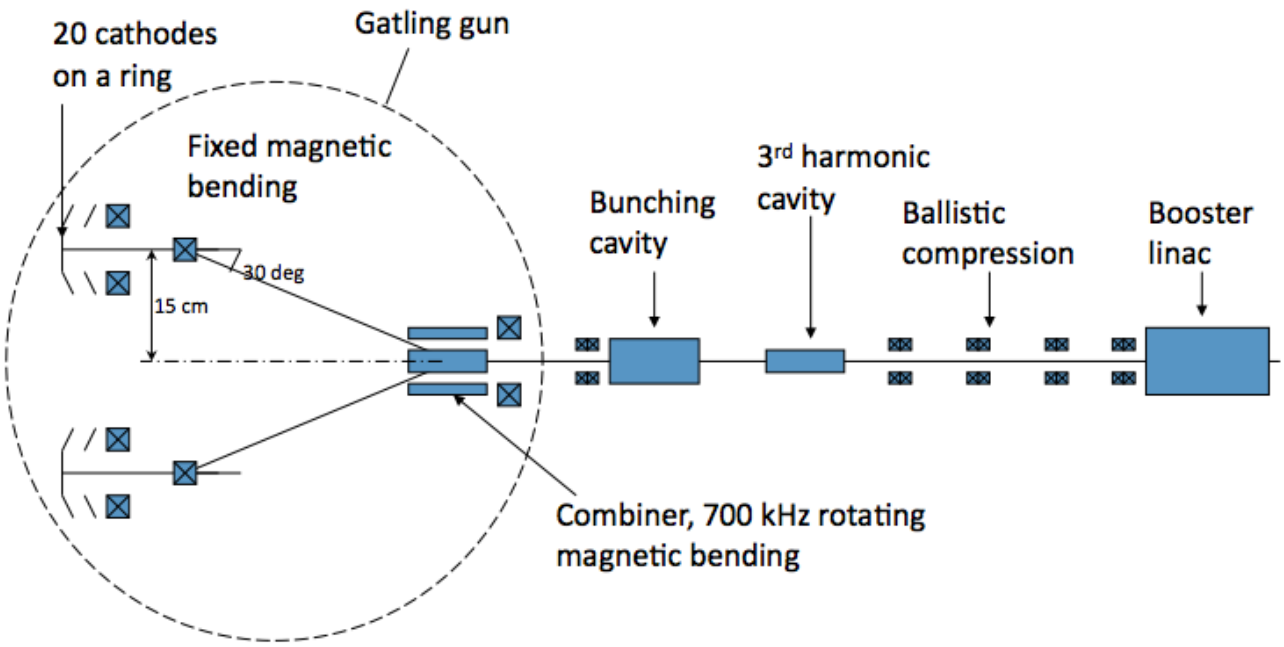

Figure 1: Gatling gun and 10 MeV injector layout.

BNL group has been developing the Gatling gun with 20 cathodes which should be able to produce 50 mA average current. The detailed mechanical design of the Gatling gun has been done. 2-D simulations have been done with results which are very close to the gun goal parameters. 3-D tracking is in progress. Diagnostic section and Depressed Collector have been included in the design. The Gatling Gun Environmental Enclosure has been designed.

The Figures 2,3 and 4 show details of the gatling gun design. In the Figure 2 the cathode preparation components are presented. The Figure 3 shows the sectioned view of the gun. The diagnostic section and the depressed collector are shown in the Figure 4.

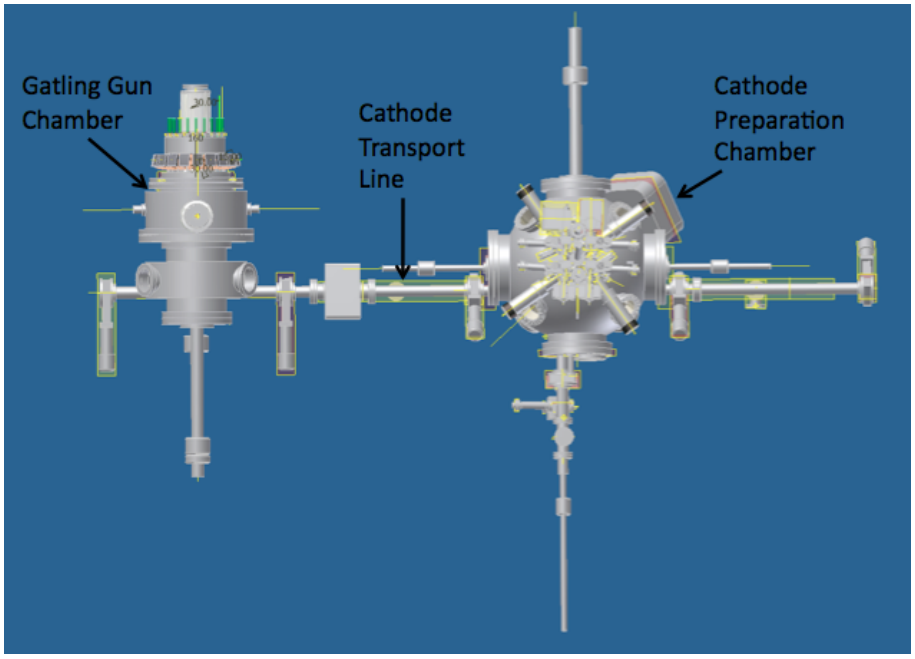

Figure 2: Gatling gun (Left, without the depressed collector) and Cathode Preparation System (

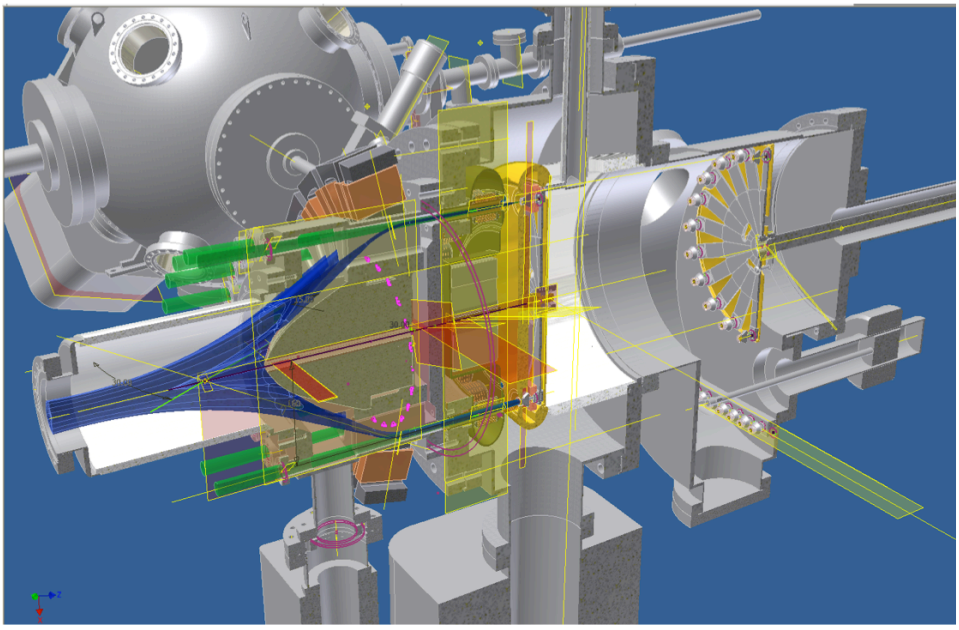

Figure 3: The sectioned view of the gun. From left, Green –indicate Laser, Blue- indicate electron beam paths. Near center is the cathode shroud and anode, and to the right is the cathode magazine.

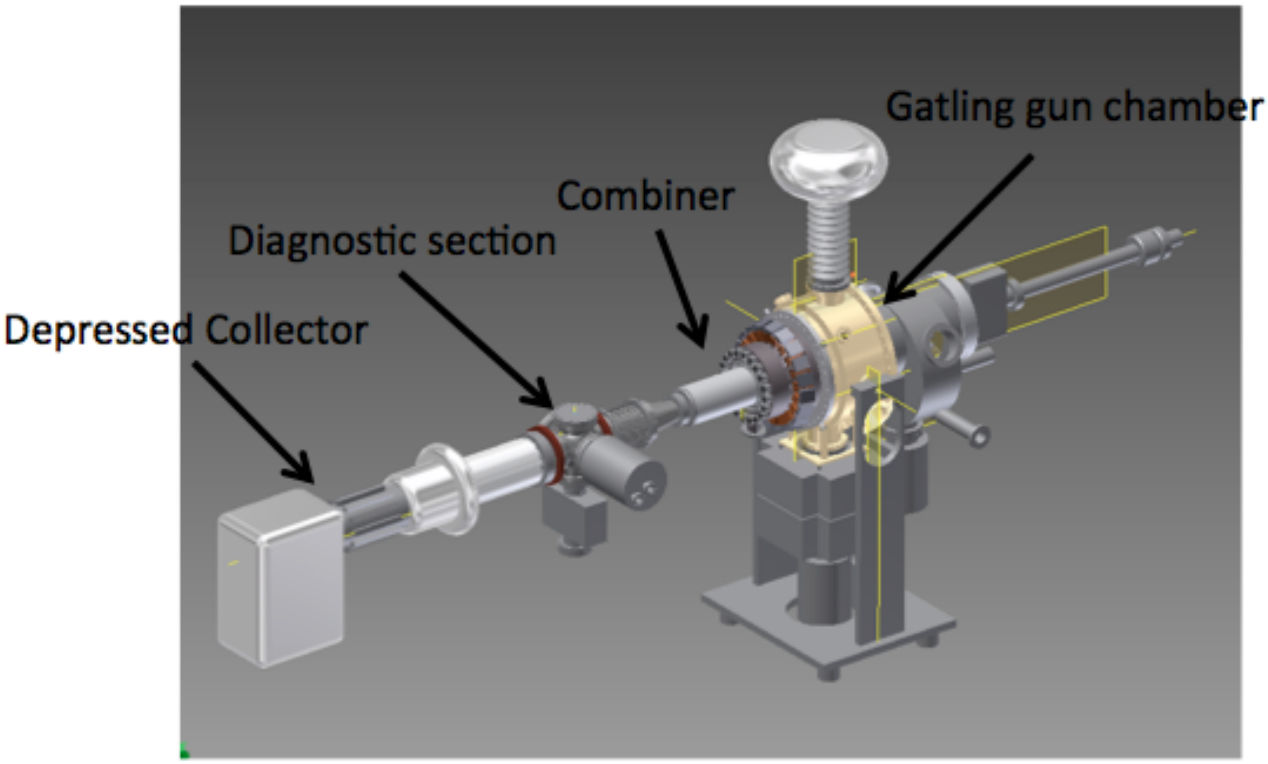

Figure 4: Gatling gun with diagnostic section and Depressed Collector

The Combiner uses the bending by the magnetic field to put the trajectories of bunches from different cathodes on the same straight trajectory. Besides the dipole magnetic field the Combiner uses quadrupole field to keep the beam round during bending. The Combiner and its windings details are shown in Figures 5 and 6. In present design, the peak dipole current on each dipole coil is 135.5 A to bend the 200 kV beam by 30°. The total power loss in dipole coils is about 600 W. A water cooled coil can easily handle this power density. The peak quadrupole current on each quadrupole coil is 2.4 A (power is negligible).

The simple combiner prototype, shown in the Figure 7, was used for initial tests which proved that the dipole and quadrupole fields were independent. Large good field range (>60% in core) with limited coils (4 sets). Improved prototype test is in progress.

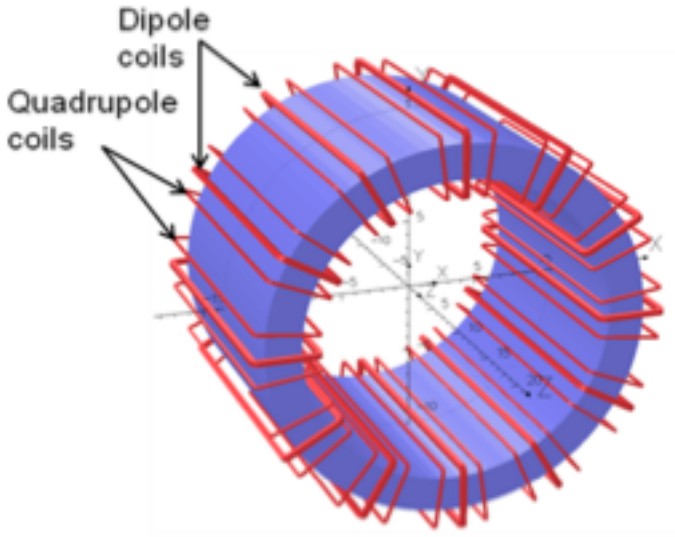

Figure 5: The Combiner with dipole and quadrupole coils.

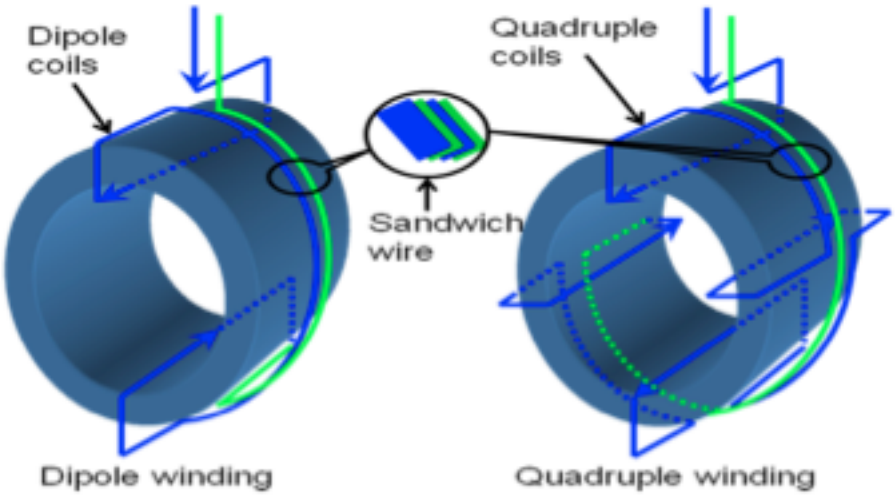

Figure 6: Dipole and quadrupole windings of the Combiner.

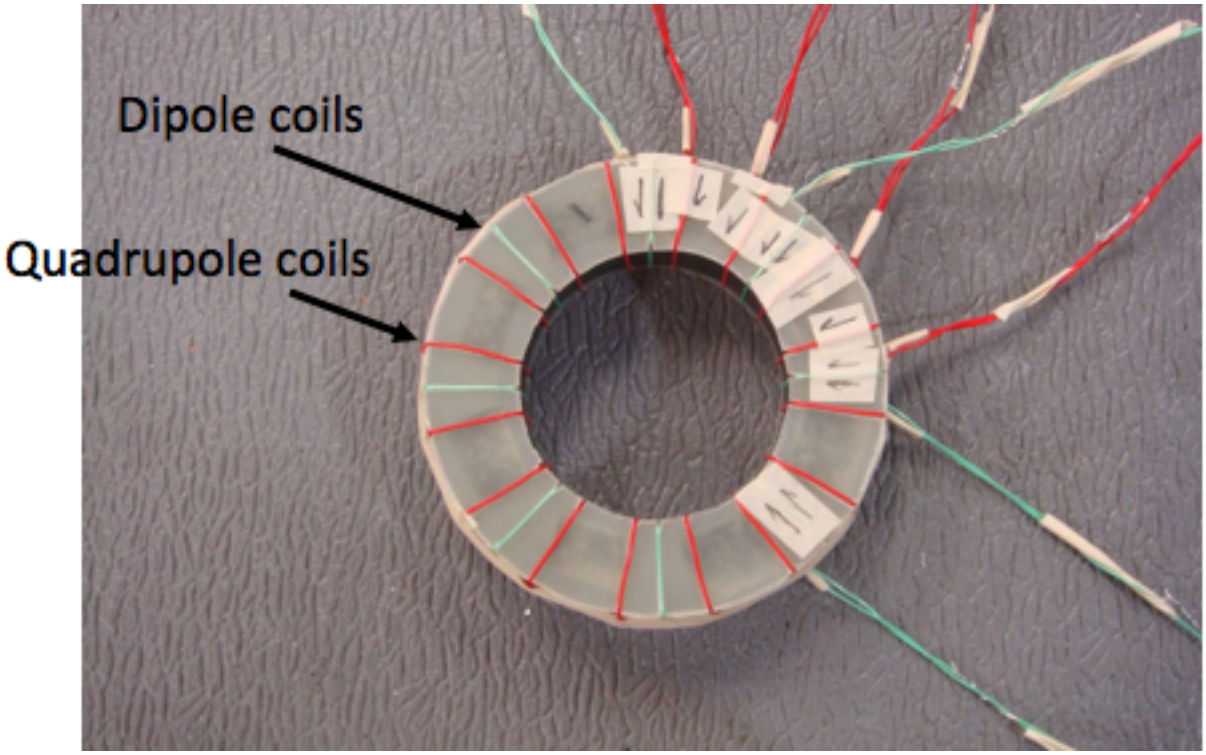

Figure 7: Simple Combiner prototype.

The Gatling gun development is in the process of building a gun prototype. All critical parts have been purchased. Laser system is ready for use. Further information on this R&D can be found at: http://www.c-ad.bnl.gov/ardd/ecooling/Photocathode.htm

Large cathode gun

In this design the gun uses a single cathode. To achieve the high current the size of the cathode is increased keeping the extracted current density at acceptable level. The design of such polarized source has been developed in MIT-Bates, and the source layout is shown in this figure:

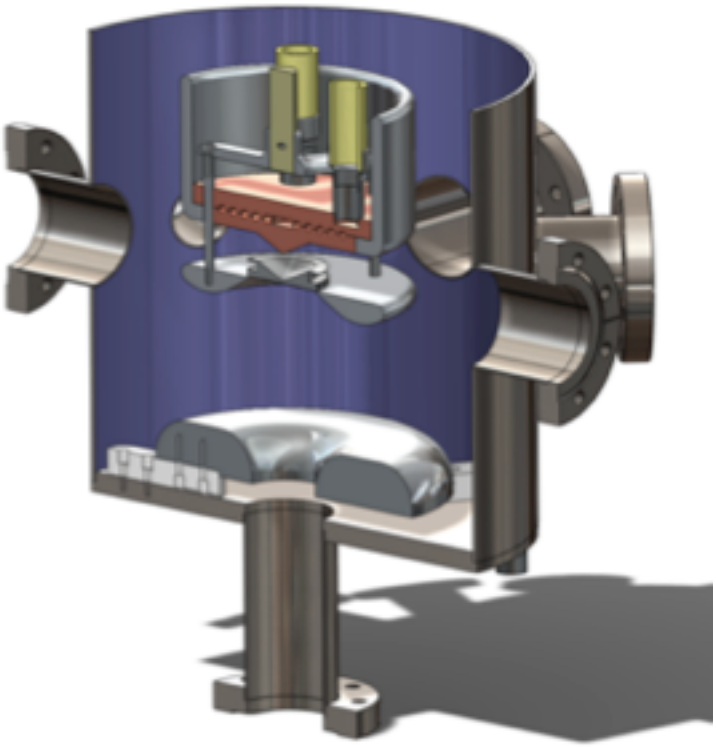

Next stage is to built a prototype of the large cathode gun.

10 MeV Injector

The basic required parameters of the electron 10 MeV injector system are listed in the table:

'	*Parameters for 20(e)x325(p) operation mode*	*Parameter ranges for all operation modes*
Energy, MeV	10	10
Bunch charge, nC	3.5	0.7-3.5
Bunch frequency, MHz	14.075	14.073-14.075
Average beam current, mA	50	10-50
Normalized rms transverse emittance, μm	20	5-200
rms bunch length, mm	2	2
rms energy spread, %	< 1	<1

Figure 1 presents the layout of the whole electron injector system. It consists of the gatling gun, the energy modification cavities including the chirping cavity and the 3rd harmonic cavity, the drift space for ballistic compression and the booster linac. Long beam bunches (rms 250ps on cathode) from the gun are used to reduce the space charge effect. This requires a large ratio bunch compression which the traditional "chicane" can hardly do it. The ballistic compression technique is the best choice here.

The initial long beam bunch also requires the use of low frequency cavity for energy spread modification. 112MHz cavity is used with accelerating gradient (~2MV/m) and the RF power is about 100kW. Also a 3rd harmonic cavity (336MHz) is introduced into the design for better longitudinal phase space modification. The 3rd harmonic cavity not only has low field gradient but also is a passive cavity.

The booster linac also employs 112 MHz cavities to accelerate the beam to 10MeV.

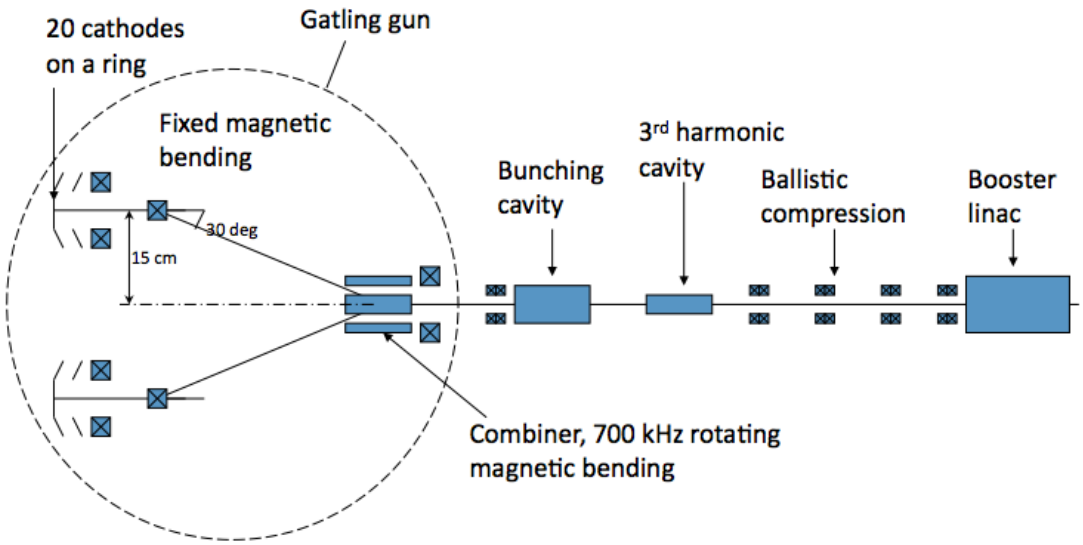

Figure 2: 10 MeV injector layout.

Figure 2 shows the simulations of the beam envelope and longitudinal phase space evolution, considered for the injector parameters for the 20(e)x325(p) eRHIC operation mode. The bunch compression to 3.6 mm has been demonstrated with output transverse emittance 20 μm

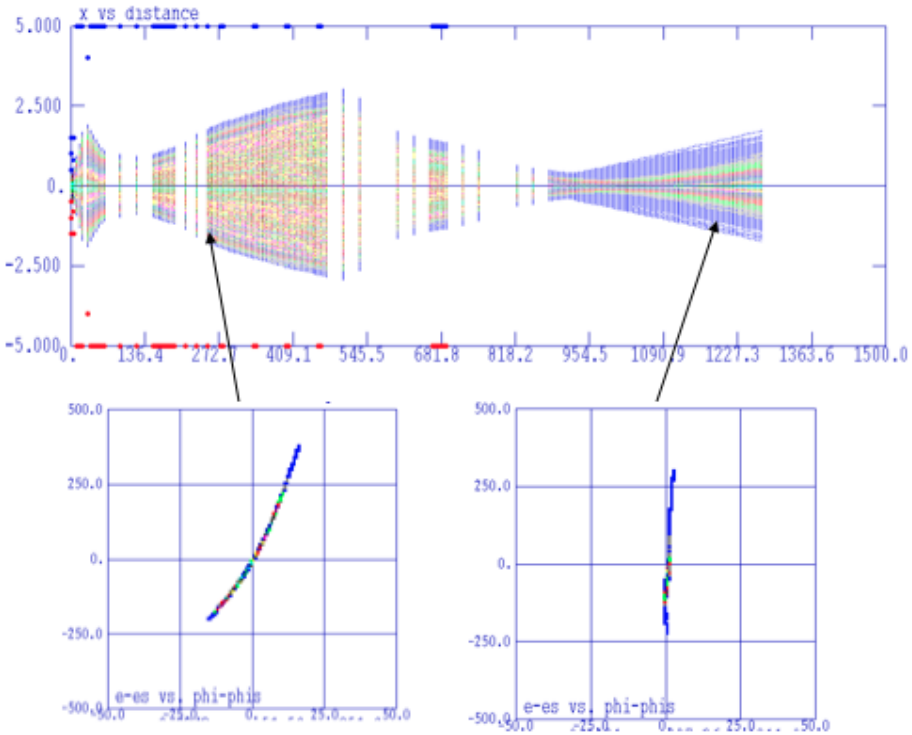

Figure 2: Results of the beam envelope and the longitudinal phase space evolution.

Beam dump

The beam dump has to be able to absorb the 500 kW power from 10 MeV electron beam. Presently the beam dump of Cornell ERL Injector is taken as the basis for the eRHIC dump because of the similarity of the beam parameters. Here is the description of the Cornell beam dump:

The beam dump for the Cornell injector is based on a SLAC klystron collector and is designed to absorb up to 600 kW average power for beams between 5 and 15 MeV. The beam is defocused using a pair of strong quadrupole magnets and rastered in a circle to reduce the instantaneous power on the dump walls. It is made using aluminum instead of the copper to reduce neutron production. The dump is made of two sections: the body and a outer shell to contain the cooling water. The body is 20 mm thick and the shell is 13 mm thick, with the total thickness enough to stop the beam. The sections are e- beam welded together and the welds are inspected for voids and cracks. The interior shape of the cone was designed using GEANT to distribute the scattered electrons (and thus the heat) as uniformly as possible around the cooled surface. A flow of 60 gpm is sufficient to extract ~40 W/cm2 with a 600 kW heat load.

Lattice

Electron beam stays within the envelope of RHIC tunnel while providing maximum possible length (201 m) for SRF linacs, which are located in the IR2 and IR10 straight sections of the RHIC tunnel. All recirculating passes have similar lattice. The lattice components are shown in the figure below, which presents exact layout plotted on the basis of the MAD survey file.

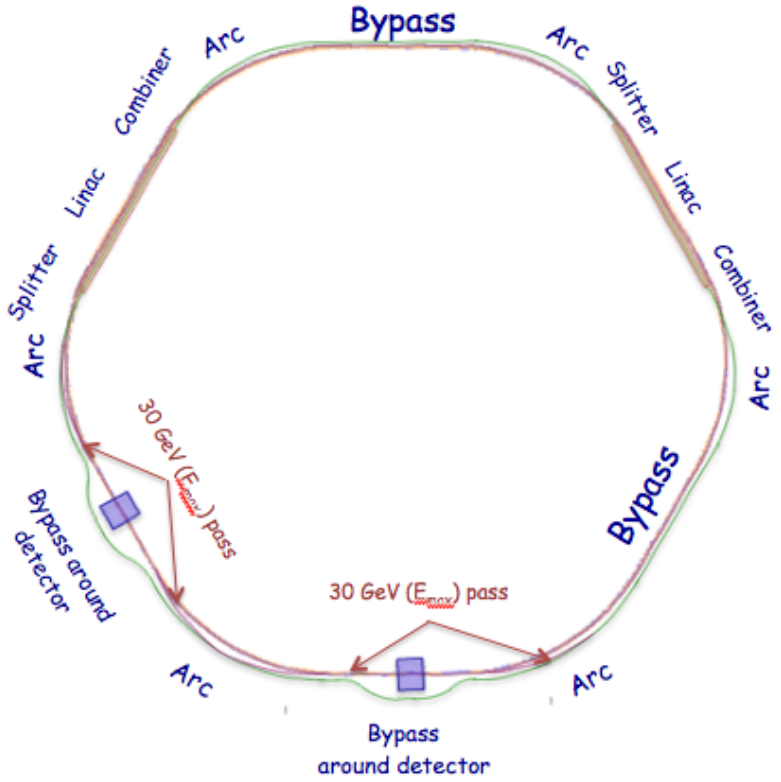

The lattice components include:

- Arcs, which transfer the electron beam in each recirculating pass through the curved sections of the RHIC tunnel.
- Main ERLs lattice presently does not include quadrupole magnets.
- The four splitters/mergers provide the transition between the beam line in the linacs and six, or seven, vertically arranged recirculating passes in the arcs.
- Top energy (up to 30 GeV) beam line(s) through the experimental detector(s) in the interaction region areas.
- The by-pass lines transfer the electron beam around the experimental detectors, or through the straight sections. In e-ion detector location the by-pass line are provided for all recirculation passes except the top energy pass. If the experimental detector is dedicated only for ion-ion collisions the top energy beam line is also included into the by-pass.
- The insertion to vary the path length of the electron circumference (up to 15cm) is included in the IR4 straight section. The path length variation is required to match the electron and proton bunch frequencies at different proton energies.

Arcs, bypasses and the top energy line bringing the electron beam to the IR are based on asynchronous cell lattice.

Arc Lattice

After collisions, electron energy is reduced down to their initial value, by multiple passes through the linacs at the negative side of the sinusoidal RF voltage. The electron energy in the dump is equal to the injection value. The time of flight of electrons is the most important parameter in this process allowing them to reach the sinusoidal voltage function at the right time:

$$L_p = -\frac{dL}{dp} = M_{5,6},$$

$$X_{out} = M\ X_{in},\ X = (x, x', y, y', -ds, \frac{\delta p}{p}, 1).$$

The recirculation passes should be isochronous to provide complete energy recovery for off-momentum electrons and to relax the tolerances on RF system. To ensure the isochronous condition the lattice has to be flexible to adjustments of the M_{56} parameter, if needed. The equation of the longitudinal synchrotron motion is:

$$\frac{\delta T}{T_o} = \left(\alpha - \frac{1}{\gamma^2}\right)\frac{\delta p}{p} \qquad [3]$$

Where γ is the relativistic factor, and a is the momentum compaction:

, [4]

where γ_T is the transition energy, θ_i is a bending angle of the dipole *"i"*, $\bar{D}_i$ s average dispersion through the dipole *"i"*, and the C_o is the circumference of the accelerator. A lattice design method to avoid the transition crossing where the momentum compaction $\alpha < 0$ had been previously presented [1]. To produce $M_{5,6} \cong 0$ can be achieved if the total sum of the horizontal dispersion through dipoles is equal to zero: $\Sigma_i\ D_i\theta_i \cong 0$. The method is best explained by the Floquet transformation and "normalized dispersion" function [2].

$$\chi = D'\sqrt{\beta} + D\frac{\alpha}{\sqrt{\beta}} \quad \xi = \frac{D}{\sqrt{\beta}} \quad , \qquad [5]$$

where a vector $\chi = D_x' \sqrt{\beta}$ or as the change in the slope of the dispersion function is equal to the bending angle θ: $\chi = \theta \sqrt{\beta}$, it represents the dipole effect on the dispersion function. These vectors need to be equally distributed on the ξ axis making the overall sum equal to zero or $M_{5,6} = 0$. The normalized dispersion space for the eRHIC arc basic module is shown in Fig. 1.

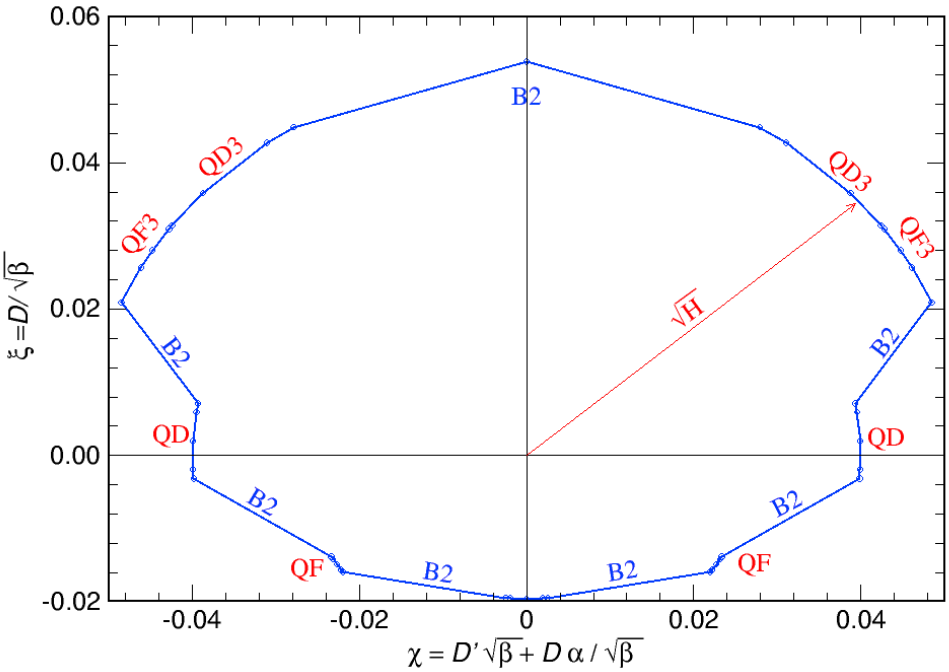

Figure 1: The normalized dispersion space for the basic module of the eRHIC arc. The *B2* dipole vectors $\chi = \theta \sqrt{\beta}$ shown are placed symmetrically with respect to the zero of the ξ axis making for the presented module the momentum compaction equal to zero ($\alpha = 0$).

The eRHIC magnets are placed inside of the existing RHIC tunnel, arcs follow the shape of the tunnel while the two linacs are in the 10 and 2 o'clock straight sections.

The synchrotron radiation in the arcs presents a significant concern. An average radius of the arcs is 381.23 m. Geometry of arc lattice needs to follow the average radius. The basic cell, as shown in Figure 2, has one and a half FODO cells on both sides and two doublet quadrupoles for a "π" flip of the dispersion function phase in the middle. It has strong focusing, good compaction, low values of betatron and dispersion functions, and tunable momentum compaction. The basic parameters of the arc cells are: length of the dipoles is L_d=3.12 m, defocusing and focusing quadrupoles in the FODO cells are 0.8385 m and .892 m, respectively. The lengths of the doublet defocusing and focusing quadrupoles are 0.926 m and 1.525 m, respectively. The drift lengths are 19.5 cm between the quadrupoles and dipoles in the FODO cells, 48.15 cm between the dipole and the focusing doublet quadruples, and 62.64 cm between the defocusing and focusing doublet quadrupoles. Ten basic blocks make an arc with a circumference of 356.3 m with a total bending of θ_{arc} = 0.93241 rad. The arc tunes are ν_h = 9.11802 and ν_v = 6.47184, with horizontal and vertical chromaticities of ξ_x = -10.789, and ξ_y = -8.11403, respectively. The momentum compaction is equal to zero (α = 0). The maximum of the betatron functions β_{xmax} =14.37 m and β_{ymax} =16.147 m, with a dispersion function oscillating between -0.2343 m < D_x < 0.3945 m. Tuning is achieved by the doublet quadrupoles as explained in a separate momentum compaction corrections. Six arcs in the eRHIC collider, are assumed to be vertically above each other with the same arc elements, but with scaled down with energies of magnet excitations. Connections to the two linacs are provided with spreaders or mergers at the ends of the arcs. The achromatic cells at the end of the arcs are designed either by the missing dipole method or by [4] using two basic module cells but with different gradients of the quadrupoles as shown in the normalized dispersion space in Figure 4 and x, y – s space in Figure 5.

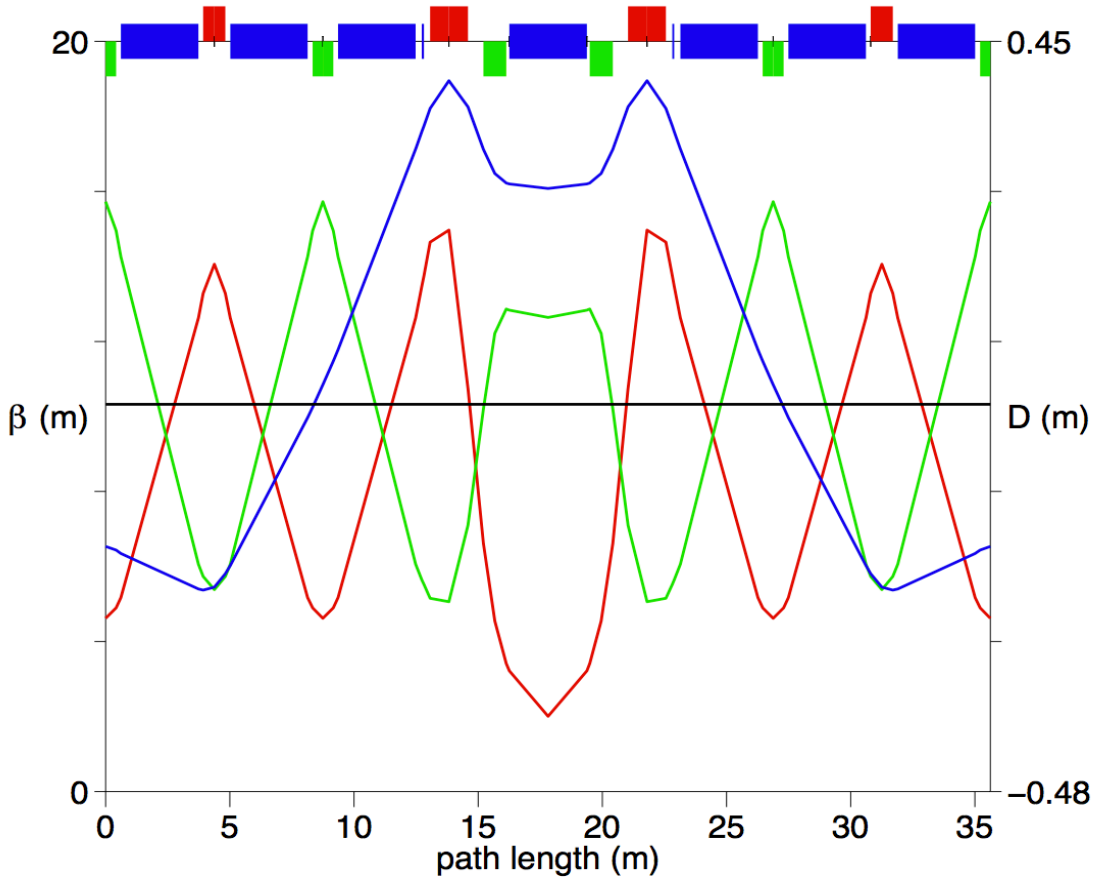

Figure 2: Betatron and dispersion functions in the basic eRHIC arc cell.

Three types of connections between the arcs and straight sections are developed:

1. First the special vertical cells with very small bending magnets to provide connection to the interaction region,
2. Second, spreaders and combiners to provide connection to the linacs, and
3. Third, cells which either pass parallel to the present RHIC straight section or bypass the detectors.

The linacs in both examples do not have quadrupoles, as the energy range is too large for them to provide significant difference in focusing. The splitters and combiners define the betatron functions for each energy pass. The center of the linac has the minimum of the betatron functions. The combiner and spreader are shown in a separate part of this report. In addition, the cavities electrical fields provide the RF focusing.

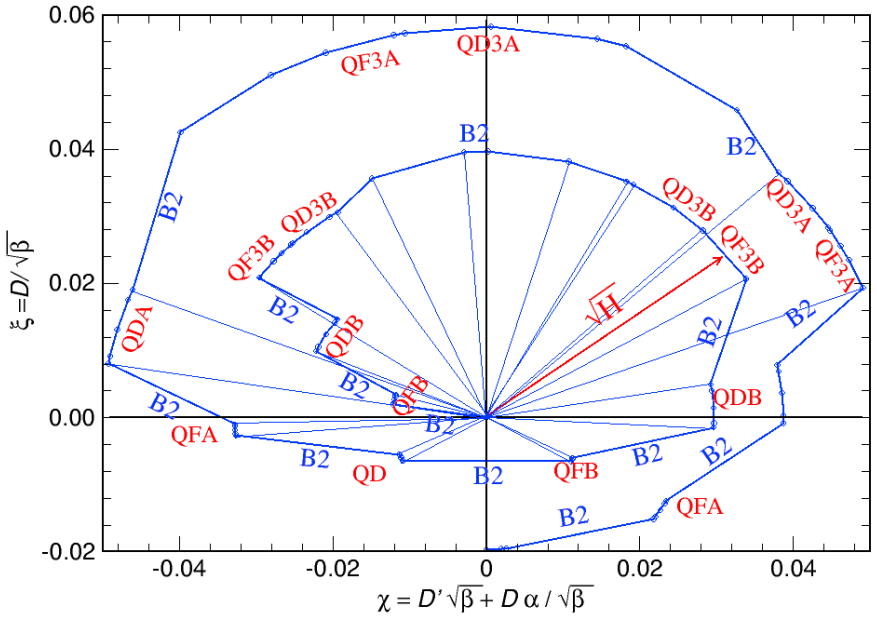

Figure 3: The achromatic cells of the eRHIC in the normalized dispersion space.

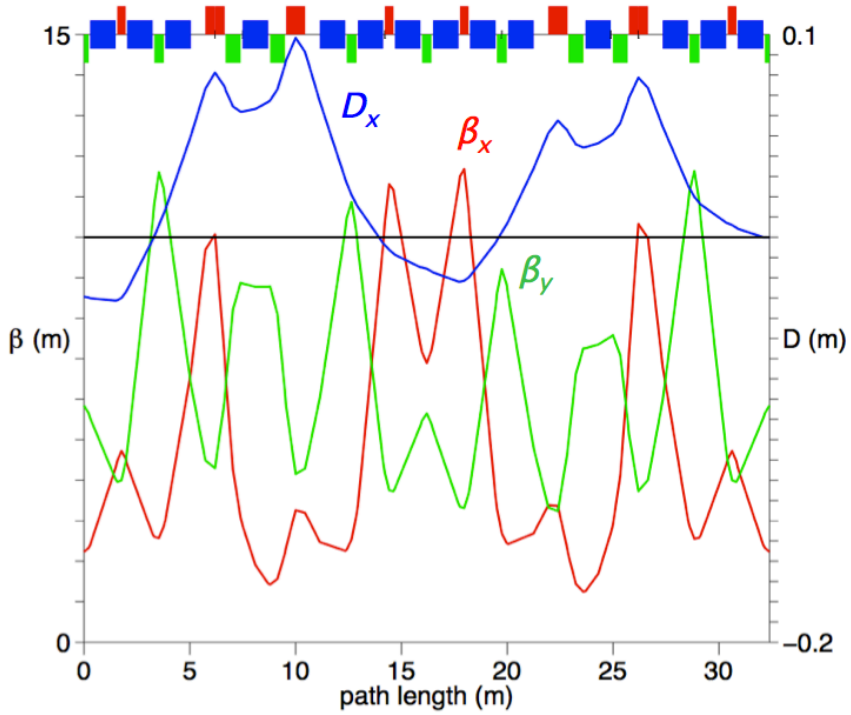

Figure 4: Achromatic cells at the end of the eRHIC arc with the structure as the arc cells but with different gradients in quadrupoles.

The lengths of the quadrupoles are selected to provide the smallest number of power supplies as shown in Figure 5.

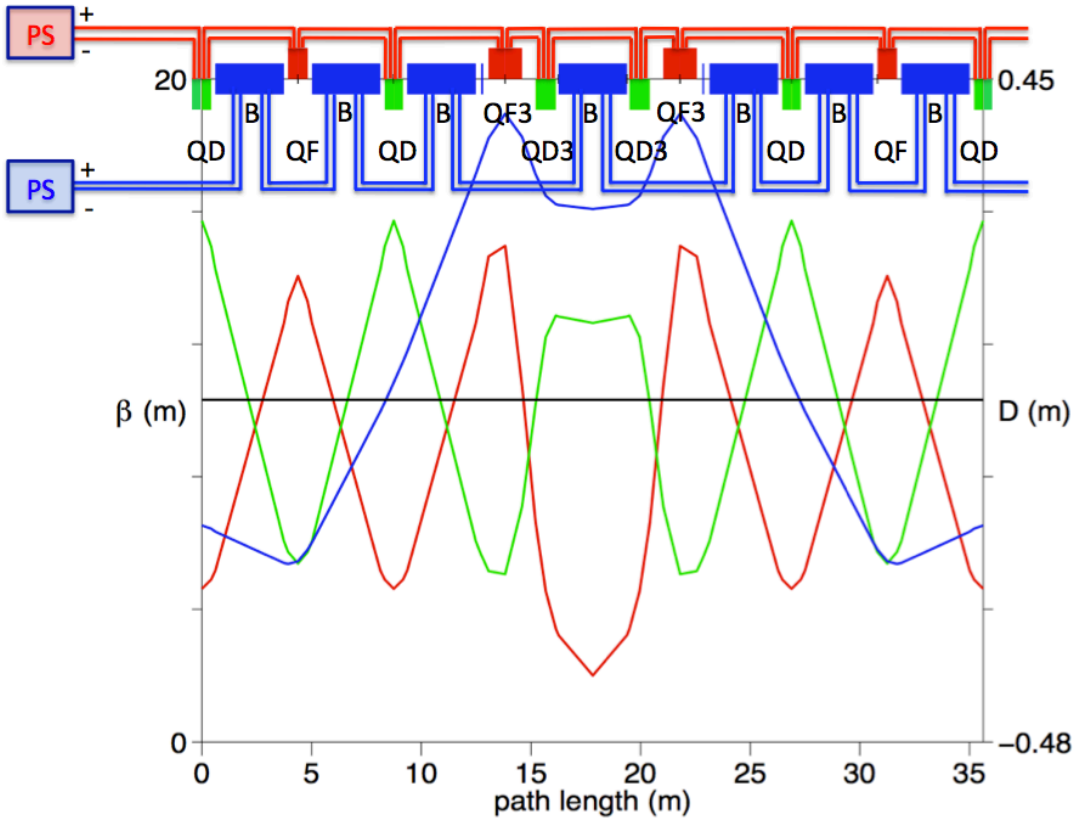

Figure 5. The quadrupoles and dipoles eRHIC arc power supplies

Splitters/Combiners

Splitters/combiners make the transformation from one beamline for all beam energies in the main linacs to the multiple beamline structure in the arcs, and vice versa. There are four splitters/combiners, one on each sides of two linacs. Splitters and combiners are vertical and are bringing the e-beam over the RHIC magnet cryostats to the outside of the RHIC ring.

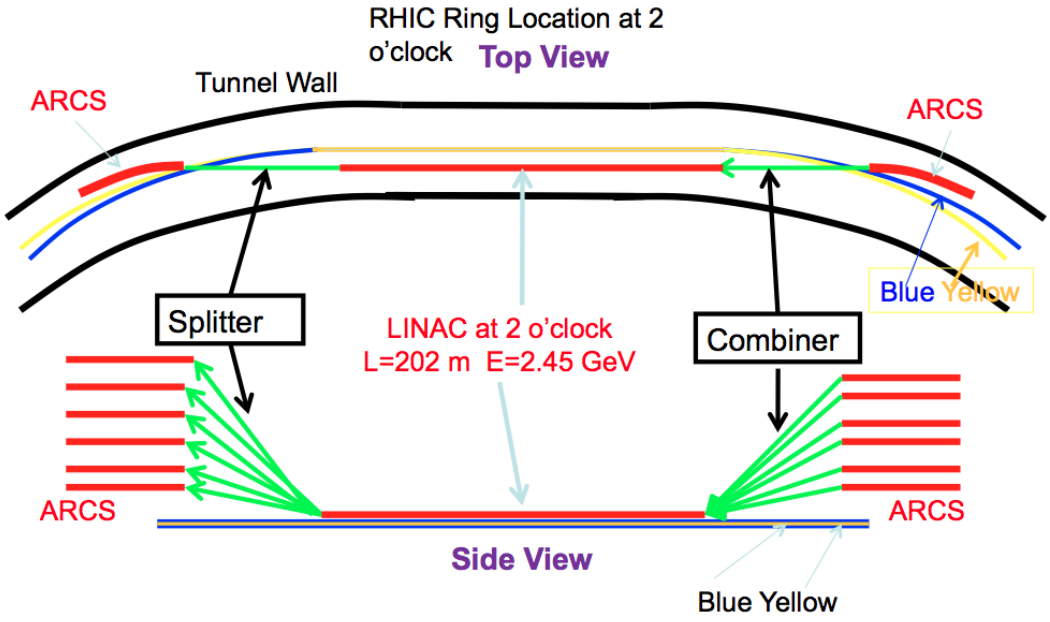

Figure 1:Splitter and Combiner at IR2

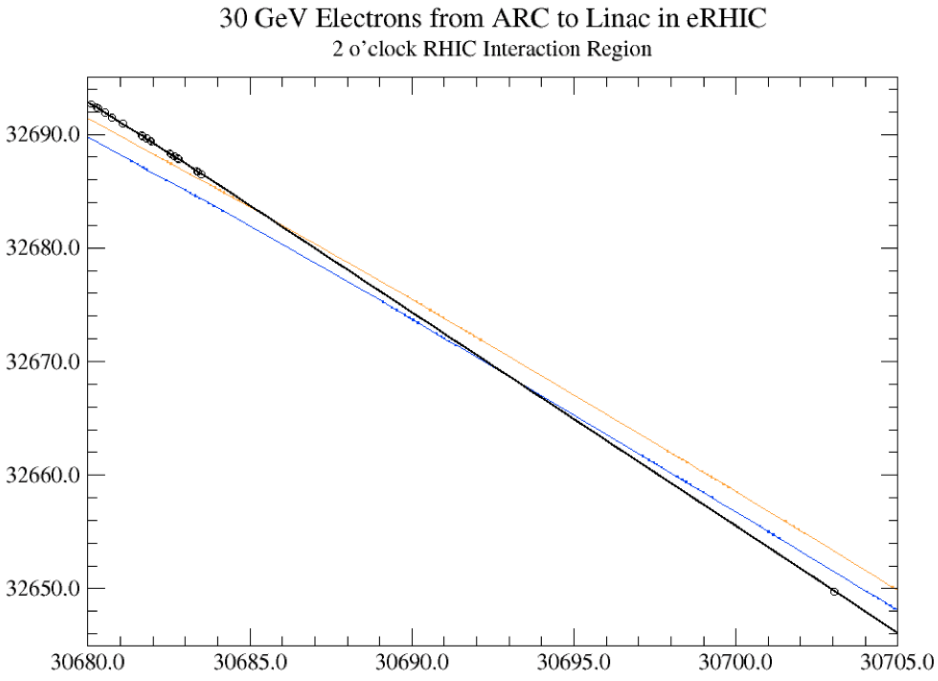

Figure 2: Splitter layout at IR2. Top view

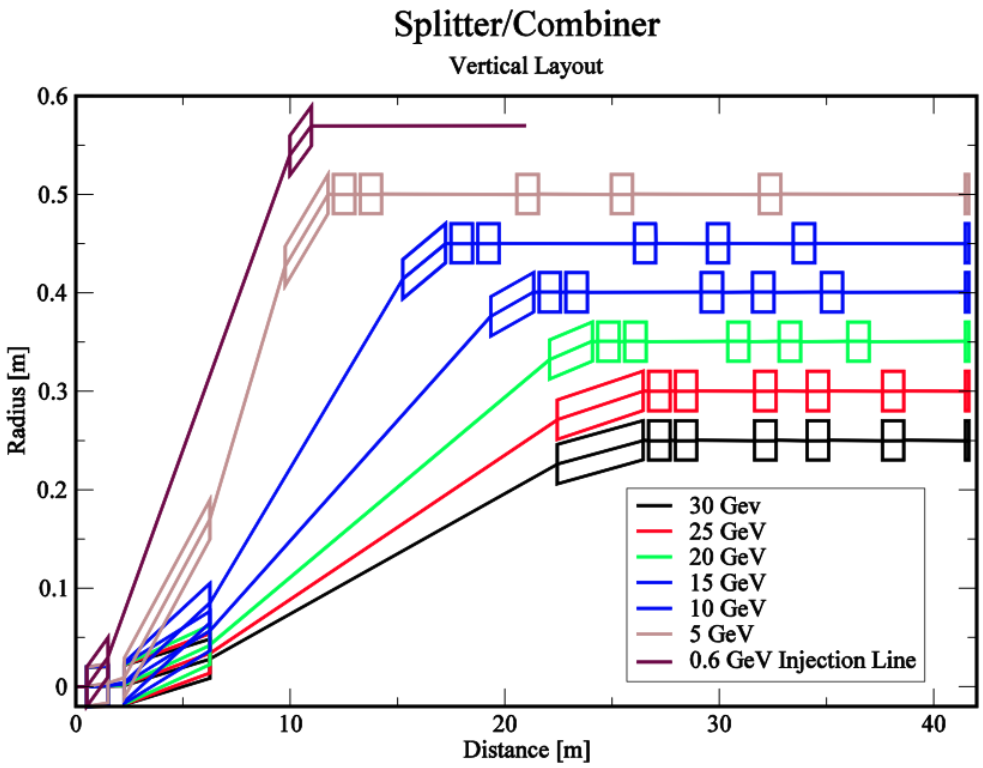

Figure 3: Splitter side-view scheme.

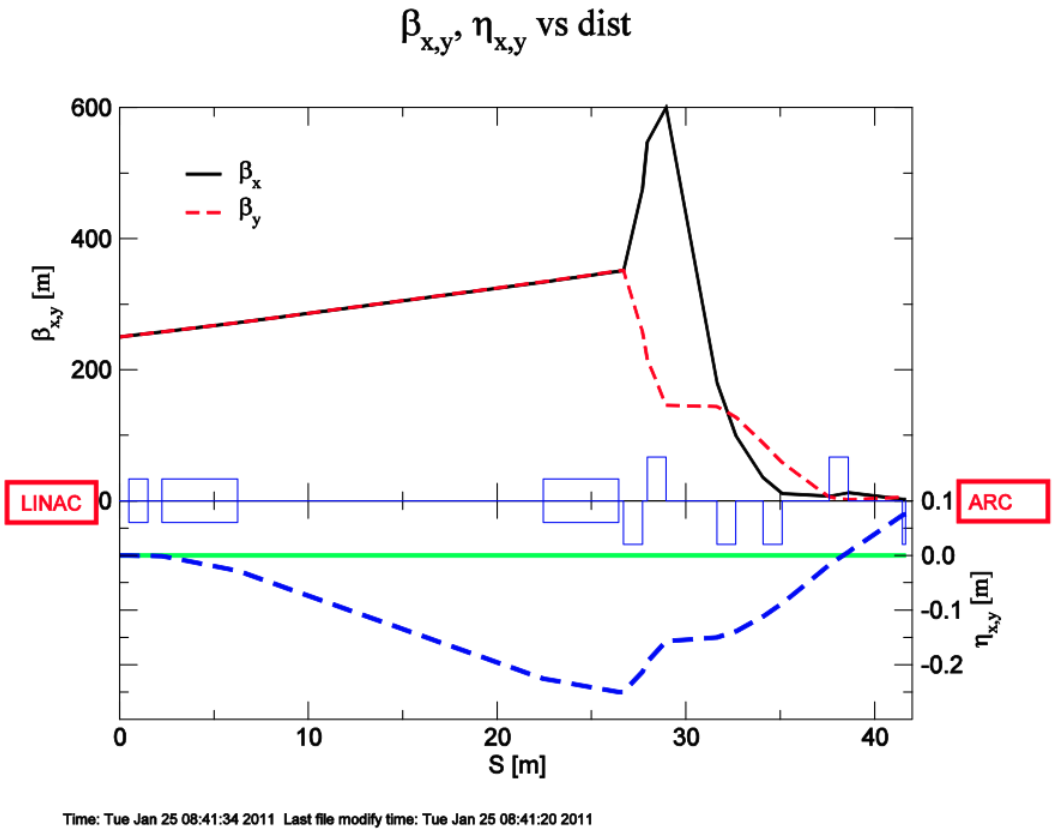

Figure 4: Splitter optics functions for 30 GeV line

Maximum fields required for 30 GeV:

- dipole = 0.31 [T] Length=4 [m]
- quadrupole= 93.0 [T/m] Length=1 [m]

The vertical dispersion is not completely compensated in the present design, in order to preserve the merger compactness. Leaking dispersion to the arcs is nor expected to be a problem. Maximum beam size at the straight section of Combiner (at T=2.5 GeV) is = 4.3 [mm] (One standard deviation) .

The longitudinal position of the dipole magnets of the individual splitter arms needs adjustment at the operation at different top beam energies, because of the beam energy loss - energy compensation process change slightly the average beam energy. At the baseline design of the energy loss compensator the largest longitudinal adjustment, up to 12cm, is required for the dipole magnet of the splitter at the exit of first ERL.

By-pass lines

Function of the By-Pass-Lines

This section describes the function, the layout and the beam optics of the by-pass-lines of the eRHIC collider. As mentioned earlier, there are six beam lines involved in the acceleration and the deceleration cycle of the electron bunches. These beam line are located inside the RHIC tunnel and are positioned vertically. At the Interaction Point (IP) region only the 30 GeV line guides the beam to the IP and the rest of the beam lines deflect the beam bunches transversely to clear the detector located at the IP. A schematic diagram of the top view of the by-pass line at the interaction point is shown in Figure 1.

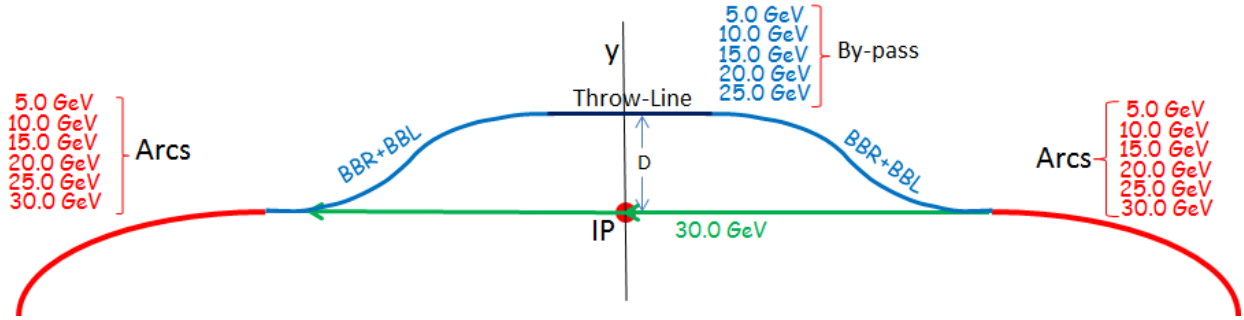

Figure 1: Schematic diagram of the top view of the Interaction Point (IP) region with the arcs and the by-pass lines. Only the 30 GeV transfer line passes by the IP point. The rest of the lines are displaced by a distance D to clear the detector located at the IP.

It is clear from the schematic diagram of Figure 1 that one of the functions of the by-pass lines is to displace transversely all the arc-beam-lines, except the 30 GeV line, by a distance D to clear the detector of the Interaction Point.

Layout of the by-pass-lines

As each of the six beam bunches exits the corresponding arc shown at the left side of Figure 1, the 30 GeV beam is directed to the (IP) and the remaining five lines are bypassing the IP. The five by-pass lines are displaced transversely by a transverse distance D to clear the detector of the IP. Each of the five by-pass lines is symmetric with respect to a plane which passes through the IP and is normal to each of the five lines. This plane contains the line which is labeled (y) shown in Figure 1. Each of the by-pass lines consists of the following sections: a) two Basic Blocks one bending to the right and the other to the left (BBR+BBL), b) a straight “throw line” located at the center of the line c) followed by two Basic Blocks one bending to the left and the other to the right (BBL+BBR). Each Basic Block deflects the beam by the same angle.

Figure 2 shows the layout of the top view of one of the by-pass lines. The rectangular blocks shown in Figure 2 represent the dipoles and the quadrupoles of the basic block. This particular by-pass line displaces the beam bunches by 3.3 m from the IP. The line may displace the beam by a larger of smaller distance then the 3.3 m, depending on the angle that each Basic Block bends the beam.

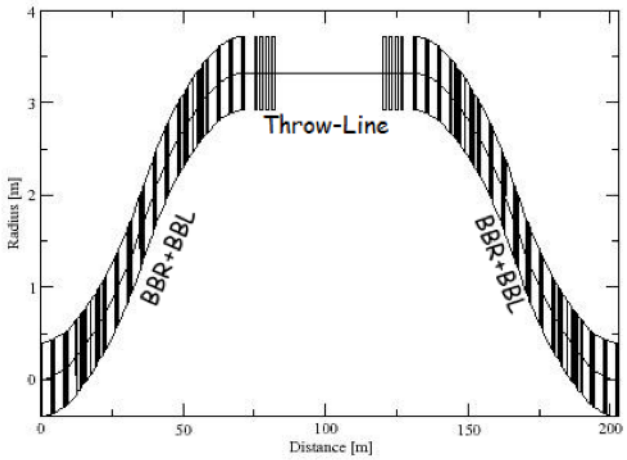

Figure 2: The layout of the by-pass line which consists of two basic blocks bending to the right

Optics of the by-pass-lines

An additional function of the by-pass line is to match the beam parameters and dispersion functions from the exit of the arcs prior to the IP to the entrance of the arcs which follow the IP. Figure 3 is a plot of the horizontal and vertical beta and dispersion function of half of a by-pass line. The first section of the by-pass line (BBR+BBL) form an achromatic beam at the exit. The "Throw-line" section which consists of eight quadrupoles transports the achromatic beam at the entrance of the BBL+BBR section which matches the beam to the arc.

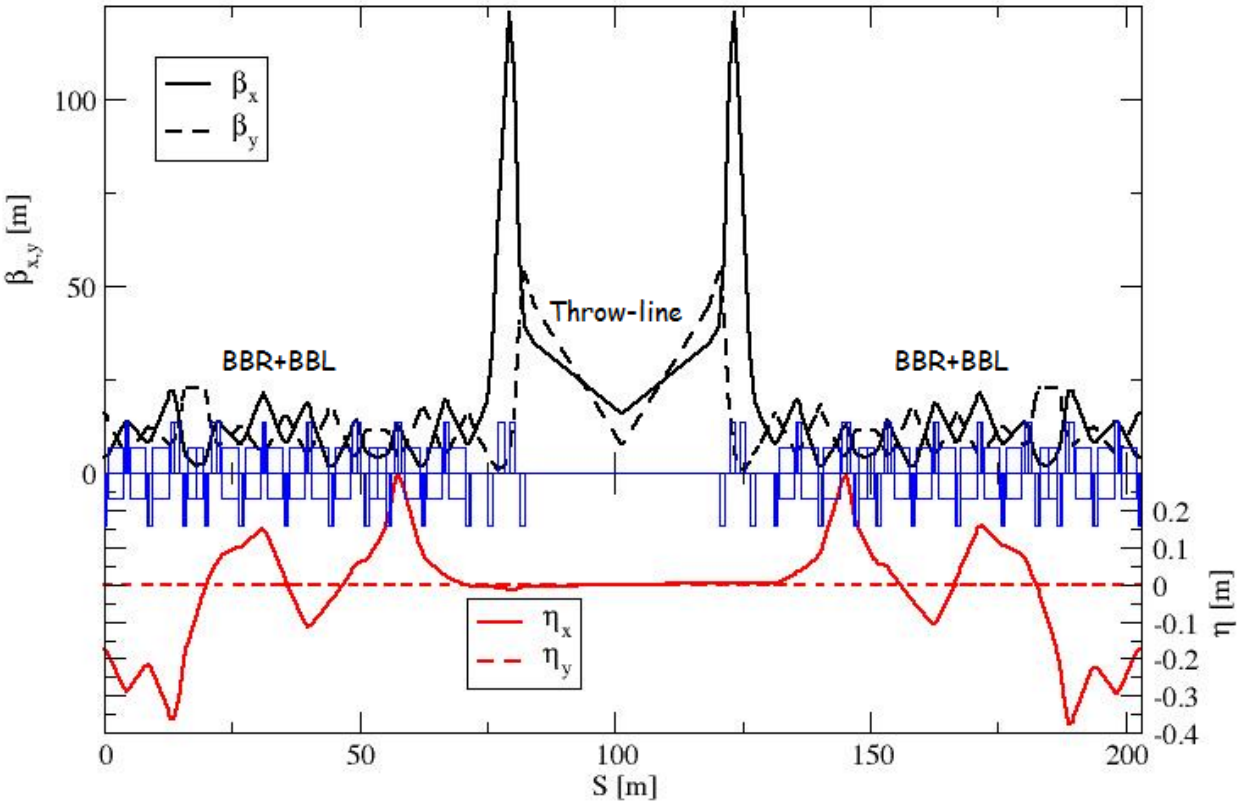

Figure 3: The beta and dispersion functions of the by-pass lines. The by-pass line consists of three main sections. The BBR+BBL section, the "Throw-line" section, and the BBL+BBR section, all discussed in the text.

To accomplish an achromatic beam at the exit of the beam line section which consists of two basic blocks (BBR+BBL) I was necessary to adjust the strength of the following quadrupoles which are included in the basic block. I.

Main Linacs

The present solution for the electron optics in the ERLs does not include any quadrupole magnets, still providing reasonably low beta-functions. The plot below shows the evolution of the beta-function in the ERLs during the whole acceleration process. The recirculating beam lines between the ERLs are shown as delta-function transformation in the locations marked by the vertical lines.

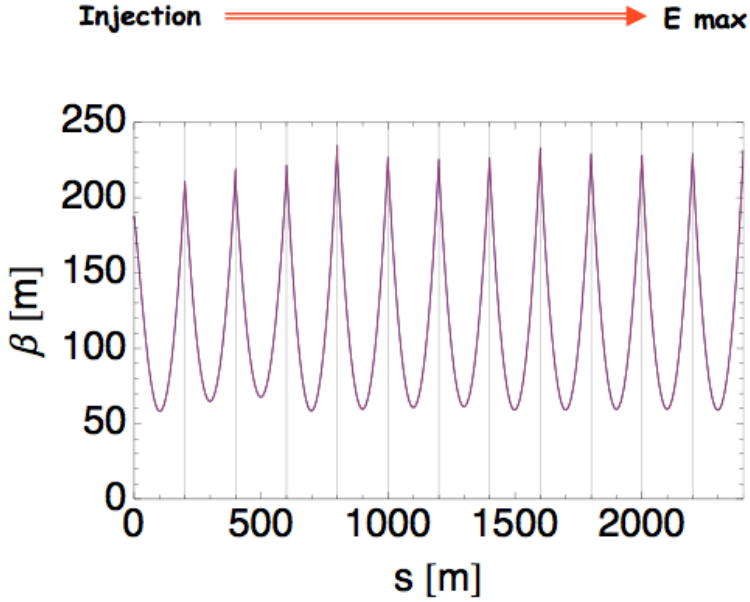

Alternative (backup) solution of the ERL lattice includes FODO focusing structure in the linac. This solution can be used in the case if there would be problems with the beam breakup in the baseline (without quadrupoles) lattice variant.

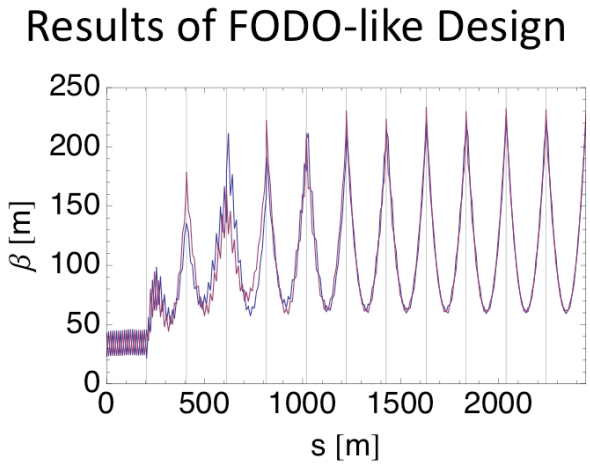

With Quadrupole strength from 0.72T/m to 2.93T/m that scales with the electron beam energy in the first linac. The quad length is assumed to be 0.2m. The resulting length of one linac is 203.8m+cold warm transition.

Path lengthening for frequency matching

Requirements

The requirement to have the ability to change the path length of all passes up to 15cm comes from the necessity of the bunch frequency variation, depending on the proton beam energy. For the collision with 325 GeV protons the required path lengthening is 0, for the collision with 100 GeV protons (or ions) the required path lengthening is about 15cm. The circumference of each path has to be tuned with the accuracy of few microns.

Main design features

- Located in IR4 straight section of the tunnel (on the outside part). The total length of the insertion is ~200m.
- Maximum magnetic field in the dipoles is limited to 3.5 kGs (that is does not exceed the field in the arc dipoles)
- The connection between all the magnetic elements of the beam line should allow a slight increase and decrease (~ 2-3 mm) of drift space for the total length of the line to vary from 0 to 15 cm
- For 15cm the maximum orbit excursion will be 1.5m. The excursion is created in the vertical plane in all six beam lines.

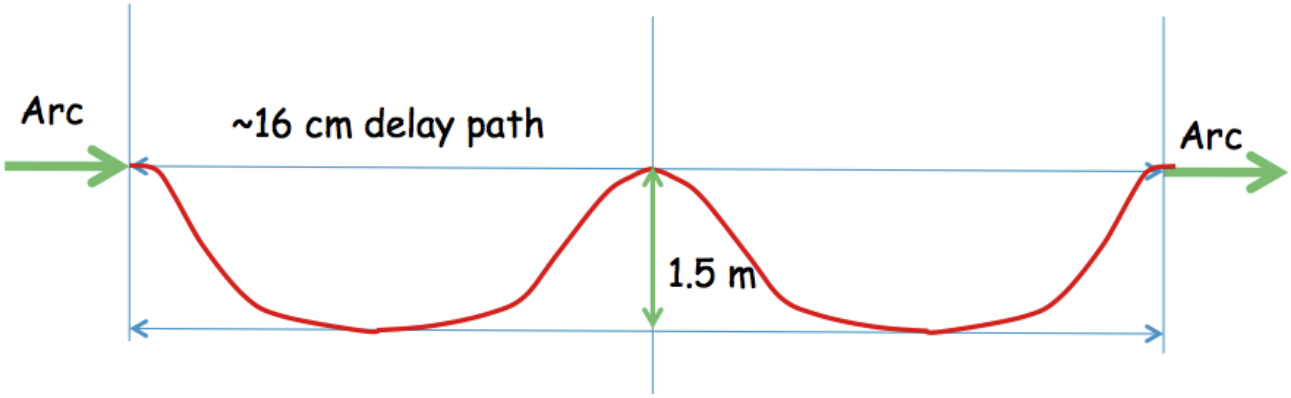

Two variants are being considered:

1. The variant with dipole magnets only. The movement of the magnet can be simpler realized, but the optics functions are quite large.

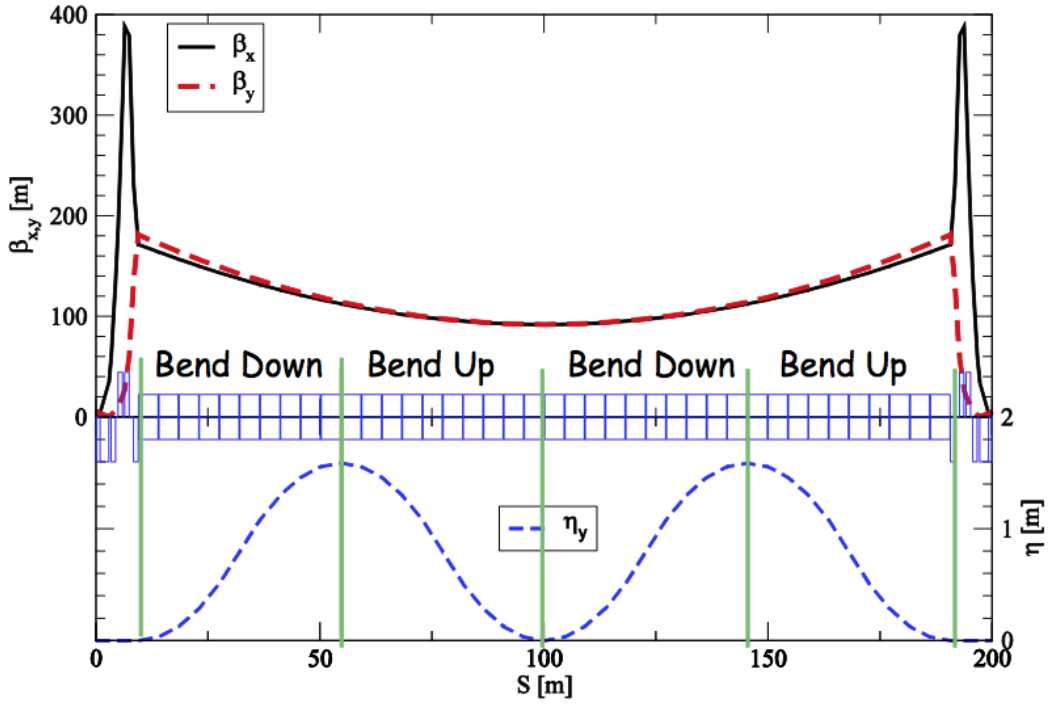

2. The variant with combined function magnets. The reduced optical functions, but potential problem with the magnet movement and alignment.

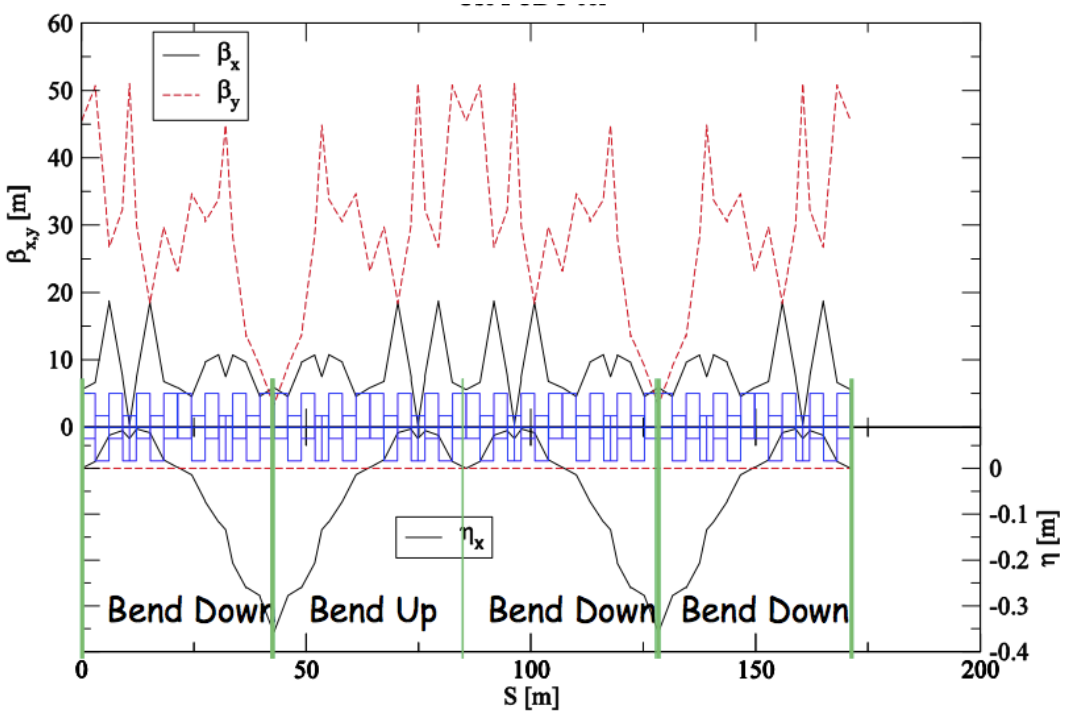

Small path length and R_{56} adjustment

Path length adjustment is critical for eRHIC, an ERL-based EIC design with 6 acceleration passes and 6 deceleration passes. It is required to ensure the acceleration passes being on the crest with maximum positive voltage and the deceleration passes being on the valley with maximum negative voltage. Such that the resulting energy spread and variation are minimal and beam power can be recovered as much as possible. The half wavelength path length change for transitioning from acceleration to deceleration is discussed in previous section. The path length adjustment will be discussed here is for ensuring the time-of-flight for acceleration passes and/or deceleration passes between the two linacs are exactly $k\lambda$ (k is an integer). For multi-pass ERL, the path length correction unit can only be located in the arcs to be able to adjust the path length of acceleration passes individually. Six units are needed in the upper part of the complex and five for the lower part. The energy of acceleration pass and deceleration pass in the same arc will be different due to synchrotron radiation. To make sure the deceleration passes being on the right phase for energy recovery, the arcs should be isochronous (R_{56} being zero).

For ultra-relativistic ERL machine, a four-dipole chicane which changes path length physically is an efficient way to adjust the time-of-flight of the electron passes. Even though the R_{56} introduced by the chicane can be suppressed to some extent by adding quadrupoles in the chicane, the adjustment of components is necessary for achieving an isochronous arc. To cancel the R_{56} from chicane and residual from arcs, the quadrupoles in the arcs will be adjusted which introduces no path length change.

The path length adjustment range is assumed to be +/- 0.25 mm for all passes based on adjustment required at CEBAF [1]. The relative energy difference for acceleration pass and deceleration pass in the same arc is expected to be around 1.5%. Less than 0.1 deg phase slippage of the deceleration pass requires the R_{56} be less than 7 mm, which we take as the control precision of R_{56}. The adjustment range of R_{56} needed will be determined by simulations.

Path length chicane

We considered the path length chicane design consisting of 3 magnets with the lengths (L_1,$2L_1$,,L_1) and with drift space L2 between the magnets The highest electron beam energy that requires small path length adjustment is 27.55 GeV. The limit of the magnetic field of the dipoles is set to be the same as the dipole field in the same arc, for 27.55 GeV the field is 0.427 T.

We get the bending angle

$$\theta = \frac{BL_1}{B\rho} = 0.425\frac{L_1}{100*27.55/30} = 0.00465L_1$$

The maximum excursion in x plane

$$\Delta x = 2L_1(1-\cos\theta)/\sin\theta + \frac{(4L_1 - 4L_1\theta/\sin\theta + 0.005)\tan\theta}{2/\cos\theta - 2}$$

The drift length

$$L_2 = \frac{(4L_1 - 4L_1\theta/\sin\theta + 0.005)}{2/\cos\theta - 2}$$

The total length of the path length unit

$$L = 2\frac{(4L_1 - 4L_1\theta/\sin\theta + 0.005)}{2/\cos\theta - 2} + 4L_1$$

For saving cost, the dipole length is designed to be the same as the dipoles in the arcs, which is 3.12 m. The chicane parameters for 27.55 GeV electron beam are listed in **Error! Reference source not found.**.

Table 1 Design parameters of path length (PL) chicane for 27.55 GeV electron beam

Beam energy	PL adjustment range	X excursion	Dipole length	Dipole field	Drift space	Total length
27.55 GeV	+/- 0.25 mm	49.6 mm	3.12 m	0.427 T	0.293 m	13.071 m

The R_{56} introduced by the chicane is (to second order approximation) [2]

$$R_{56} = (4L_1/3 + 2L_2)\theta^2 = 1mm$$

This should be in principle canceled by the R_{56} adjustment next. However, the value is quite small comparing with the R_{56} control precision.

R_{56} adjustment

There are ten basic blocks in each arc, eight in the middle are identical, and the two on both ends are for matching. The configuration of a basic block and its baseline parameters are shown in **Error! Reference source not found.**. Either the two focusing or defocusing quadrupoles in the middle will be used for R_{56} adjustment for keeping the symmetry of the basic block [3].

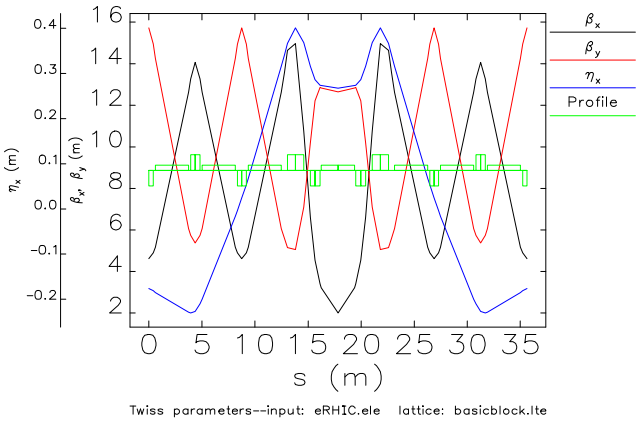

Figure 2: Configuration of a basic block and baseline Twiss parameters

The betatron transfer matrix of a focusing quadrupole is

$$M_f = \begin{pmatrix} \cos\sqrt{k}l & \sin\sqrt{k}l/\sqrt{k} & 0 \\ -\sqrt{k}\sin\sqrt{k}l & \cos\sqrt{k}l & 0 \\ 0 & 0 & 1 \end{pmatrix}$$

The betatron transfer matrix of a defocusing quadrupole is

$$M_d = \begin{pmatrix} \cosh\sqrt{k}l & \sinh\sqrt{k}l/\sqrt{k} & 0 \\ \sqrt{k}\sinh\sqrt{k}l & \cosh\sqrt{k}l & 0 \\ 0 & 0 & 1 \end{pmatrix}$$

The betatron transfer matrix of a dipole is

$$M_b = \begin{pmatrix} \cos\phi & \rho\sin\phi & \rho(1-\cos\phi) \\ -\sin\phi/\rho & \cos\phi & \sin\phi \\ 0 & 0 & 1 \end{pmatrix}$$

The betatron transfer matrix of a drift space is

$$M_L = \begin{pmatrix} 1 & L & 0 \\ 0 & 1 & 0 \\ 0 & 0 & 1 \end{pmatrix}$$

By stacking the matrices for all components, the betatron transfer matrix from the entrance to the middle of the basic block can be expressed as function of focusing quadrupole strength. Due to the symmetry of the basic block, the dispersion at the entrance and the middle point can be expressed in the same way.

Transfer matrix for the 1st half mirror symmetric lattice

$$M = \begin{pmatrix} m_{11} & m_{12} \\ m_{21} & m_{22} \end{pmatrix}$$

Transfer matrix for the 2nd half mirror symmetric lattice

$$M_{mirror} = \begin{pmatrix} m_{22} & m_{12} \\ m_{21} & m_{11} \end{pmatrix}$$

Transfer matrix for the whole mirror symmetric lattice:

$$M_{mirror}M = \begin{pmatrix} 1+2m_{12}m_{21} & 2m_{12}m_{22} \\ 2m_{21}m_{11} & 1+2m_{12}m_{21} \end{pmatrix}$$

Due to periodicity

$$\beta = \sqrt{-\frac{m_{12}m_{22}}{m_{11}m_{21}}}$$

Compaction factor contributed by a dipole magnet is

$$\alpha_c = \left\langle \frac{D}{\rho} \right\rangle = \frac{1}{l}\int_0^{\varphi} D(\theta)d\theta$$

$$\alpha_c = \frac{1}{l}[D_0\sin\varphi - D'_0\,\rho(\cos\varphi - 1) + \rho\varphi - \rho\sin\varphi]$$

Here, l is the length of 8 basic blocks, D_0 and D'_0 are the dispersion and dispersion prime at the entrance of the dipole, ρ and φ are the bending radius and angle. Compaction factor of the basic block is the sum of contributions from all dipoles

$$\alpha_{c,t} = \alpha_{c,1} + \alpha_{c,2} + \alpha_{c,3} .....$$

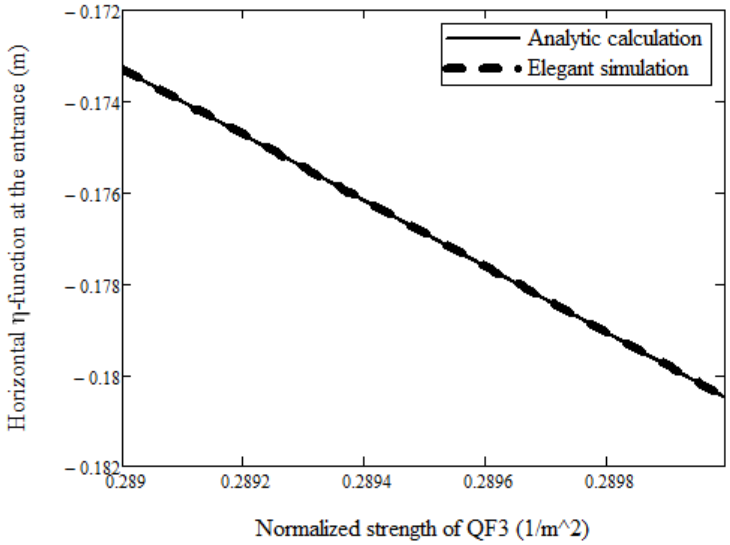

Figure 3: Horizontal dispersion function at the entrance of the basic block when adjusting the focusing quadrupole strength by +/-5%, solid line is from analytical calculation; dashed line is from ELEGANT simulation

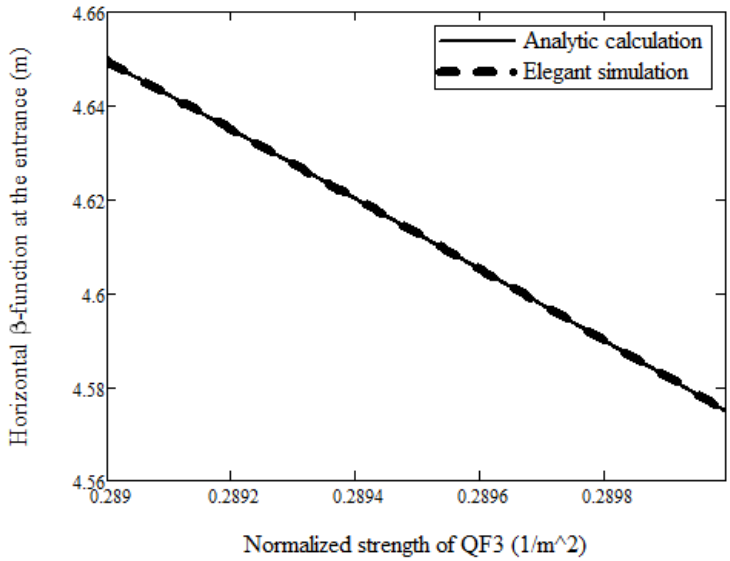

Figure 4: Horizontal beta function at the entrance of the basic block when adjusting the focusing quadrupole strength by +/-5%, solid line is from analytical calculation; dashed line is from ELEGANT simulation

The beta-function and dispersion at the entrance while adjusting the focusing magnet strength by +/-5% are calculated analytically, which was confirmed by ELEGANT simulation [4]. The results are shown in **Error! Reference source not found.** and **Error! Reference source not found.**. The two end basic blocks need to be re-matched for the dispersion and beta-function after adjustment of

compaction factor. In addition, the phase advance changes by +/- 0.25% in horizontal plane, +/- 0.1% in vertical plane.

Due to nonzero dispersion at the entrance and exit of the 8 basic blocks in consideration, we choose to calculate compaction factor instead of the R_{56}. The following is defined as the production of compaction factor and the length of 8 basic blocks. The analytical calculation and simulation of compaction factor are shown in **Error! Reference source not found.**.

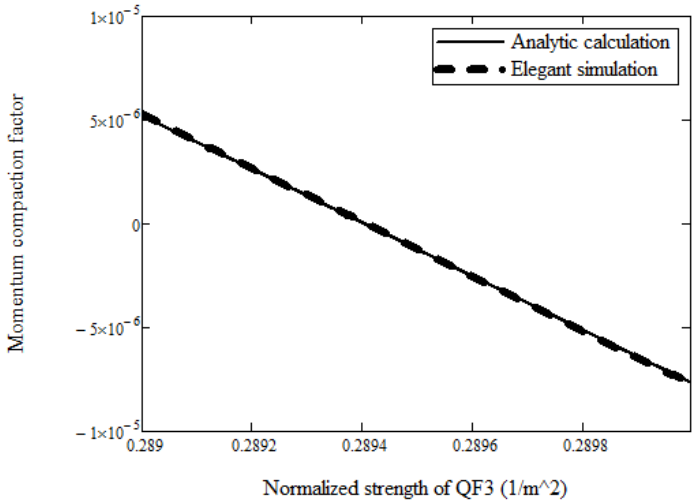

Figure 5: Compaction factor of the basic block when adjusting the focusing quadrupole strength by +/- 5%, solid line is from analytical calculation; dashed line is from ELEGANT simulation

The compaction factor range in Fig. 5 is converted to adjustment range for R_{56} by multiplying the length of 8 36-meter-long basic blocks. The adjustment range of R_{56} is -59 mm to 49 mm if varying the focusing quadrupole strength by +/-5%. The same correction can be done by varying the defocusing quadrupoles, the corresponding R_{56} range is -18 to 17 mm. For higher resolution, the defocusing quadrupoles is a better knob. On the other hand, the focusing quadrupoles can achieve a wider control range. These two knobs can be activated simultaneously to achieve wide range adjustment and fine tune R_{56}.

[1] Krafft, G. A., et al. "Measuring and Controlling the Energy Spread in CEBAF."*arXiv preprint physics/0009087* (2000).

[2] Owen, Hywel, and Peter Williams. "A modular path length corrector for recirculating linacs." *Nuclear Instruments and Methods in Physics Research Section A: Accelerators, Spectrometers, Detectors and Associated Equipment*(2011).

[3] D. Trbojevic , D. Finley , R. Gerig and S. Holmes "Design Method for High Energy Accelerator without Transition Energy", *Proc. of Second European Particle Accelerator Conference*, pp.1536 - 1538 1990

[4] Borland, M. *Elegant: A flexible SDDS-compliant code for accelerator simulation*. No. LS-287. Argonne National Lab., IL (US), 2000.

Superconducting RF

eRHIC utilizes state-of-the-art superconducting RF technology for electron as well as for hadron beams.

- Main Linacs: Two main linacs of a six-pass ERL are based on 704 MHz 5-cell elliptical SRF cavities (currently BNL-3 design). At full energy of 30 GeV, the length of each linac will reach 200 m. All 200 meters are cold with short 1-meter warm-to-cold transition sections at each end.
- 600-MeV Pre-Accelerator Linac: The 600-MeV pre-accelerator is a single-pass 704-MHz SRF ERL. It is based on cryounits designed for the main linac.
- 10-MeV Injector Linac: Long (250 ps) bunch produced by the gatling gun dictates use of low-frequency cavities for bunching. Superconducting QWR-type structures will be used as buncher cavities. 704 MHz SRF cavities will be used in the linac.
- Energy Loss Compensator Linac: This linac compensates energy losses by the electron beam due to synchrotron radiation, higher-order modes, and other effects, see details in Energy Loss Compensation. The linac will be installed in a highest-energy pass and will provide beam with up to 9.8 MW of RF power. Because both accelerating and decelerating electrons will pass through the linac, it will operate on the second harmonic of main RF.
- Energy Spread Compensator Linac:
- Crab Cavities: A crab-crossing scheme will be used to alleviate negative effects of the crossing angle collision. Superconducting crab QWRs are proposed for eRHIC. Due to long hadron bunches, low RF frequency is required. To keep the frequency and cavity voltage reasonable, a two-frequency scheme will be used with the main crab cavities operating at 183 MHz and the harmonic cavities operating at three times this frequency.
- CeC Linac: The 177-MeV single-pass 704-MHz SRF ERL will provide electrons for coherent electron cooling of hadron beams in RHIC. It utilizes cryounits designed for the main linac.
- CeC SRF gun: A 112-MHz QWR SRF gun will be based on a prototype recently developed by a collaboration of Niowave and BNL as a DOE SBR project.

The tables below attempt to summarize requirements and parameters of various SRF systems.

Parameter	ERL main linacs	600 MeV pre-accelerator	10 MeV injector	Energy loss compensator	Energy spread compensator
Location	IP2 and IP10	IP2	IP2	IP12	TBD
Energy [MeV/linac]	2450	600	10	98	
Linac length [m]	200	60		21	
Number of cavities	120 x 2	30	5	49	
Cryounit length [m]	1.66	1.66	0.8		
Cryostat dia. [in]					
Height over RHIC [cm]	35	35			
Cavity type	Elliptical	Elliptical	QWR	Elliptical	Elliptical
Number of cells	5	5	1	2	
Frequency [MHz]	703.8	703.8	112.6	1407.6	3519 or 4926.6
Energy gain [MeV]	20.4	19.7	2	2	
R/Q [Ohm]	506.3	506.3			
Eacc [MV/m]	19.2	18.5		9.4	
Epk/Eacc	2.46	2.46			
Bpk/Eacc [mT/(MV/m)]	4.27	4.27			
G [Ohm]	283	283			
Q_0	3.5e10	3.5e10			
Q_L	5.9e7	5.9e7			
Cavity detuning al low energies [kHz]	-105.7	-105.7			
Loss factor at 2 mm rms bunch length [V/pC]	3.6	3.6			
Static load at 2 K [W]	3	3			
Dynamic load at 2 K [W]	25	25			
Heat load at 50 K [W]	50	50			
Installed RF power [kW]	10	10		250	
208 V AC power [kW]	26	26		500	
HOM power [kW]	7.56	7.56			
HOM water cooling [GPM]	3	3			

Parameter	Crab cavities for protons	Crab cavities for electrons	CeC linac	CeC SRF gun
Location	IP6 and IP8	IP6 and IP8	IP10	IP10
Energy [MeV/linac]	100? (transverse kick)		177	
Linac length [m]			19	
Number of cavities			10	1
Cryounit length [m]			1.66	0.8
Cryostat dia. [in]				
Height over RHIC [cm]				
Cavity type	QWR	QWR	Elliptical	QWR
Number of cells	1	1	5	1
Frequency [MHz]	224?		703.8	112.6
Energy gain [MeV]			17.7	2
R/Q [Ohm]			506.3	
Eacc [MV/m]			16.6	
Epk/Eacc			2.46	
Bpk/Eacc [mT/(MV/m)]			4.27	
G [Ohm]			283	
Q_0			3.5e10	
Q_L			5.9e7	
Cavity detuning al low energies [kHz]				
Loss factor at 2 mm rms bunch length [V/pC]			3.6	
Static load at 2 K [W]			3	
Dynamic load at 2 K [W]			25	
Heat load at 50 K [W]			50	
Installed RF power [kW]			10	
208 V AC power [kW]			13	
HOM power [kW]			7.56	
HOM water cooling [GPM]			3	

Main Linacs

Two main linacs of a six-pass ERL are based on 704-MHz 5-cell elliptical SRF cavities (currently BNL3 design). The BNL3 SRF cavity is optimized and designed for applications such as eRHIC and SPL [2]. Its preliminary design is shown below:

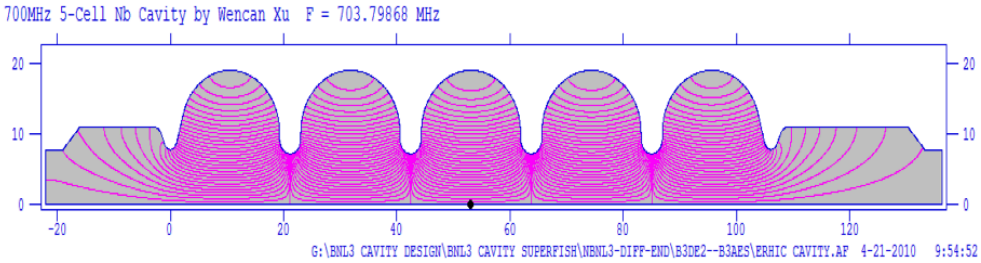

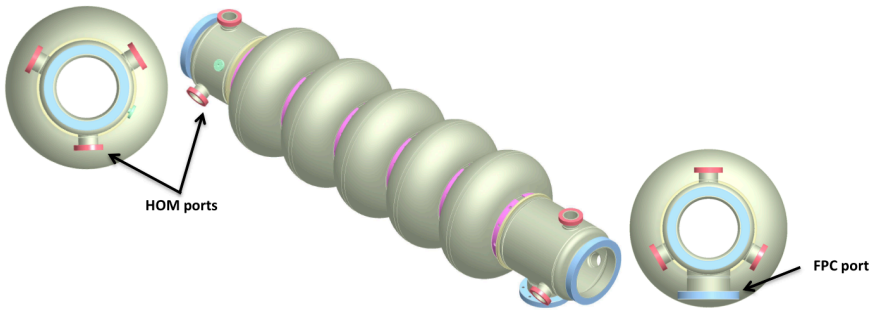

This table compares parameters of the BNL1 cavity, previously designed for the ERL Prototype, and the BNL3 cavity:

Parameter	BNL1	BNL3
Geometry factor	225 Ohm	283 Ohm
R/Q	404.0 Ohm	506.3 Ohm
Epk/Eacc	1.97	2.46
Bpk/Eacc	5.78 mT/(MV/m)	4.26 mT/(MV/m)
Beam pipe radius	120 mm	110 mm

The BNL1 cavity demonstrated quite remarkable performance during vertical tests as shown in the plot below [3]. With similar treatment we expect to achieve similar results with the BNL3 cavity.

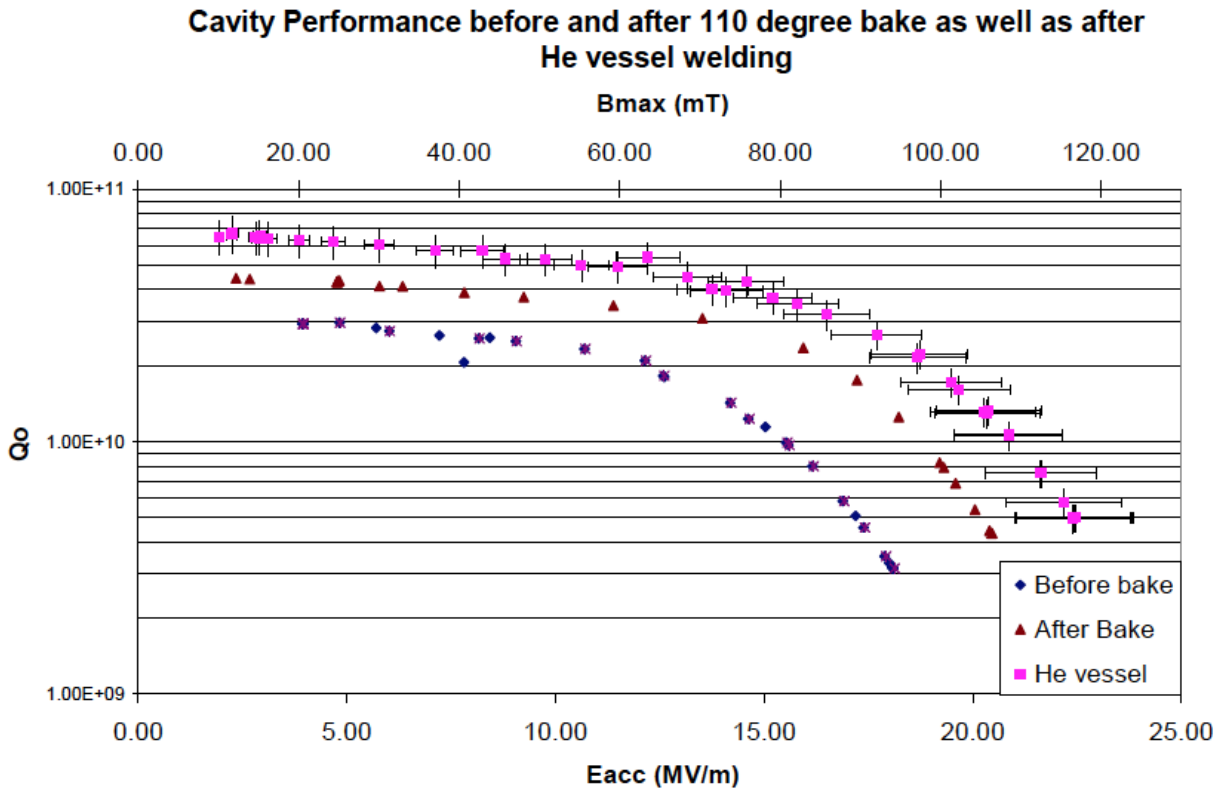

Figure 1. The plot of Qo vs Eacc for three tests on the 5 cell cavity. The blue circles are before the 110 degree bake, the red triangles are after the 110 degree bake and the pink squares are with the He vessel attached.

Three antenna-type couplers will be attached to a large diameter beam pipes at each end of the cavity and will provide strong HOM damping while maintaining good filling factor for the linac. A two-stage high-pass filter rejects fundamental frequency, but allows propagation of HOMs toward an RF load.

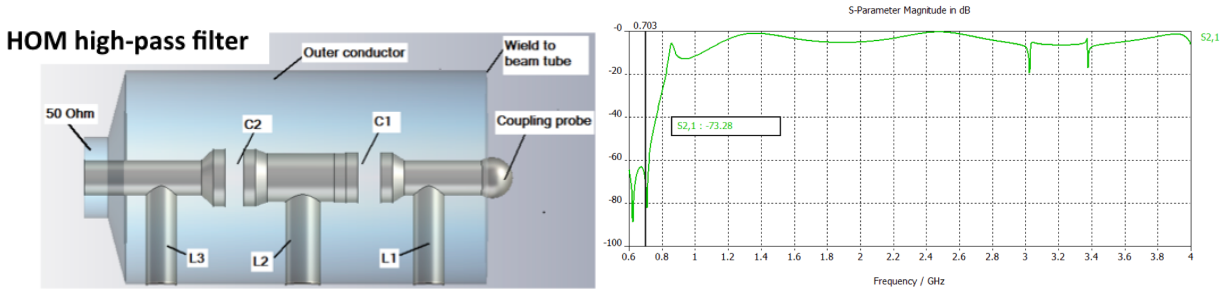

A copper model of the cavity is fabricated to study effectiveness of the HOM damping scheme. The niobium cavity is expected to be ready in early 2012. After testing, it will become part of the prototype eRHIC cryounit. The latter will eventually be used in the Coherent electron Cooling Proof of Principle (CeC PoP) experiment.

At full energy of 30 GeV, the length of each linac will reach 200 m, delivering energy gain of 2.45 GeV. Each linac will have 120 cavities operating at the accelerating gradient of 19.2 MV/m. All 200 meters are cold with short 1-meter-long warm-to-cold transition sections at each end. The main cryo connection will be in the middle of the linac. The linac will consist of single-cavity cryounits with short interconnections between them. Design of the cryounits will provide easy access to allow *in situ* maintenance/repair. Preliminary layouts of the cryounit and string assembly of multiple cavities are pictured below:

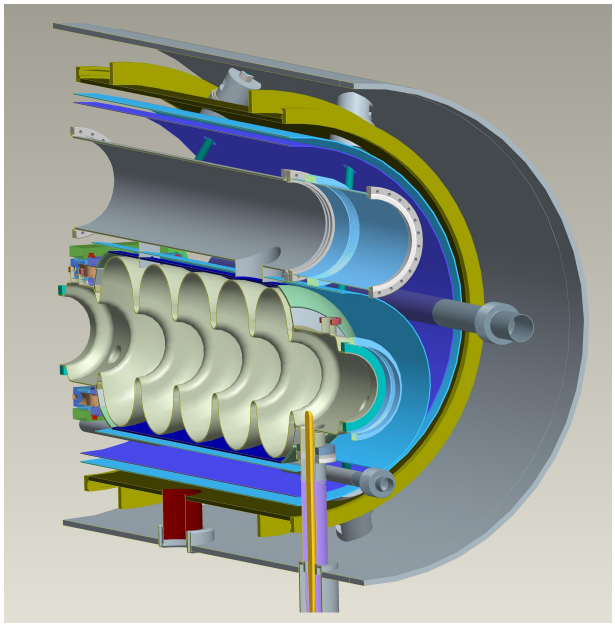

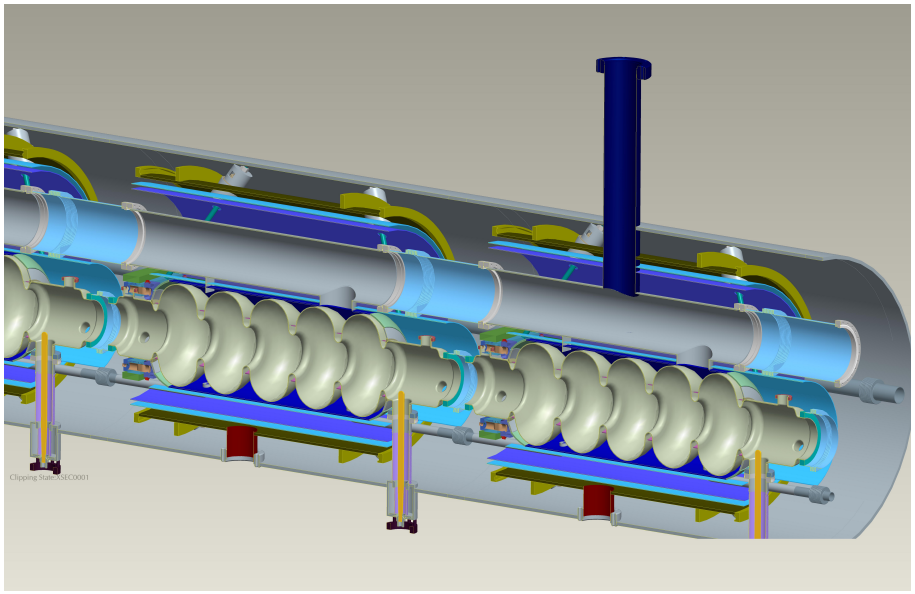

Energy Loss Compensator

This linac compensates energy losses by the electron beam due to synchrotron radiation, higher-order modes, and other effects, see details in Energy Loss Compensation. The linac will be installed in a highest-energy pass and will provide beam with up to 9.8 MW of RF power. Because both accelerating and decelerating electrons will pass through the linac, it will operate on the second harmonic of main RF, 1407.5 MHz.

The main performance limitation for this linac will be RF power per Fundamental Power Coupler (FPC). With two FPCs per cavity and 100 kW per FPC, the linac will consist of 49 SRF elliptical cavities operating at accelerating gradient of 9.4 MV/m. Assuming filling factor of 50%, the linac length is 21 m.

Crab Cavity Design

A Crab-Crossing scheme will be used to avoid more than one order of magnitude of the luminosity loss due to 10-mrad crossing angle collisions. The schematic of the crab-crossing is shown in Figure 1. Both electron and hadron beams come to the collisions rotated by 5 mrad in the horizontal plane. The beam rotation is realized using superconducting crab cavities. The beam crabbing scheme of both electrons and hadrons is local, so that the beam rotation does not propagate outside of the interaction region area.

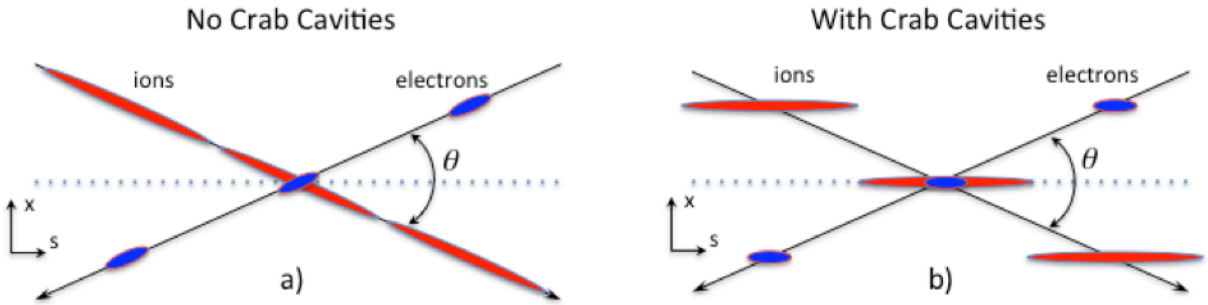

Figure 1: Crossing angle collisions without and with crab cavities

Due to the long hadron bunches, low RF frequency is required. To keep the frequency and cavity voltage reasonable, a two-frequency scheme will be used with the main crab cavities operating at 183 MHz and the harmonic cavities operating at three times this frequency. As the frequency is still rather low to use elliptical cavities, use of superconducting crab QWRs was proposed for eRHIC. Such structure have the following advantages:

- It is the most compact structure of proposed so far.

- There is no Lower Order Modes (LOMs)
- There is no Same Order Modes (SOMs).
- The first Higher Order Mode (HOM) has frequency factor of 2 to 3 above the crabbing mode.
- Items 2, 3, and 4 make it easy to damp HOMs.

The only disadvantage is that there is parasitic acceleration imparted on the beam. However, the acceleration is small and can be eliminated with shape optimization. A conceptual design of the crab QWR is shown in Figure 2.

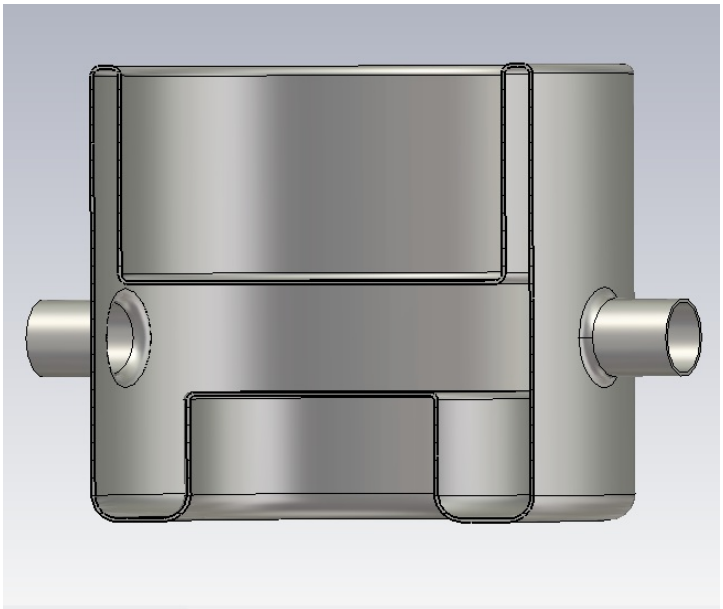

Figure 2: Sketch of the crab cavity for eRHIC.

Cavity Parameters

The parameters of the current design are shown in the table:

	Units	Parameter
Crab mode frequency	MHz	181
Nearest other mode frequency	MHz	251
Cavity length	cm	75.2
Cavity width	cm	38.1/25.1
Deflecting voltage*	MV	6.1
Peak surface electric field*	MV/m	39
Stored energy*	Joules	100
$R_t/Q\#$	Ohm	291
Accelerating voltage	MV	0

(*) for peak surface magnetic field of 100 mT.(#) circuit definition.

Field Distribution

The advantage of the design is the cancellation of the acceleration voltage. The cavity will provide transverse deflection to the bunch, while keeping the net accelerating effect zero. The field distribution along the beam axis of the cavity is shown in the figures below.

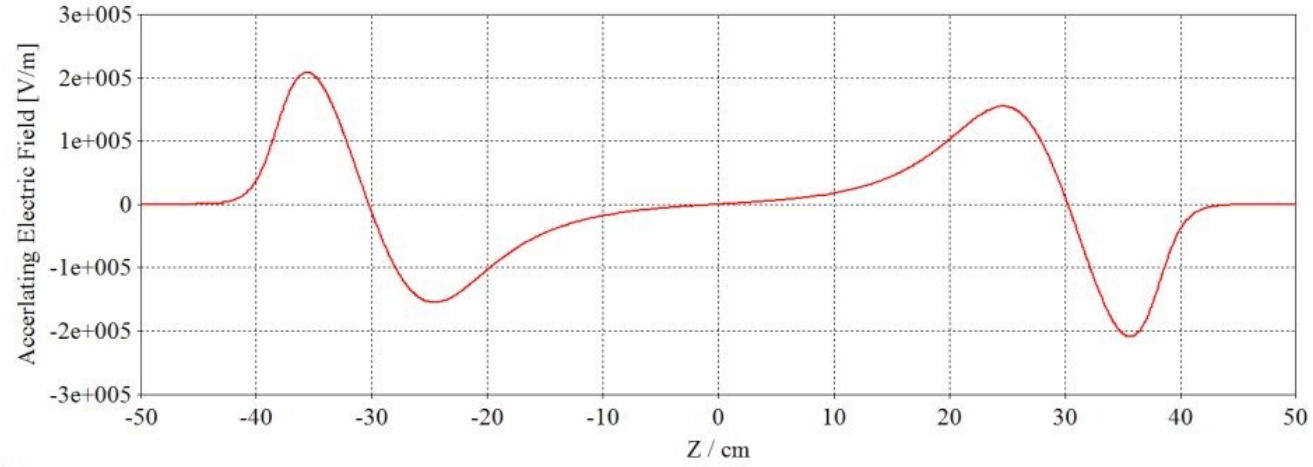

Figure 3: Accelerating electric field along the beam axis of the crab cavity

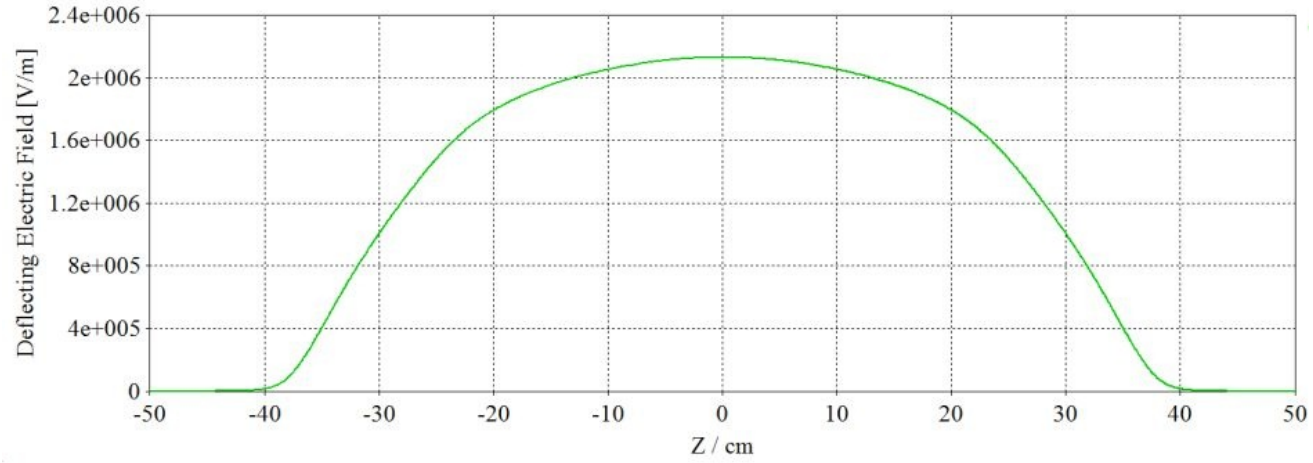

Figure 4: Deflecting electric field along the beam axis of the crab cavity.

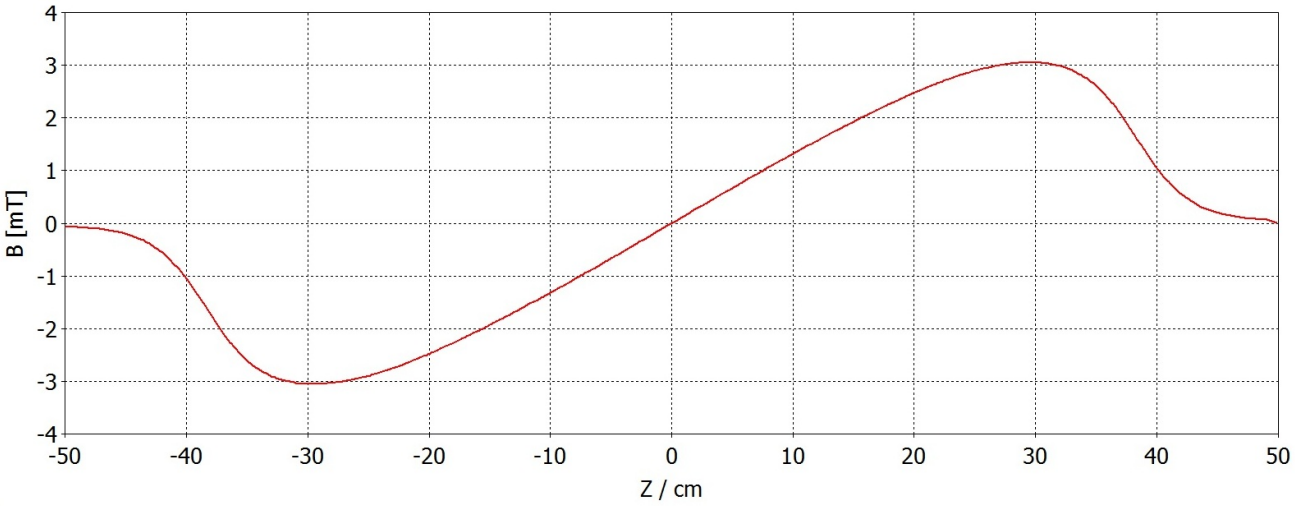

Figure 5: Magnetic field along the beam axis of the crab cavity.

Beam Dynamics

Energy Loss and Energy Spread

eRHIC employs the energy recovery linacs to accelerate high average current electron beam. According to the energy recovery, the energy given to the beam during the acceleration into the cavities of main and pre-accelerator linacs is taken back from the beam during the deceleration and recycled. However, during the beam propagation through the accelerator there are several processes which lead to the energy loss that can not be recovered. This energy loss has to be compensated thus contributing to the total power requirement for the accelerator. Also, the same processes induce the energy spread in the beam, which is accumulated during the beam travel in the accelerator. After the beam deceleration the energy spread has to acceptable to realize the lossless beam transport in 10 MeV transport line to the dump.

The processes contributing considerably to the energy loss and energy spread are the synchrotron radiation, and the interaction of the beam with the environment, especially, the resistive wall effect, high order mode losses in RF cavities and wall roughness. The effect of coherent synchrotron radiation also has been considered.

Synchrotron Radiation

The following calculations included the synchrotron radiation produced in the dipoles of recirculating arcs. The bending radius of those dipole in the baseline lattice with separated function magnets is 234m. The effect from the dipole magnets of splitter/mergers, the detector by-passes and interaction regions is not accounted there.

- For the baseline design with 6 recirculating passes, the beam energy losses and induced energy spreads are shown in the table:

Top energy, GeV	**30**	**20**	**15**	**10**	**5**
Total loss power, MW	7.6	7.6	2.4	0.47	0.03
Power load at top energy, kW/m	1.3	1.3	0.4	0.08	0.005
DE/E at the collision, 1e-4	3	1	0.5	0.2	0.03
DE/E in lowest energy arc after deceleration, 1e-3	22	7.9	3.8	1.4	0.25
Energy spread after deceleration, MeV	13	3.1	1.1	0.28	0.025

The energy spread after deceleration for the top beam energy of 30 GeV is very large and has to be reduced before the beam arrives to 10 MeV transport line to the beam dump.

- The plot below demonstrates how the SR loss power is accumulated over 6 accelerating and 6 decelerating turns for the various top beam energies:

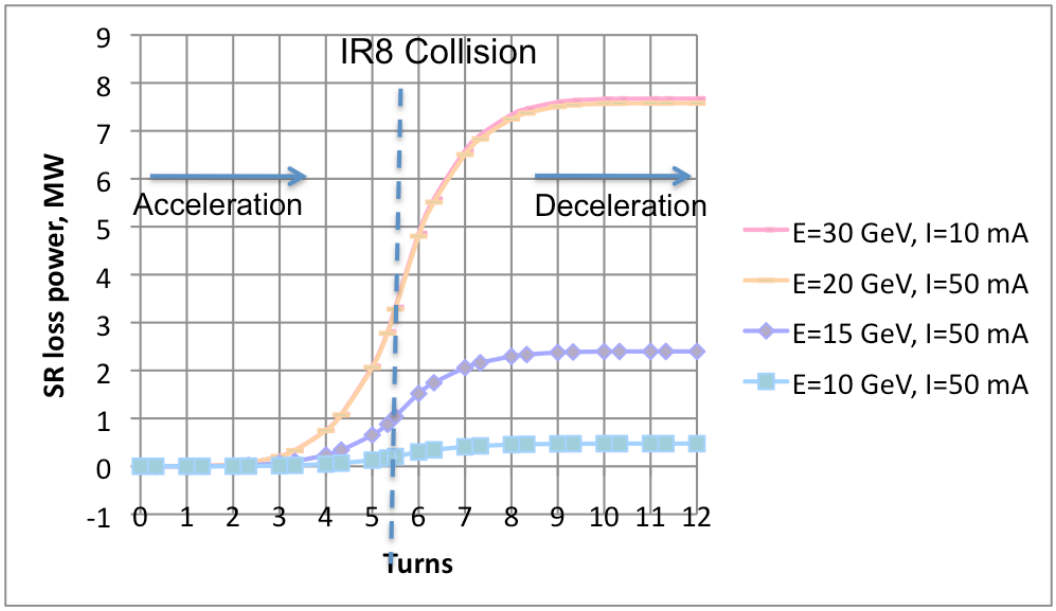

- This plot presents SR accumulated induced energy spread on all 12 turns (6 accelerating + 6 decelerating) for the various top beam energies:

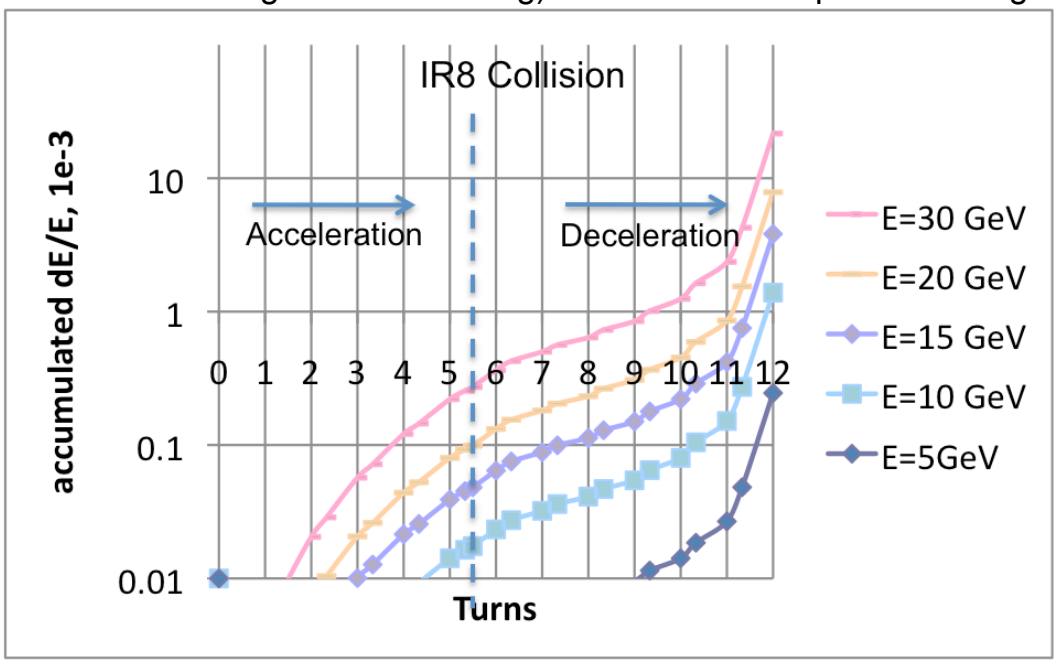

The aperture of lowest energy turn (turn 12) has to be large enough to accommodate the resulting large energy spread.

Coherent Synchrotron Radiation and Shielding

When an electron bunch goes through a bend, each electron gives out synchrotron radiation. For radiation wavelength longer than the bunch length, the radiation from individual electrons add constructively which is called Coherent Synchrotron Radiation (CSR).

Simple estimates of CSR effect for eRHIC shows that electron beams would have significant energy spread and energy loss if one does not take into account the shielding effect of beam pipe walls. When the walls of beam vacuum chamber are conducting, induced charges will decrease the EM fields created directly by bunches. This phenomenon is referred to as shielding and is the stronger the closer the induced charges. Analytic theory of CSR shielding suggests that CSR can be suppressed if beam-pipe dimension is small or the bunch length is large. For the eRHIC bunch length parameters (2-4mm rms) these analytic estimates show that CSR effects will be strongly suppressed for the present value of the vertical size of the vacuum chamber with a significant safety margin.

In addition, experiments were conducted at BNL's ATF to study effects of CSR shielding both on energy loss and energy spread even in the regime where modest shielding supression could be expected [1].

- This plot shows limiting rms bunch length for which CSR is completely suppressed as a function of full beam pipe gap size:

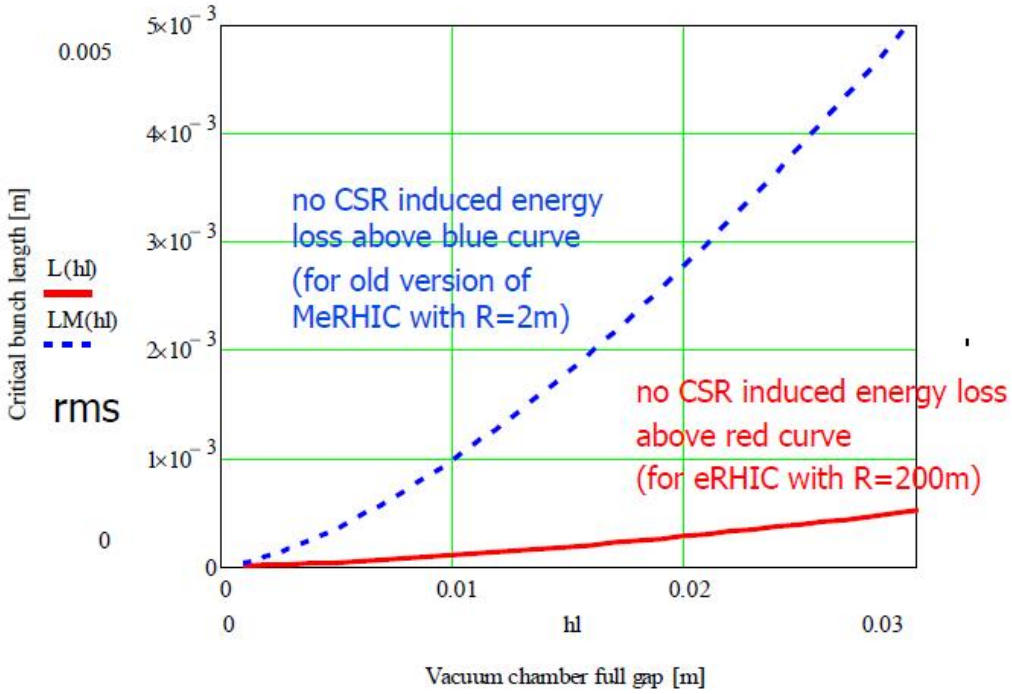

Resistive Wall

The results of the calculations for 6 recirculating pass eRHIC, assuming the Gaussian longitudinal distribution with 2 mm rms, and for different pipe materials are shown here:

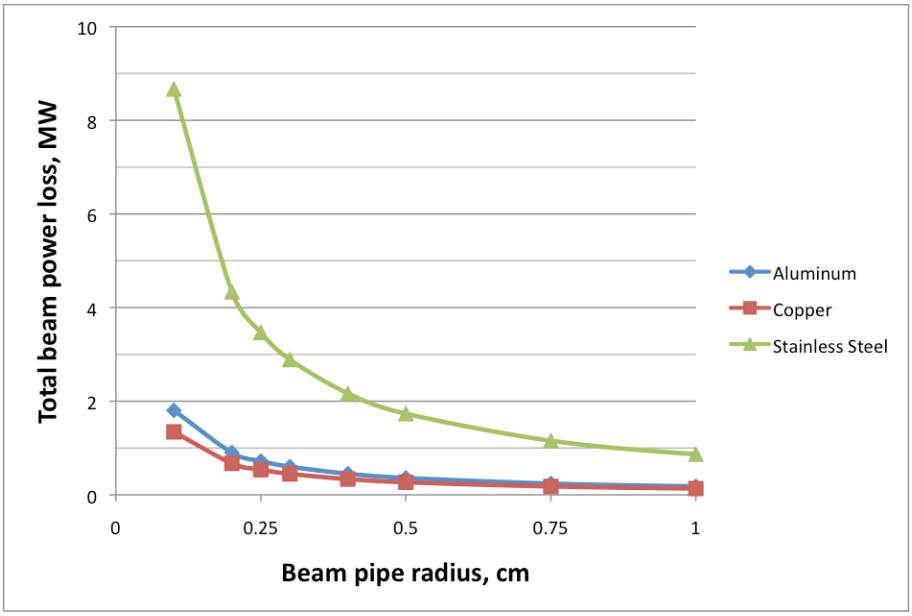

The calculation assumes round beam pipe (for elliptical beam pipe the maximum deviation from this calculation is at 10% level). Aluminum or copper-coated pipe has to be used for 0.25mm pipe radius.

The summary table (in bold are present nominal design parameters):

	Second Stage		First Stage	
Pipe material	**Aluminum**	Copper	**Aluminum**	Copper
rms bunch length, mm	**2**	2	**4**	4
Total beam power loss, MW	**0.72**	0.54	**0.21**	0.19
Beam power loss per m, W/m	**17.5**	13	**6.2/3.1**	4.6
Average particle energy loss per turn, MeV	**1.2**	0.9	**0.43/0.21**	0.32
Total induced energy spread, MeV	**14.4**	10.8	**4.36**	3.37

The parameters calculated in the table are for Gaussian longitudinal bunch profile. In the case of rectangular longitudinal distribution, with the same rms value, the energy loss ~30% higher and the induced energy spread ~60% higher.

Cavity Wakes

- The loss factor for the 704 MHz cavities of the eRHIC main linacs is shown here versus the rms bunch length, assuming Gaussian longitudinal profile:

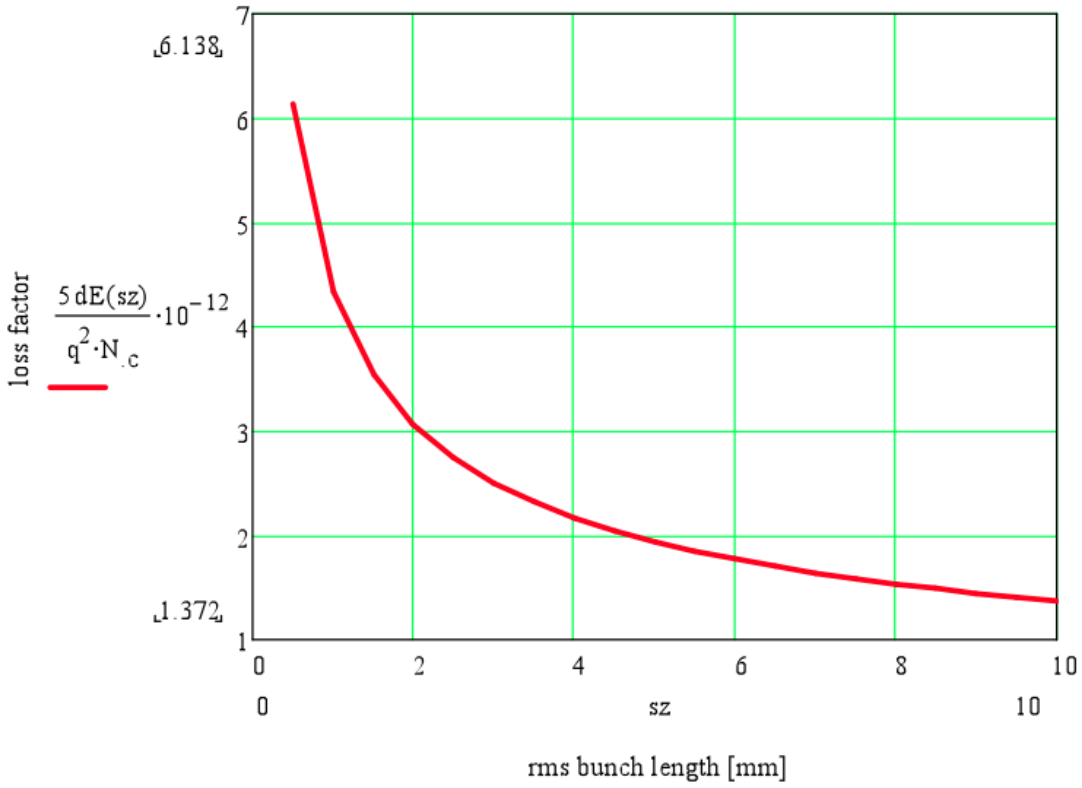

- The table below summarizes the energy loss and induced energy spread due to the beam interaction with the cavity wakes in the main linacs. This lost beam energy goes into the High-Order Modes of the cavities and has to be extracted from the cavity and accommodated in the dampers. The word "Total" in the table means the total effect over all 12 passes through the main ERLs (two linacs). The baseline design column shows the values calculated for the beam energy up to 20 GeV. Above 20 GeV the bunch charge is reduced, so are the energy loss and energy spread values.

	Second Stage (20 GeV)	**First stage (5 GeV)**
Bunch length, mm	2	4
Cavity loss factor, V/pC	3.0	2.45
Number of cavities per linac	120	24
Total power loss per cavity, kW	6.3	5.2
Total power loss, MW	1.5	0.25
Average energy loss per linac per pass, MeV	1.3	0.22
Total induced RMS energy spread, MeV	12.7	2

The parameters calculated in the table are for Gaussian longitudinal bunch profile. In the case of rectangular longitudinal distribution, with the same rms value, the energy loss is about the same.

Wall Roughness

[

Considered models

Several models ("inductive", "statistical", "resonator") used for calculating the wall roughness impedance and related beam energy loss and energy spread have been considered.

The main conclusions are:

- Models with identical bumps (height comparable to length) – give largest estimate of impedance. However, such models do not reflect correctly real wall roughness characteristics.
- The real roughness is typically characterized by the large aspect ratio of the characteristic size along the surface (correlation length) and the height of the bumps. Corresponding models give much smaller impedance.
- For short bunches (comparable or smaller than correlation length) one may need to worry about synchronous modes and energy loss even for smooth bunch distributions. More pronounced effect for sharp edge distributions. The effect becomes suppressed for large aspects ratios of wall roughness.

Energy loss and energy spread

For eRHIC:

- Approximation of “long bunch” is valid (Inductive wake).
- Contribution to energy spread becomes within specs for correlation length > 20 microns.
- Extruded aluminum should correspond to “very long” correlation length.
- We do not have to worry about energy loss ("long bunch limit" and large aspect ratio for roughness)

For following parameters:

- gap size of 5mm
- bunch length of 2mm rms
- extruded aluminum vacuum chamber with 1 μm (or less) roughness height and large correlation length
- **Energy loss is negligible effect.**
- **Energy spread is projected to be below 10 MeV for expected roughness aspect ratio of extruded aluminum.**

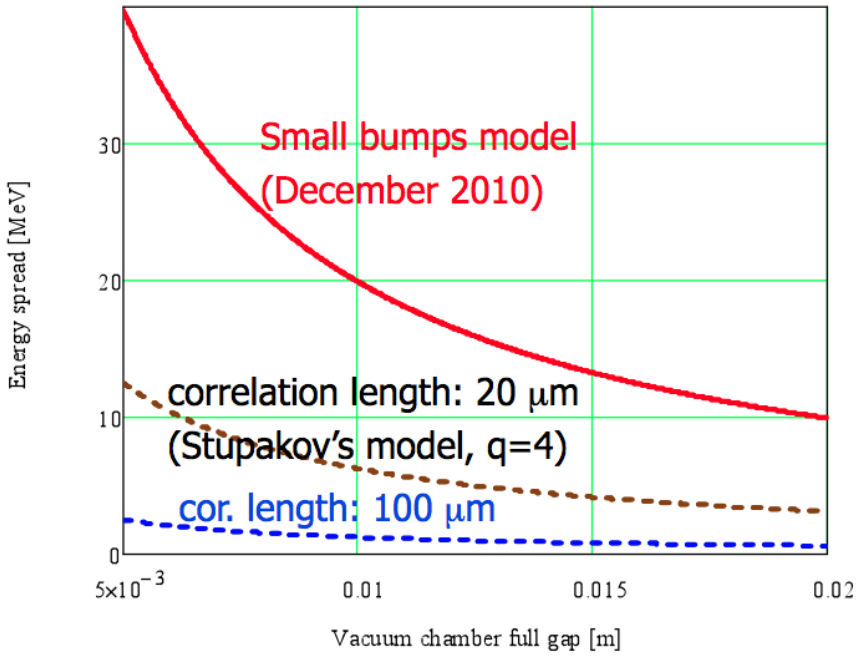

Parameters:

Roughness height 1 μm rms. Bunch length 2 mm rms

Total Energy Loss Budget

The table summarizes the energy losses for the baseline design for different beam energies. For 5 GeV energy the values shown for the first stage design (that is for shorter main linacs). The contributions from the effects of wall roughness and coherent synchrotron radiations were found to be negligible and not shown here.

Top beam energy		Synchrotron radiation	Resistive wall	Main linac cavity HOMs	All combined
30 GeV	Total power loss, MW	9.7	0.01	0.1	9.8
	Average electron energy loss per turn, MeV	0.2-277.2	0.2	0.5	up to 278
20 GeV	Total power loss, MW	7.6	0.7	1.5	9.8
	Average electron energy loss per turn, MeV	0.05-54.8	1.2	2.6	up to 58.6
5 Gev first stage	Total power loss, MW	0.03	0.21	0.25	0.5
	Average electron energy loss per turn, MeV	0.0002-0.24	0.43/0.21	0.43	up to 1.1

The plot shows the energy loss budget for the baseline design for different beam energies.

For 5 GeV energy the parameters are taken for the first stage design.

Energy Loss Compensation

In order to compensate for the energy losses we have considered the string of 2nd harmonic cavities placed on one or several recirculating passes in the location of IR12 straight section. The compensator makes full energy loss compensation, so that the energy of the decelerating beam coming into the pre-accelerator ERL is the same as the energy of the accelerating beam coming out of the pre-accelerator. The several variants of the compensator have been considered which differ by the number of recirculating passes put through the compensator. The compensator variants with smaller number of passes assumes the lower energy passes are excluded from the compensator. Let's note that even if the compensator put only on one recirculating pass the electron beam passes through the compensator two times: on the acceleration and deceleration loops. at the plots below the compensator variants are compared by the value of relative energy difference between accelerating and decelerating beam in the same recirculating arc. This energy difference comes due to the energy loss accumulated during the acceleration and deceleration process. First plot corresponds to the top beam energy of 30 GeV (with losses dominated by synchrotron radiation), and the second plot corresponds to the 5 GeV top energy with the domination of resistive wall and cavity wake energy losses.

We concluded that putting the 2nd harmonic compensator just on one recirculating pass is acceptable and preferable, since no additional spreader/combiner system needs to be installed. The variant to install the compensator just on the top energy pass can also be considered, with the advantage of using fundamental (704 MHz) cavities instead of 2nd harmonic one.

The table shows the required energy gain for the the compensator based on 2nd harmonic cavities.

The exact number of cavities used in the compensator depends on the achievable power input, which is discussed in SRF Energy Spread Compensator section

[

Top energy	Beam current, mA	Required energy gain per one pass, MeV		Required total power, MW
		six pass scheme	one pass scheme	
30 GeV	12.6	64.8	389.1	9.8
5 GeV, first stage	50.0	1.8	10.6	1.1

Effect on Spreaders/Combiners

With the energy losses and the energy compensation taken into the account the beam energy in the spreaders and combiners will change slightly, relative to the design values. The plots below shows the relative average energy deviation in the arms of the spreader located at the exit of 1st main ERL. The average energy means the average of accelerated and decelerated beam passing through the same spreader arm. First arm corresponds to the highest energy arm, while 6th arm presents lowest energy spreader arm. First plot shows the data for the variant of 2nd harmonic compensator placed just on one recirculating pass. The second plot corresponds to the compensator placed on all six recirculating passes.

The simple way to accommodate those energy variations is to provide the ability to shift longitudinally the dipole magnet position in spreader arms. **For instance, for the energy loss compensator put on one pass, the longitudinal position of the dipole magnet in the highest energy spreader arm should be adjusted by up to 12 cm, depending on the top beam energy.**

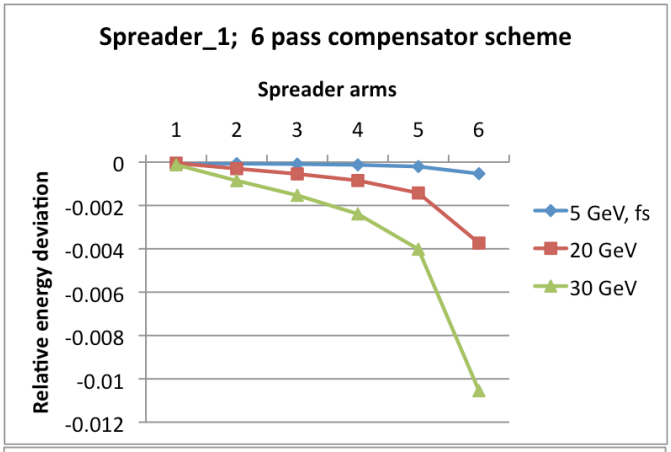

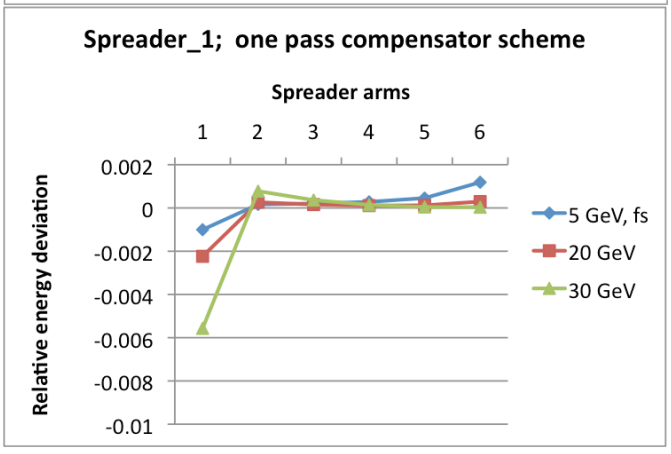

Transverse Emittance

- The transverse emittance has to be preserved during the acceleration. The major effect which may cause the emittance growth is the quantum character of the synchrotron radiation. The plot below shows the emittance increase at the acceleration up to 30 GeV. The resulting increase of 2.5 mm mrad is acceptable.

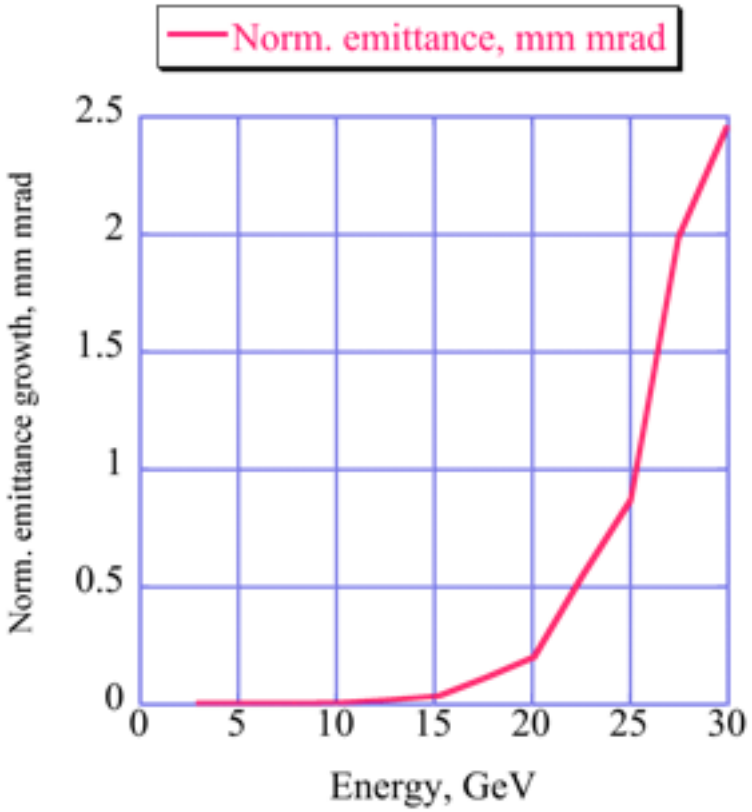

The increase of the transverse emittance and the formation of the beam halo due to the electron beam disruption at the collision points is considered in Beam Disruption section.

- Since the mean free path of the electrons is about 2.5E6 m (based on the pressure values of 1 nTorr) the emittance disruption due to multiple gas scattering is negligible.

Beam Disruption and Mismatching

Through beam-beam interaction with the opposing Proton/ion beam, the electron beam will be disrupted by the nonlinear beam-beam field and the distribution mismatches with the design optics due to the extra tune shift, which characterized by beam-beam parameter. Because of the large beam-beam parameter/disruption parameter in ERL based EIC, the effect for the electron beam is important to estimate the electron beam quality and the required aperture of the magnets and accelerators.

In eRHIC, the energy of both beam covers a large range. We studied the 2 cases followed by the methods in Ref[1]:

- Nominal parameter case: 325GeV proton beam with 20 GeV electron beam (Disruption parameter ~ 27)
- Large disruption case: 325GeV proton beam with 5GeV electron beam (Disruption parameter ~108)

325GeV proton with 20 GeV electron beam

In this case, the electron beam finish about 2π phase space rotation in the opposing proton bunch. The beam size of the electron beam reduces due to the focusing beam-beam force, which often referred as 'pinch effect'. The luminosity is enhanced to $cm^{-2}s^{-1}$.

Figure 1 shows the phase space distribution after the beam-beam interaction. Figure 2 shows the electron beam emittance and beam size evolution in the proton beam.

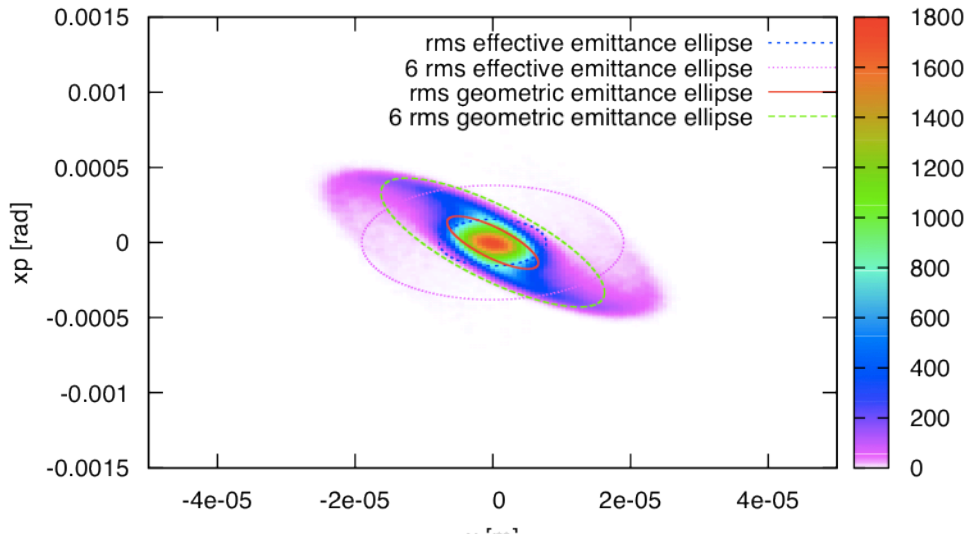

Figure 1: The phase space distribution of the 20 GeV electron beam

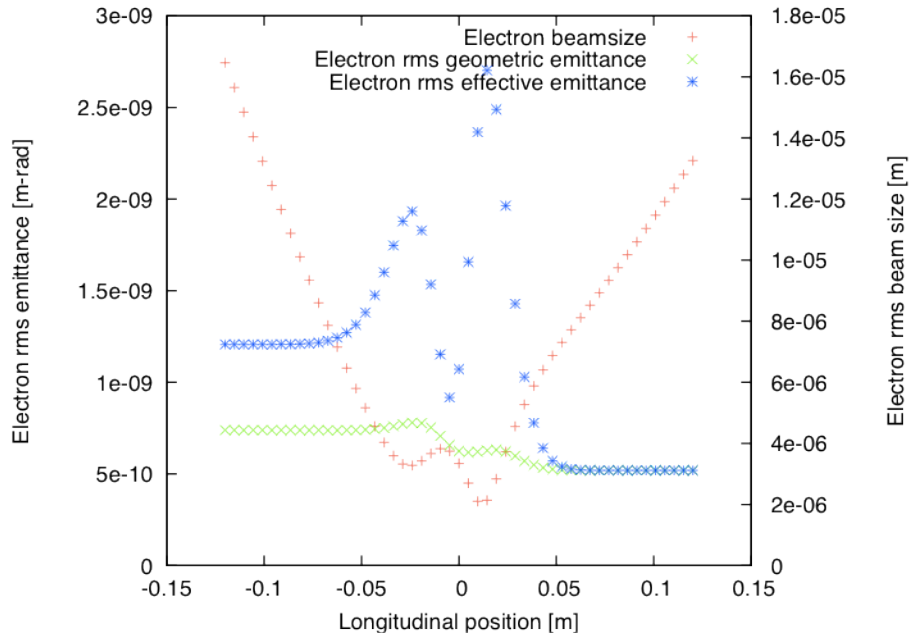

Figure 2: The beam parameter evolution of the 20 GeV electron beam

The long tail of the electron beam requires larger aperture in the decelerating stage than the accelerating stage. Figure 3 demonstrates the requirement of the aperture of the energy recovery pathes for various energies (20GeV, 1GeV and 0.2GeV) assuming the beta function is 10 meters.

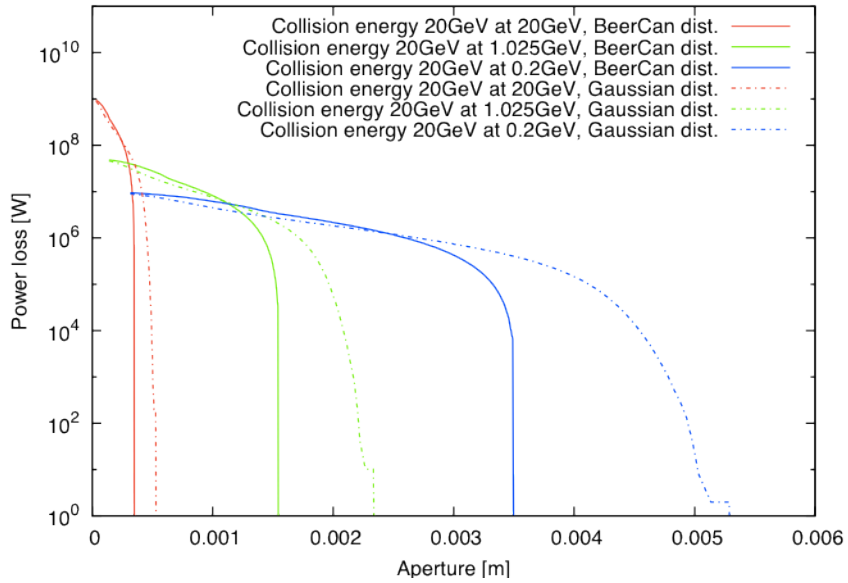

Figure 3: Beam power loss versus transverse aperture.

[

325GeV proton with 5 GeV electron beam

In this case, the electron beam finish about 4π phase space rotation in the opposing proton bunch. The beam size of the electron beam reduces due to the focusing beam-beam force,

which often referred as 'pinch effect'. The luminosity is enhanced to $cm^{-2}s^{-1}$.

Figure 4 shows the phase space distribution after the beam-beam interaction. Figure 5 shows the electron beam emittance and beam size evolution in the proton beam.

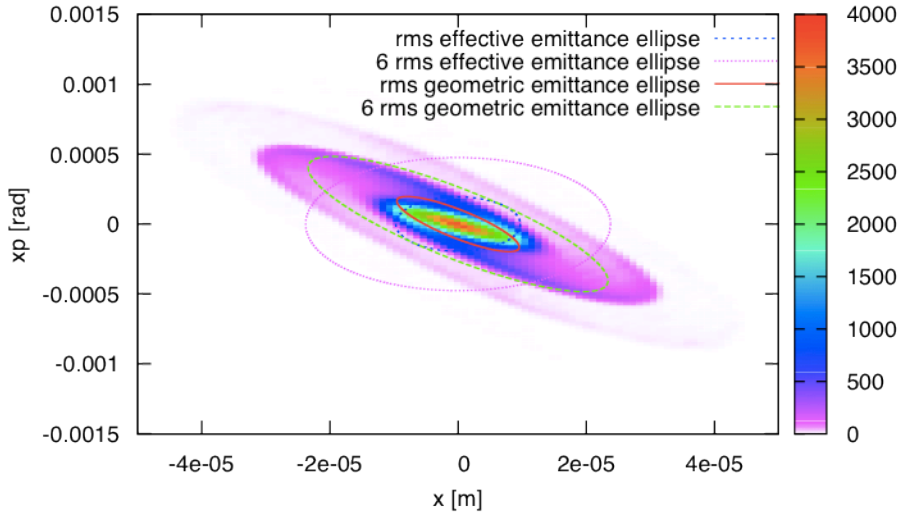

Figure 4: The phase space distribution of the 5 GeV electron beam

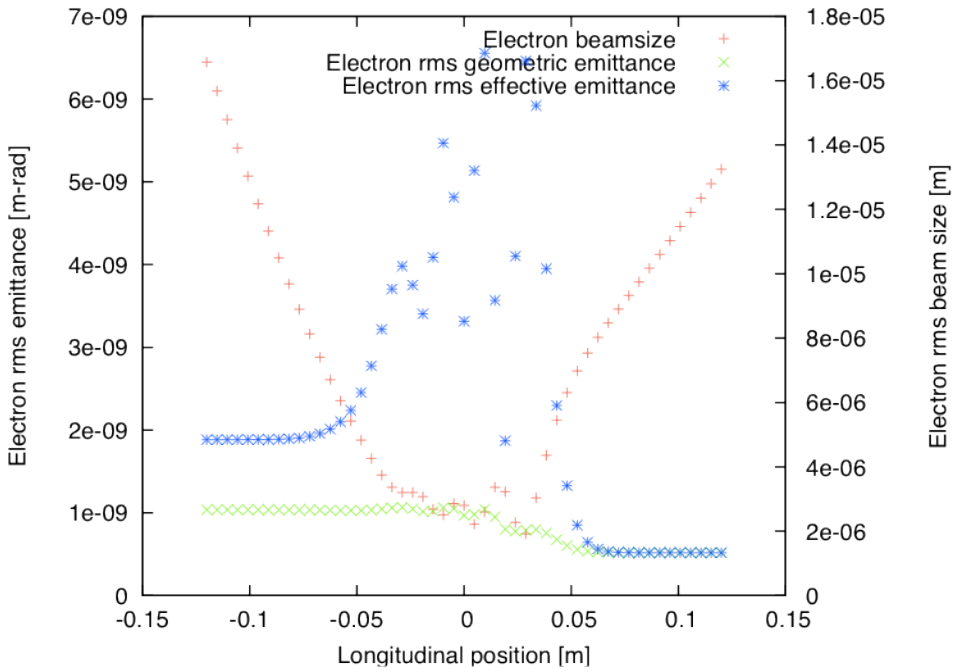

Figure 5: The beam parameter evolution of the 5 GeV electron beam

The long tail of the electron beam requires larger aperture in the decelerating stage than the accelerating stage. Figure 6 demonstrates the requirement of the aperture of the energy recovery pathes for various energies (5GeV, 0.4GeV and 0.2GeV) assuming the beta

function is 10 meters.

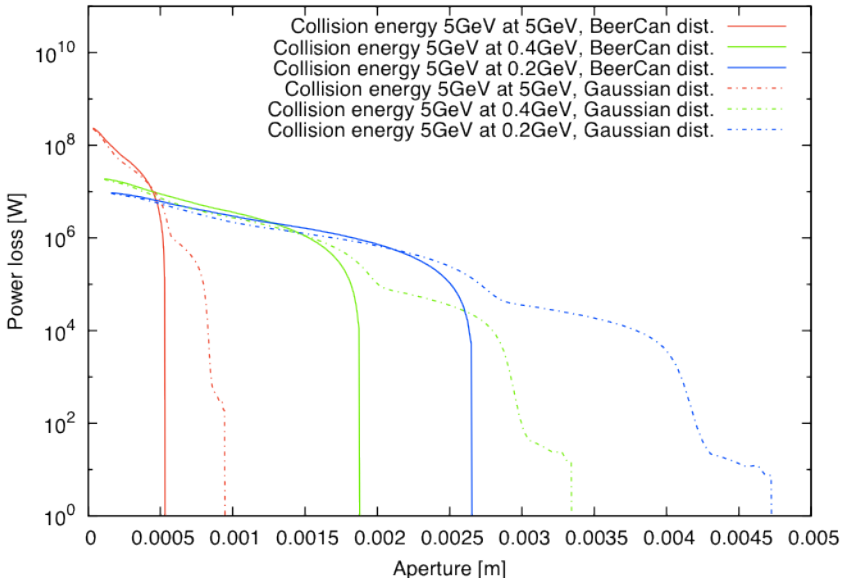

Figure 6: Beam power loss versus transverse aperture.

Requirement of the Aperture

Although we only plot the aperture for some discrete energies and fixed beta function, it is easy to scale the energy and beta functions at arbitrary locations. In both cases, for the lowest energy recovery pass and the pass to preinjector, the 5mm gap small magnet does not have sufficient aperture. Instead, minimum 10mm gap magnets are needed.

Ion Trapping in Linac

The residue molecules can be ionized by the high energy electron beam. And the ions may be accumulated at the beam pass, since the interaction between the electron beam and ions is focusing force. The situation must be avoided in linac since the ion accumulation will shield the acceleration field for the electron beam.

Model

The ion accumulation time can be calculated by $\tau i = 1 / (\sigma i n g c)$, where the cross section of ionization σi can be found by experimental results [1], and n_g is the particle density of the residue gas.

For a p-pass ERL, one ion at linac will interact with 2p electron bunch of different energies. The transfer matrix of its transverse phase space can be calculated from the linearized beam-beam force and drifting between bunches. And the stability of the ion can be determined from its matrix.

Results

For the realistic longitudinal beam pattern (Figure 1), Figure 2 shows the stability of different molecule species. In the figure, zero indicates the ion is not stable, and 1 indicates the ions will accumulate at the electron beam pass.

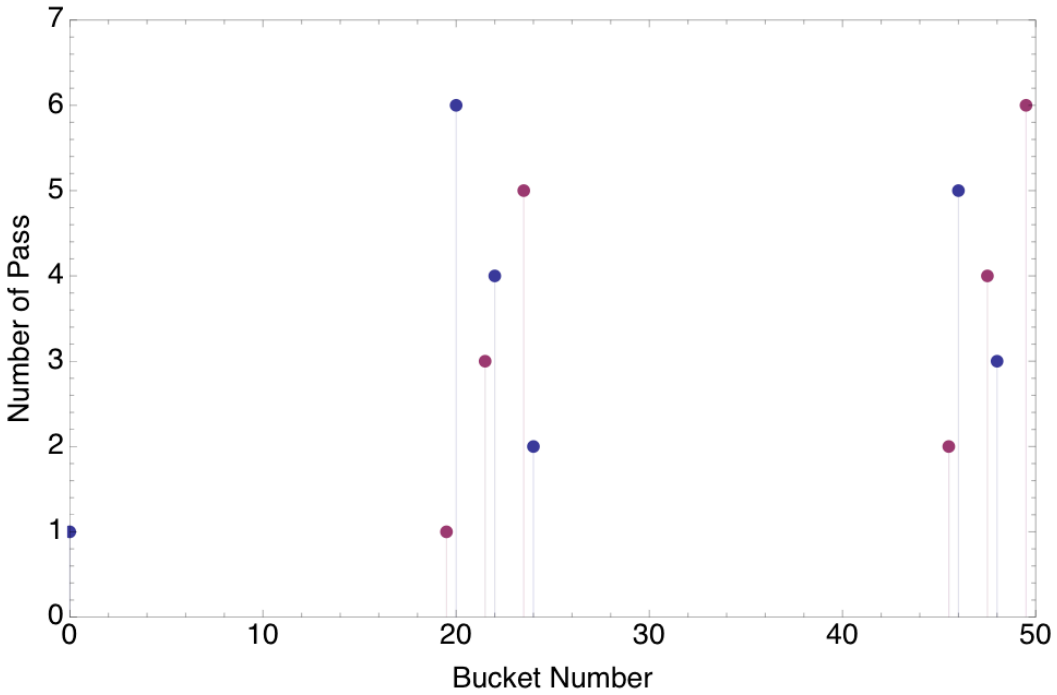

Figure 1: The electron beam pattern. There are 50 accelerating and 50 decelerating phases for 12 electron bunches of different energies to fill up.

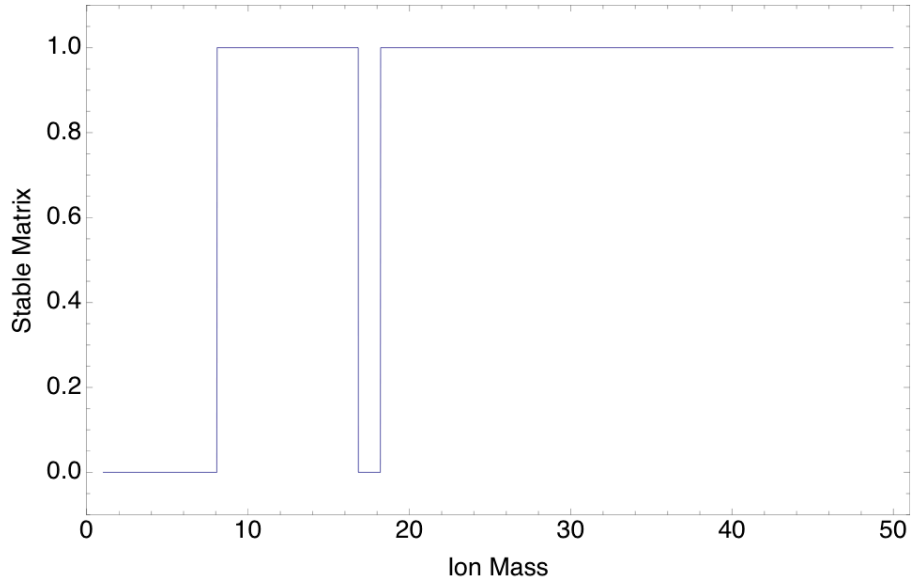

Figure 2: Ion stability for different ion species at the midpoint of the linac when the longitudinal electron bunch pattern is as shown in Figure 1.

In figure 2, we used the smallest beta function in the linac, therefore it is the best senario in the linac. In this case, small molecule with ion mass less than 8 won't accumulate. In superconducting linac, the only gas molecule left is Helium. Therefore no ion accumulation will occur at the lowest beta function region in linac.

However, the beta function at linac varies. With high energy approximation, the beta function in linac is same as in drift space, . In a 200 meter linac, the helium ion begins to accumulate at both end 40 meters (Figure 3). In those regions, the ion clearing electrodes are needed.

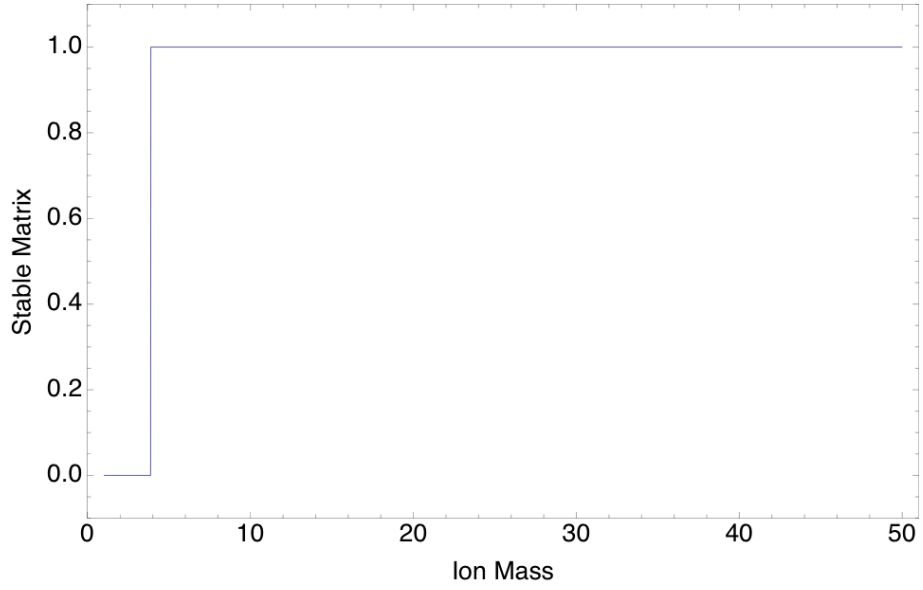

Figure 3: Ion stability for different ion species at s=40m from the linac ends.

Single Pass Beam Break Up

The growth of tail oscillation action in aluminum beam pipe with 5mm full gap during each revolution for 1mm initial offset:

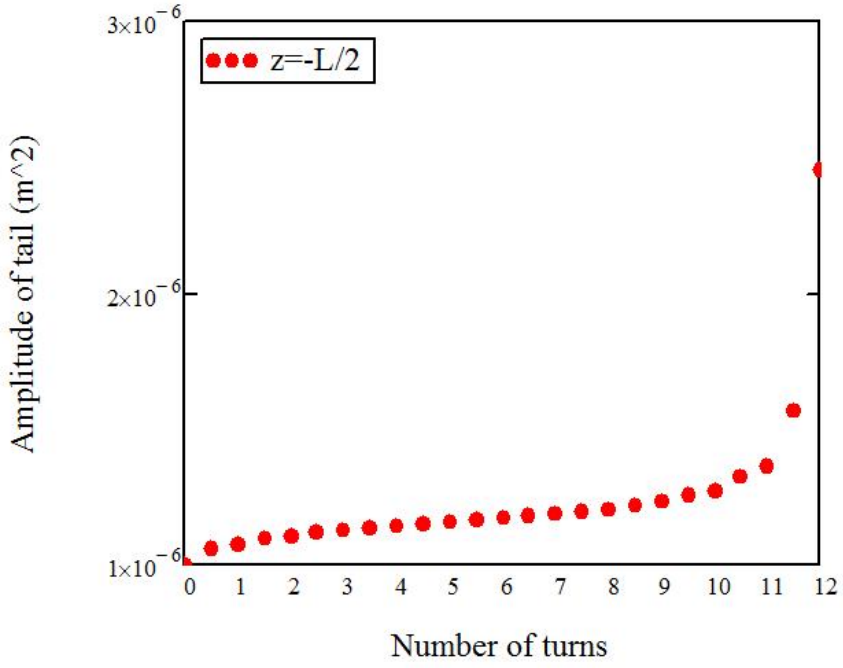

The displacement along electron bunch during the last revolution at various location:

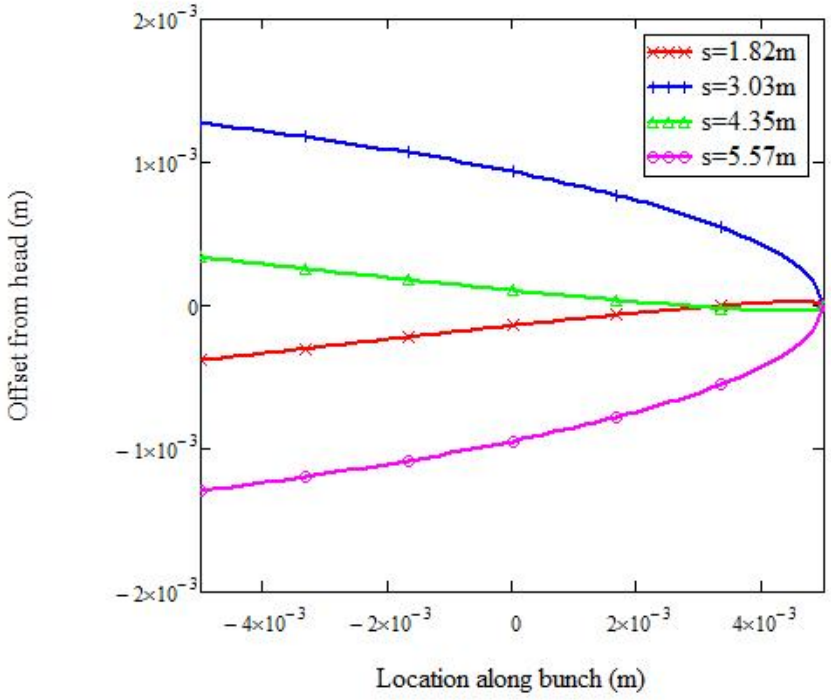

Beam Loss

Touschek Effect and IBS

When particles in a beam scatter within each other via Coulomb interaction one needs to consider both large and small angle scattering. The effect when particles can be lost as a result of a single collision event (large-angle scattering) is called Touschek effect. It happens due to transformation of small transverse momentum into large longitudinal momentum as a result of amplification by the Lorentz factor γ. When the scattering angles are small, random addition of such small scattering events leads to diffusion which primarily changes beam dimensions. Such a multiple Coulomb scattering was first applied to explain emittance growth in electron beams. Multiple Coulomb scattering was later generalized by Piwinski for proton machines without making any restrictions on the magnitude of beam temperatures, thus making it possible to transfer energy from the longitudinal into transverse via collisions. The generalized treatment of multiple small-angle Coulomb scattering was then renamed as the Intrabeam Scattering (IBS). The IBS theory was later extended by several authors to include variations of the betatron functions and momentum dispersion function along the lattice.

It is important to distiguish the Touschek effect and IBS because:

- The Touschek effect describes particle loss as a result of single collision. Here only transfer from transverse into longitudinal direction plays a role. It is important to consider this effect for ERL design to have an appropriate choice of collimation system.
- IBS results in changes of beam distribution and does not necessarily lead to a beam loss. Evaluation of IBS effect in ERL's, where beam distribution is non-Gaussian (especially in the longitudinal phase-space), requires special treatment and will be presented in the future.

For present eRHIC baseline, the Touschek effect appears to be significant and collimation system will be designed accordingly.

- This plot shows distribution of Touschek particles accumulated through all paths in ERL's on the way up and down. Parameters were taking for the case of 20GeV full energy:

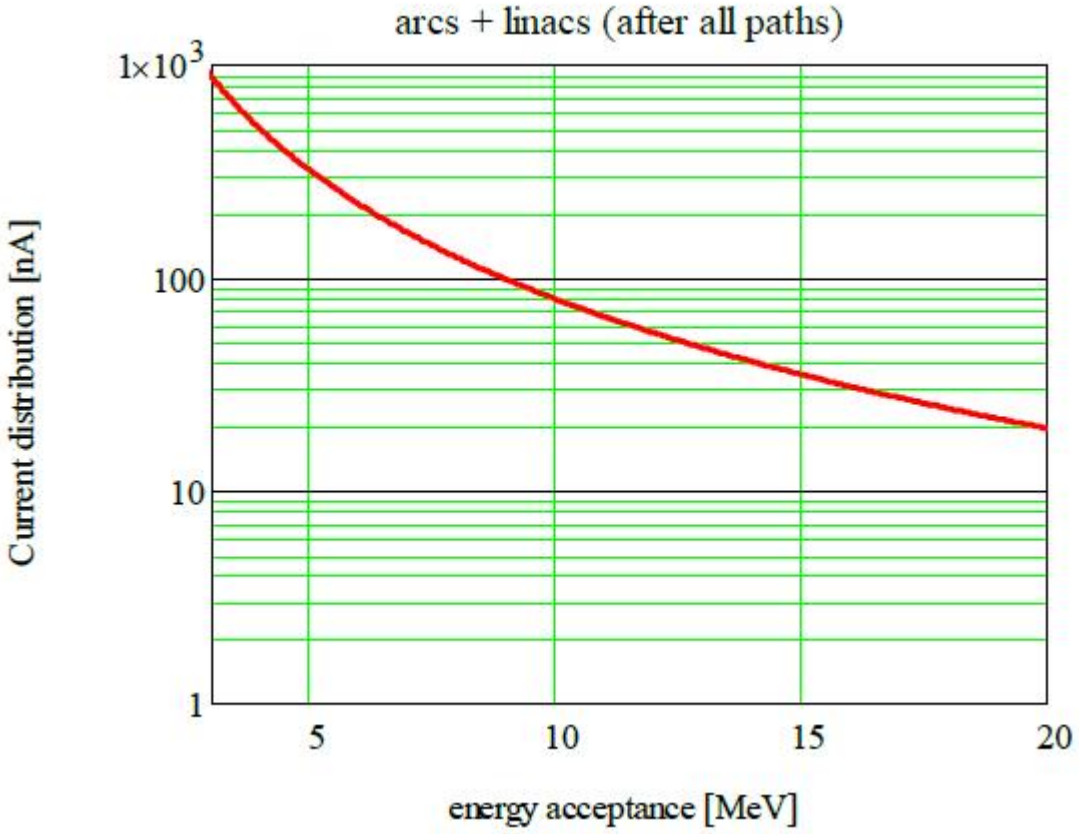

Beam-Gas Scattering

The calculation of the the beam-gas scattering processes have been done assuming the gas pressure of 1 nTorr in warm sections and 0.01 nTorr in cold section (linacs). The results show the low loss level, which can be easily accommodated.

Elastic Scattering

Depending on transverse aperture, beam loss due to elastic collision varies from 0.3 to 5.7 pA (1cm - 5cm) under the present model.

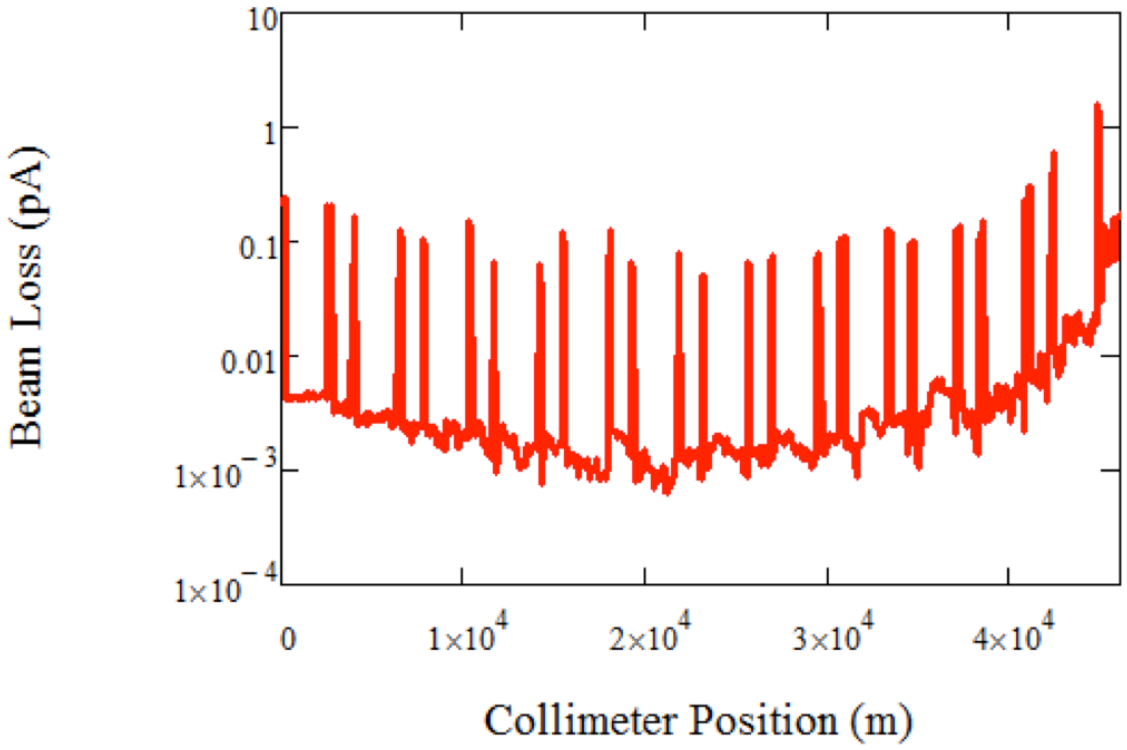

This plot shows the beam loss due to 2cm wide collimator sitting in different locations:

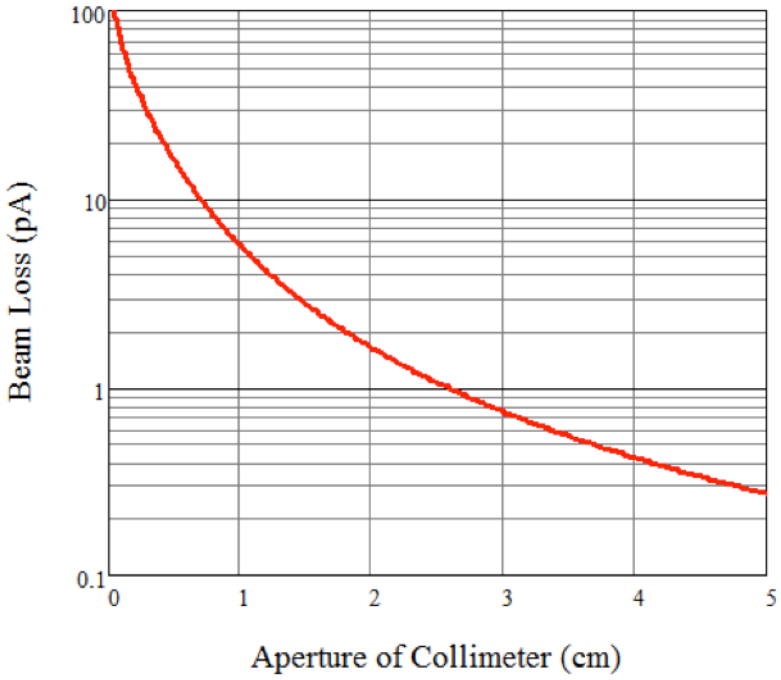

Bremsstrahlung Radiation

Depending on energy deviation aperture, beam loss due to bremsstrahlung varies from 3.9 to 5.3pA (10Mev/1Mev).

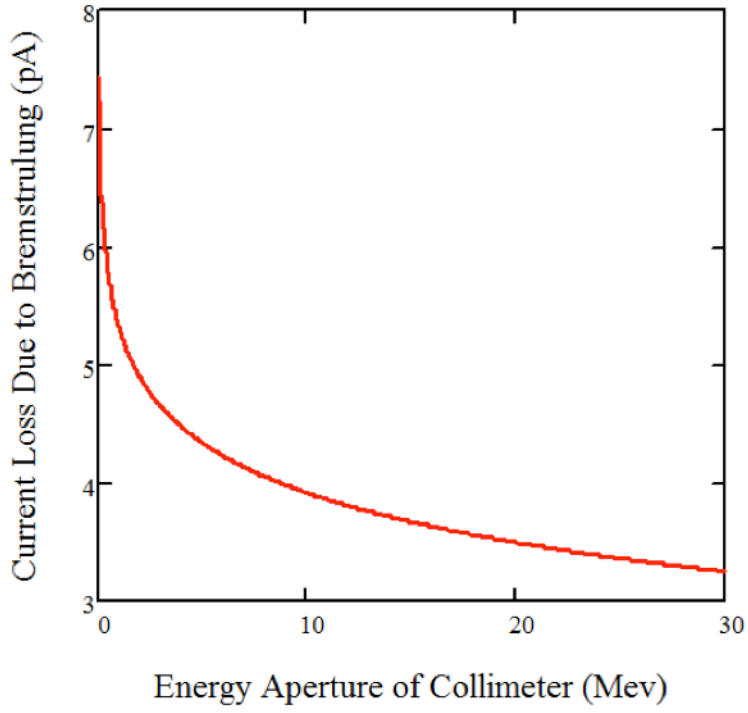

Beam Polarization

The eRHIC requirements calls for 70-80% electron polarization at the experimental detectors. Only the longitudinal polarization orientation is needed.

The following are main features of the electron polarization in eRHIC:

- High quality longitudinally polarized e-beam will be generated by DC guns with strained-layer super-lattice GaAs-photocathode
- Direction of polarization will be switched by changing helicity of laser photons in and arbitrary bunch-by-bunch pattern
- Longitudinal orientation of the spin into a collision point is arranged by arranging the multiple of 180-degrees spin rotation between the gun and the collision point by the proper beam energy selection
- Energy spread of electrons should be kept below 6 MeV to prevent the spin decoherence and have e-beam polarization in IP above 80%.

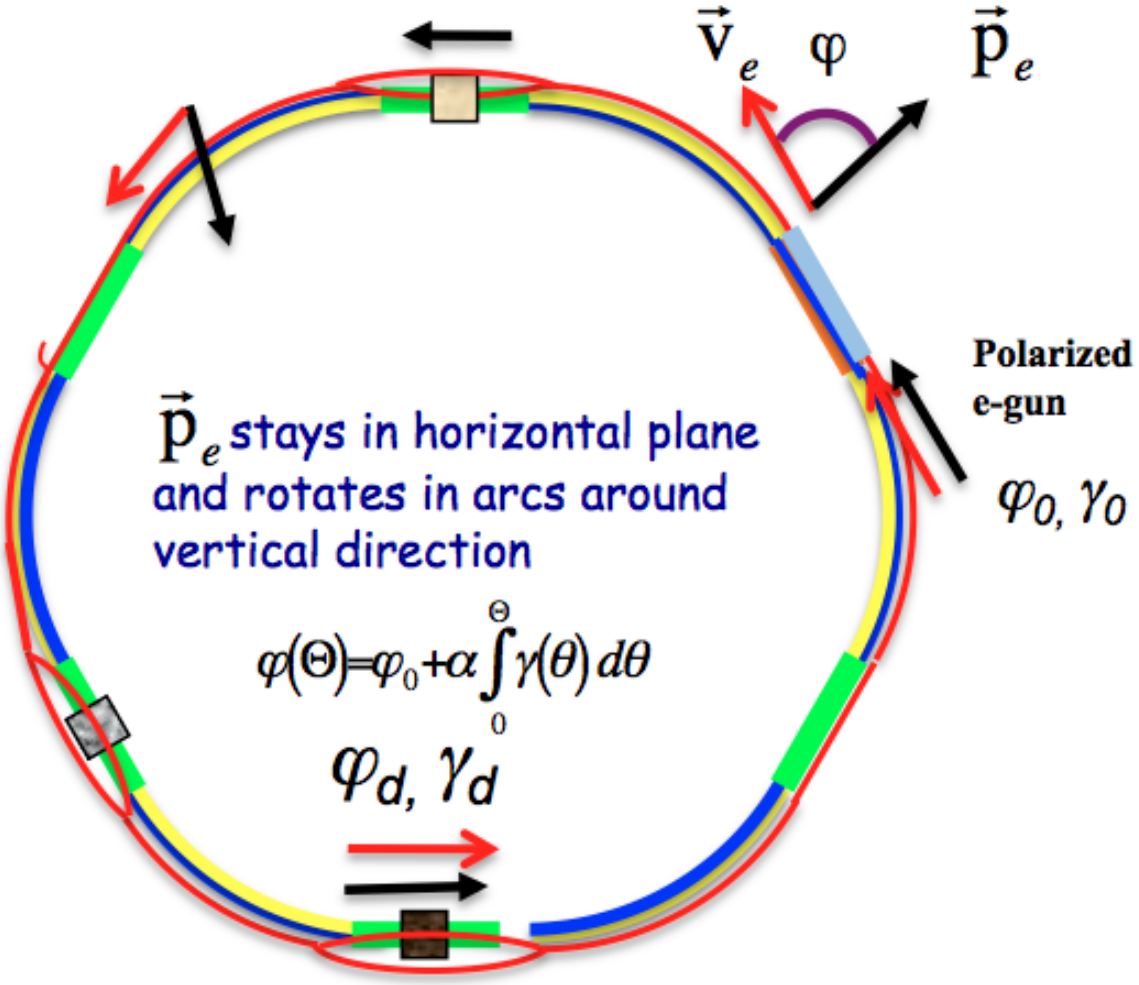

Longitudinal orientation in collision point

To provide the longitudinal spin direction in a collision point, the spin rotation

between the polarized gun and the collision point has to be a multiple of 180-degree. The selection of the top beam energy in steps of 72.2 MeV (0.24% of the top energy of 30 GeV) will provide for such condition.

Systems

Cryogenics

Linac Cold End Design

- Hybrid / Cold Compressor technology @ 1.6 to 2kHz
- Bath Cooled, Direct Pumping on superfluid bath
- SUPPLY/RETURN in middle of LINAC 60 + 60 cavities
- 8 inch diameter header
  vapor return / liquid supply header
  (2 F flow) (120 g/s each half)
- Liquid feed line to ends
  Supply feed for normal operation into 8 inch header
  Cooldown from far ends towards center
- Lower liquid communication line between cavities to aid cooldown
- 55 K Shield supply and return flow lines
  for thermal shield, support heat stationing
  FPC heat stationing

New cryogenic facilities

- Sub-atmospheric pumping& recovery system at IP2
- New 4.5K plant at IP2
- Sub-atmospheric pumping& recovery system at IP10
- Sub-atmospheric pumping& recovery system at IP12

System level diagrams

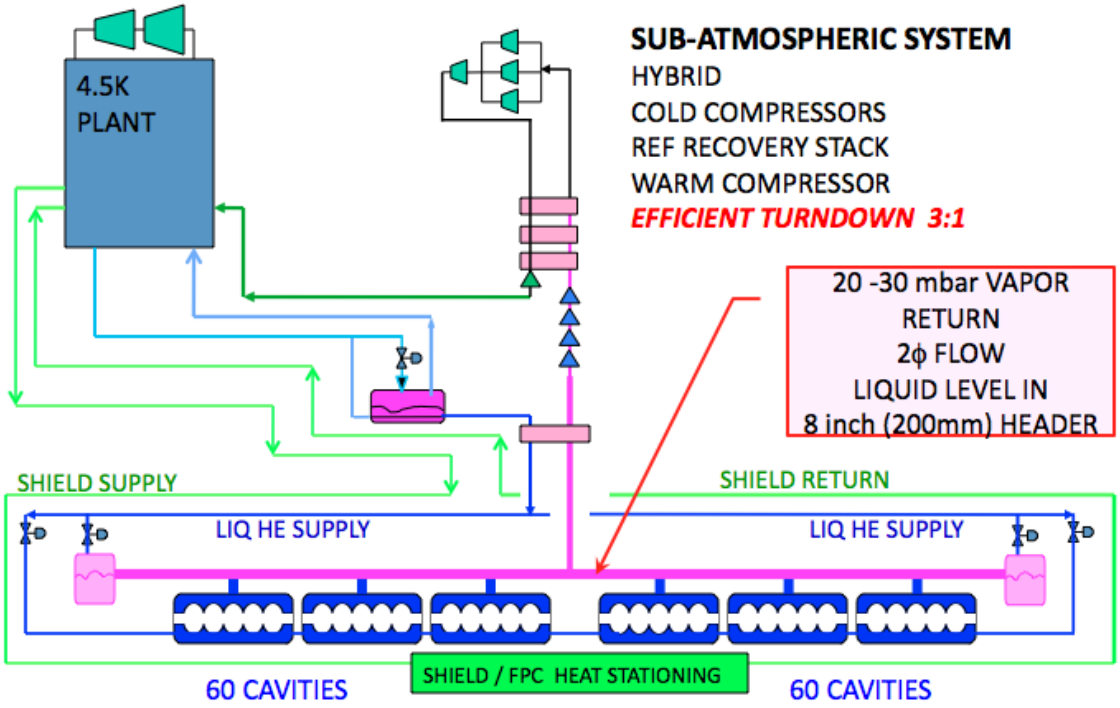

Figure 1: IP2 diagram.

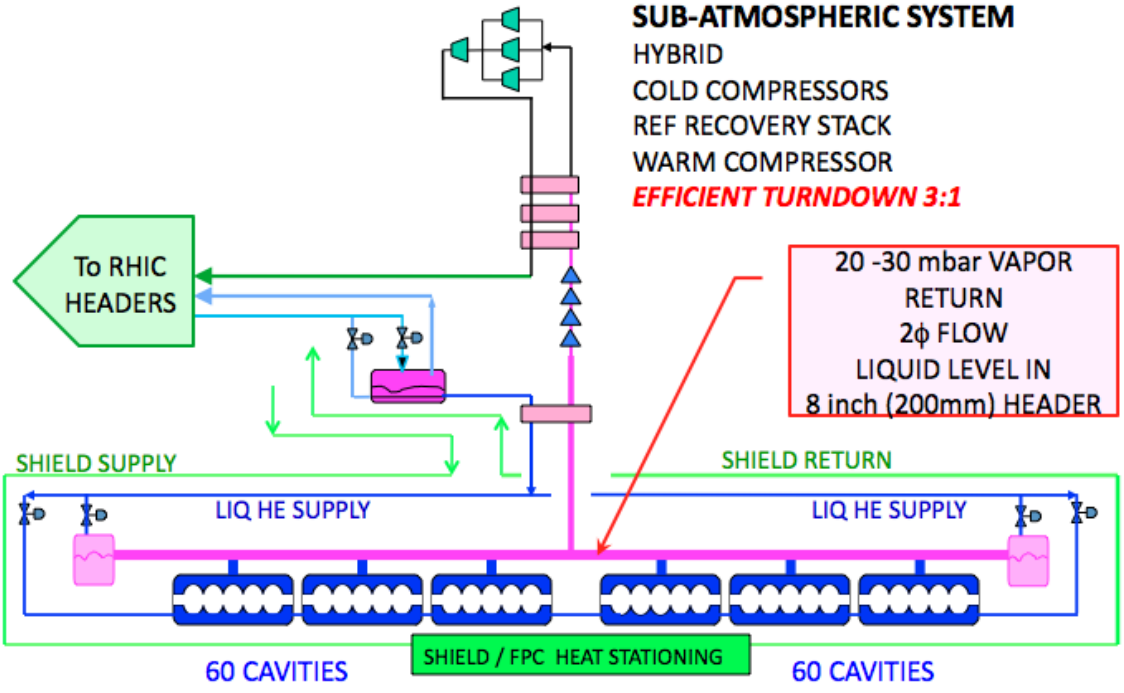

Figure 2: IP10 and IP12 diagram

Cryo loads

Main cryo loads:

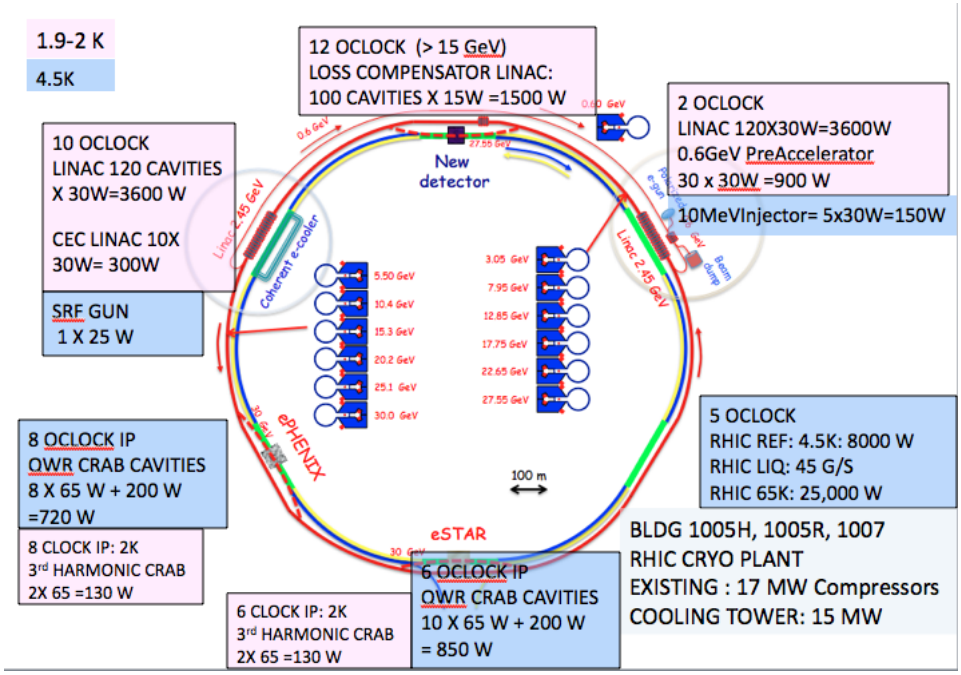

Electric Power

The distribution of required electric power for cryo systems:

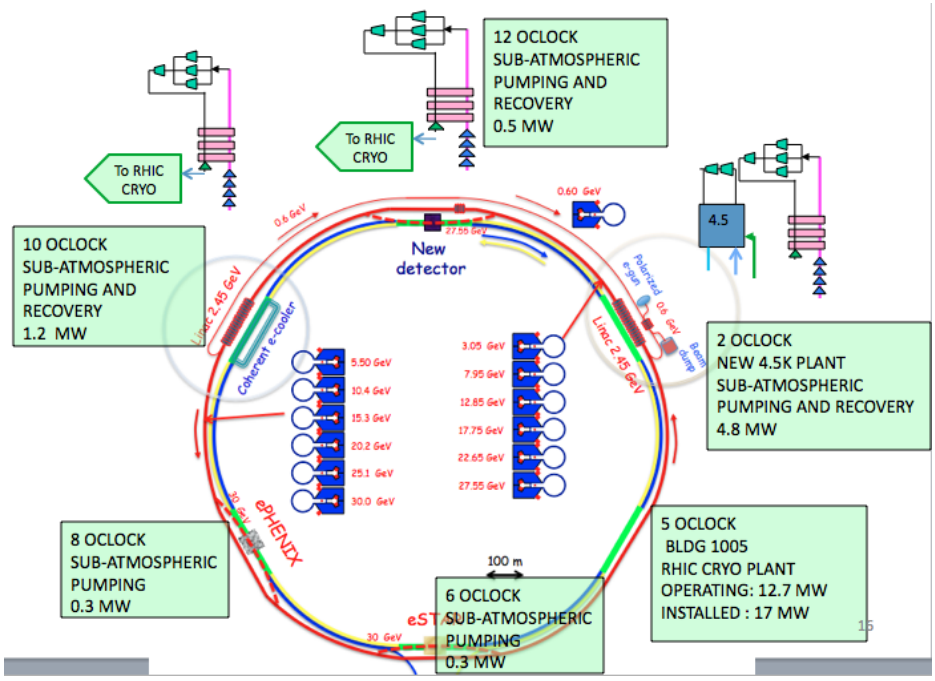

The required electric power comes to about 19.5 MW. (However, it includes also cooling the Yellow ring, which is not necessary.)

Magnets

Parameters of all magnets can be found in the attached Excel spreadsheet

With the large number of electron recirculating passes making the magnets as compact as possible is a major cost saving issue for eRHIC. Small magnet gap provides for low current, low power consumption magnets. The present design uses the magnets with the full gap of 8 mm in almost all recirculating passes, except the 3 low energy passes where the beam energy is less than 1/4 of the top energy and the magnet gap is 13 mm. The example of the vertically stacked magnets of recirculating arcs can be found in Design Concept Overview section.

Prototype Developments

The R&D effort of designing and prototyping efficient and inexpensive small-gap magnets and the corresponding vacuum chamber has been underway at BNL. The prototypes of the small gap dipoles and quadrupole have been built.

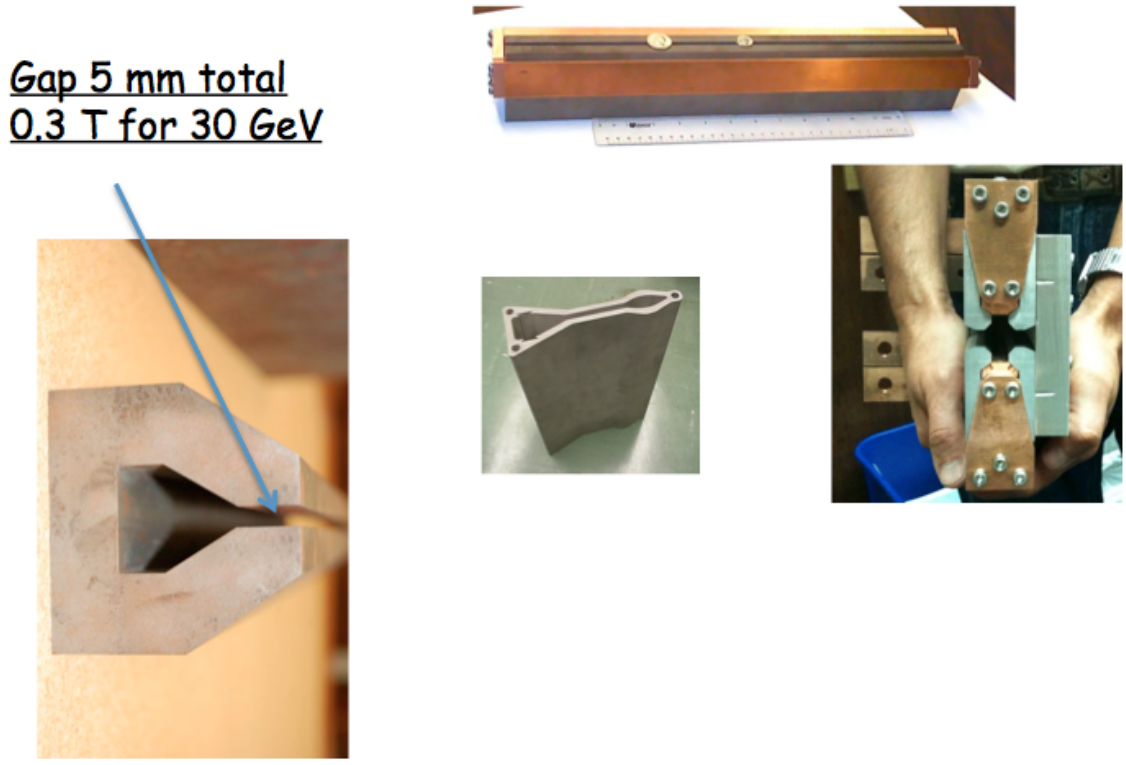

The magnetic measurements done with the dipole magnet prototypes (with the gap as small as 5 mm) showed a field close to satisfying eRHIC requirements:

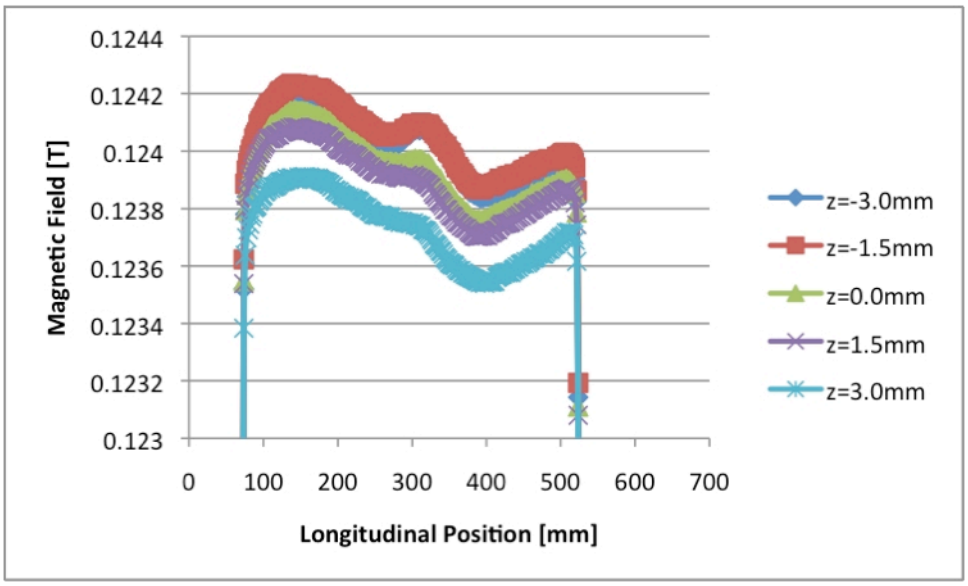

245Ampere, Transverse scan at center of the dipole

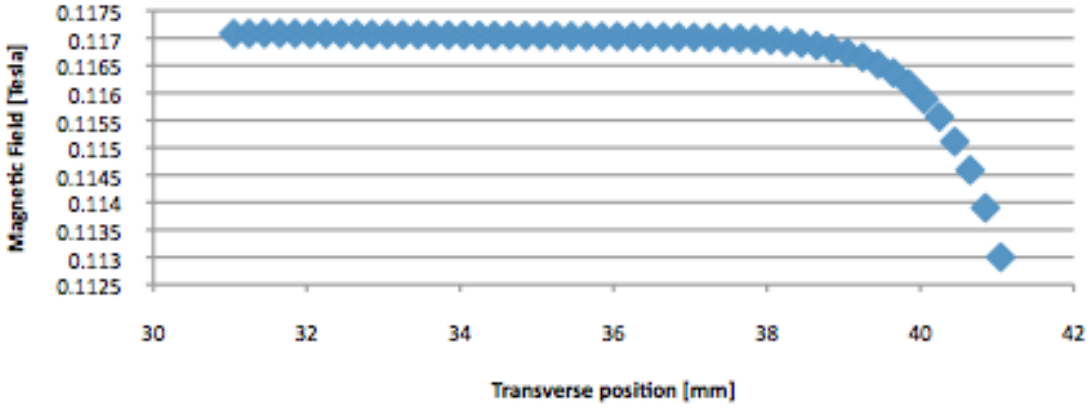

Fabrication technique used for quads did not satisfy our requirements but pawed the way to better fabrication technique.

Number of magnets

Sheet Name	Dipole	Quadrupole	Sheet Total

Main Arcs	2520	3240	5760
Bypasses	308	178	486
Combiner & Splitters	26	120	146
Delay Lines	240	60	300
Pre-Accel-to Linac	17	14	39
600 MeV Line	32	208	240
IP-8 Collision Line	43	48	91
Type Total	3186	3820	
Total Number Magnets :			7014

The table counts the total number of dipole and quadrupole magnets presented in the eRHIC electron lattice:

Magnet Correctors

In spreader/combiner, each element is assumed to have separate power supplies.

Dipole Correctors

There will be 2 horizontal and 2 vertical trim dipoles per each basic block in arc to correct the dipole field error and the quadrupole random errors.

Summary: Number of trim dipoles

	Horizontal	Vertical trims	Notes
Arcs	720	720	
Delay lines (4 OC)	24	24	12 dedicate corrector (horizontal) needed
Bypasses (6 & 8 OC)	88	44	
Straights (12 OC)	24	24	12 dedicate corrector (horizontal) needed
IR	16	20	
Spreader	48	48	24 dedicate corrector (horizontal) needed
600MeV line	80	80	
Total	992	960	48 dedicate corrector (horizontal) needed

The strength of the dipole correctors () are estimated to be 2% of the main dipoles, assuming:

- The error of dipole strength is better than 0.1%
- The alignment error of quadrupoles is better than 100 microns (rms).

The horizontal corrector in arcs can be achieved by adding corrector coil on the main

dipoles. The vertical corrector in arcs can be achieved by one of the following methods

- Adding separate magnets as corrector
- Implementing the surface coil on the vacuum chamber at the position of quadrupoles.

Currently, option #2 is the main approach for cost estimate. When there are no quadrupoles, option #1 will be used.

Quadrupole Correctors

There will be 2 trim bi-polar quadrupole per each basic block in arc and bypass lines to correct the quadruple field error, beta beating and betatron phase error.

Separately tuned quads in spreader/combiner, IR and delay lines are assumed.

Summary: Number of trim quads

	trim quads
Arcs	720
600MeV Line	40
Total	760

Beam Chamber and Vacuum System

- The vacuum chamber vertical gap (in the beam area) is 5 mm in all recirculating passes, except the 3 lower energy passes where it is 10 mm.
- Chamber material: extruded aluminum.

Arcs

In the arcs six beam lines are vertically stacked. The vertical distance between the center of the stacked beam lines is 10 cm.

Figure 1 shows all parameters of arc basic cell (lengths, gradients, fields, as well as the optical functions):

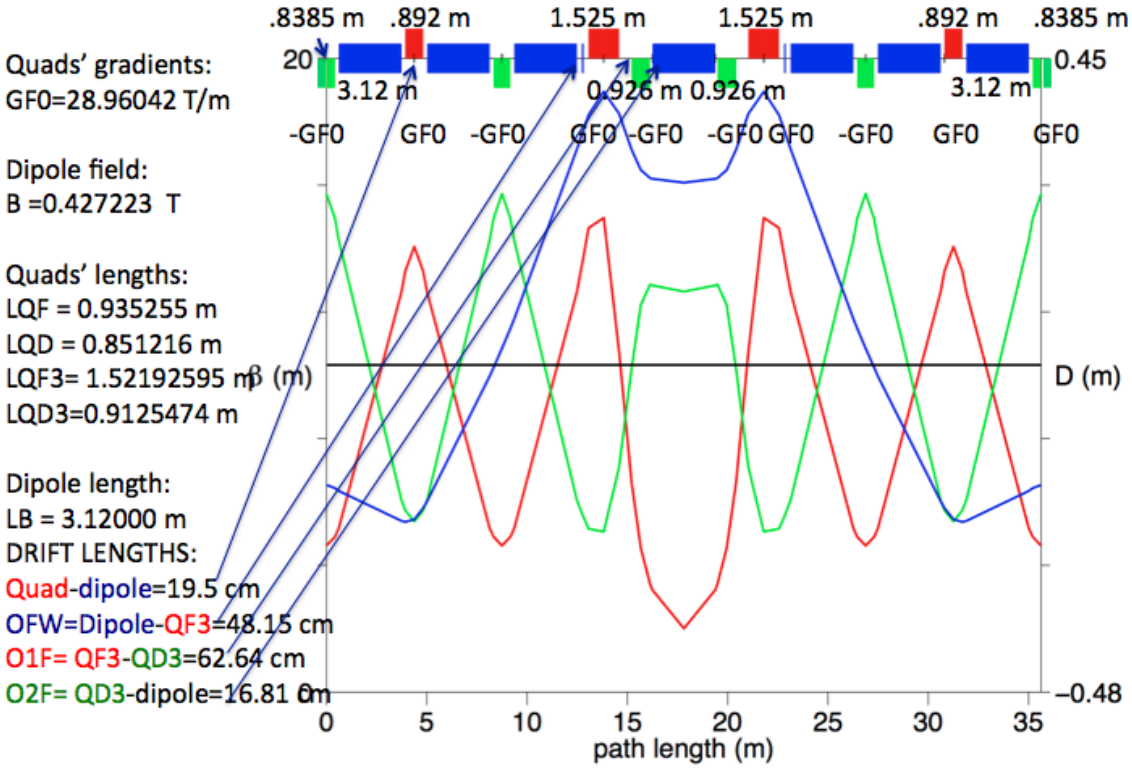

Figure 1: Basic cell parameters.

Figure 2 shows the geometry of the beam trajectory in the arc bending magnet D:

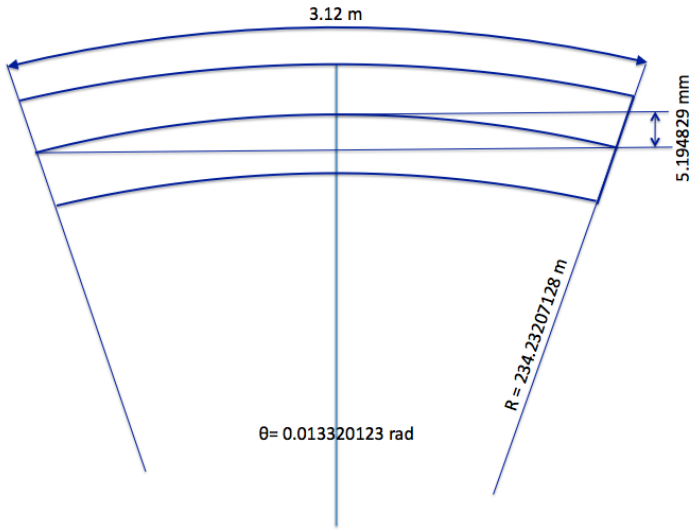

The layout of vacuum chamber in arcs is shown here:

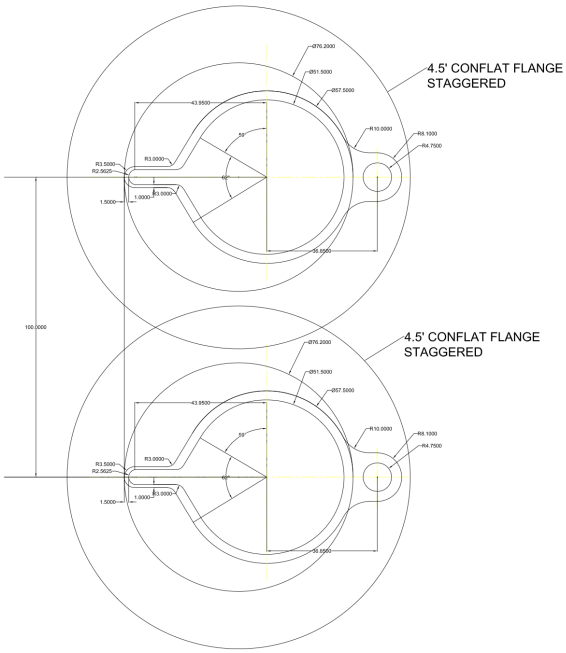

Beam Instrumentation

BPMs

Sensitivity: 0.1mA to 600mA in the linacs; 0.1mA to 100mA in the arcs, spreader/mergers and bypass lines. Single bunch capability: 0.1-5nC. In commissioning stage, a single bunch will be injected and travel throughout all the paths. It is expected the BPM can distinguish the testing bunch start to end.

Resolutions: in 5mm beam pipe <10microns; in 10mm beam pipe <20 microns

Number of BPMs

- 4 BPMs per basic cell (in the arcs)
- For long drift sections, each pass contains 3 BPMs at start, end and mid-point respectively
- In those bending area without quads (Bypasses, Delay lines), 2 bpms per pending out/back sections
- 2 BPMs for the triplets at each ends of drift.
- 4 double-plane BPMs per each pass in each Spreader / Combiner
- Around IR, 2 double-plane BPMs at Triplets and 3 double-plane BPMs at the bending magnet.
- 15 double-plane BPMs in the injection system.
- In the connection from pre-linac to main linac (Injector)

  For 30 GeV, the pre-linac has total length of 60 meters, totally 12 BPMs are assigned. The positions are shown in the schematic figure

  For 5 GeV, the pre-linac will be 10m and placed in the dump side. Therefore, both 10MeV and 100 MeV beam needs to be guided 50 meters. Assuming 4 fodo cells are used for both cases, totally 8 bpms are needed.

Summary: Number of BPMs

	2-plane BPM	Notes
Arcs	1440	

0.6 GeV Return Line	24	No final design yet
Pre-Linac To Main Linac	20	
Spreader/Combiner	144	The pass to injector is not counted
Bypasses	121	66+55 for IP 6 and 8 respectively
Straights+DelayLine	114	42 for the straight and 72 in delayline
IR	42	
Injector	15	No detail design yet, migrate from MeRHIC
Total	1920	

Analysis of Button Signal

Here is the estimated signals for the eRHIC BPMs. I used 3.5 nC charge with 4 ps r.m.s. bunch duration. The peal voltage is 300 V for 4 mm button in the vacuum chamber with 5 mm gap. Due to the high frequency content (see spectrum profile) after 180 feet of LMR240 (attenuation 4.4 dB = 1/e for 100 MHz) peak voltage drops below 1 V.

Shortening bunch will increase button voltage but unlikely the voltage at the cable end will change. The estimations were done for the on axis beam and moving beam off-axis 3 mm in each plane can increase the signal by factor 3. (I. Pinayev, 10/25/2011)

- Signal at button BPM output (pdf) (Igor Pinayev, 10/24/2011)
- Signal at end of 180ft lmr240 cable (pdf) (Igor Pinayev, 10/24/2011)
- Button BPM power spectrm (pdf) (Igor Pinayev, 10/24/2011)
-

Energy Feedback BPMs

Energy feedback BPMs are required to realize the accurate control of the path length and R56. Special cavities without significant power load may be required.

Accuracy goal for the pass length measurement

- Path length control <100 microns
- R56 control <10 microns

Beam Current Monitor

Summary: Number of Beam Current Monitor

	DCCT	ICT/FCT

Range	100 mA	0.1-10nC
Arcs	12	12
0.6 GeV return line	1	1
Injector	1	1
Beam dump	1	1
0.6 GeV injection line	1	1
Total	16	16

Beam Profile Monitor

Flags with CCD Camera:

- 1 per pass per Spreader/Merger
- 2 per linac
- 1 per Sextant in arc
- 2 for the long 0.6 GeV pass line.
- 10 for the injector

Synchrotron Radiation Ports:

- 2 for the injector
- 2 for the prelinac to linac path
- 2 per arc in energy recovery path
- 3 in 0.6 GeV pass

Halo Monitor

- 1 for the injector
- 1 for the pass from prelinac to main linac
- 1 per Sextant in arc
- 4 for the 0.6 GeV pass
- 1 per linac (before each linac)

Summary: Number of Beam Profile Monitors

	Flags with CCD Camera	SR Ports	Halo Monitor
Arcs	36	108	36
0.6 GeV return line	2	3	4

Delay lines	0	0	0
Linac	4	0	2
Spreader/Combiner	36	0	0
injector	10	2	2
Total	88	113	44

The SR critical energy can be found at various energies with current parameters (In arc, the bending radius is 208.55. In delay line the field for 30GeV is 0.35T):

SR critical energies (in KeV) at arc and delay lines if present in this energy:

Energy (GeV)	In arcs	In delay lines
30.0	287.2	209.5
27.55	222.4	162.2
25.1	168.2	122.7
22.65	123.6	90.2
20.2	87.7	63.9
17.75	59.5	43.4
15.3	38.1	27.8
12.85	22.6	16.5
10.4	12	8.7
7.95	5.34	3.9
5.5	1.8	1.3
3.05	0.3	0.2

Other beam profile monitors:

- Scrapers: for injector 4/8?
- Streak Camera: for IR and Crab Cavity, total 3;
- Emittance measurement (Pepperport with YAG screen)
- Bunch length measurement at injector.

Beam Loss Monitor

- Integrating cable monitor, total 62:
  - 1 per sextant, total 36;
  - 1 per bypass/delayline/IR line, total 24;
  - 1 for 0.6 GeV return line and injection line, total 2
- Local loss monitor: 1 per 10 meters in arc. Total: ~2400

Miscellaneous

- HOM pickup signal as BPM in linac
- Use one HOM pickup as BPM every 3 704 MHz cavity.
- Thermal Imaging Cameras: 7 locations, movable.

Abort System

- We need at least two dumps at 0.6 GeV and 30 GeV respectively in order to keep all three SRF linacs balanced while aborting beam. The layout is shown below:

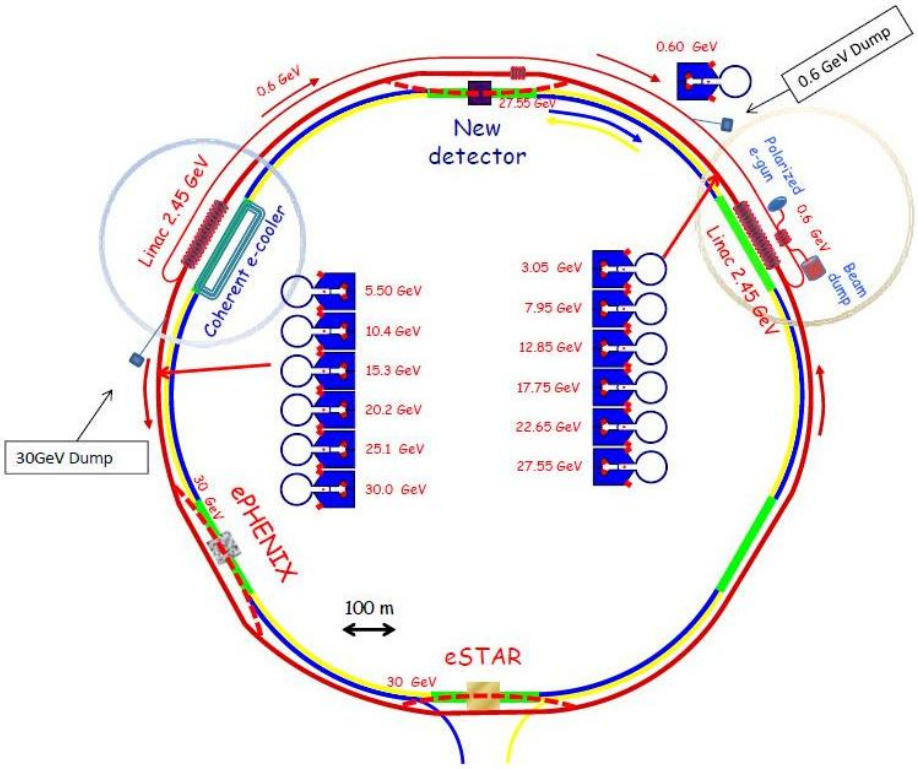

- Travelling with electron beam, the 12 passes can be represented by the following schematic block diagram:

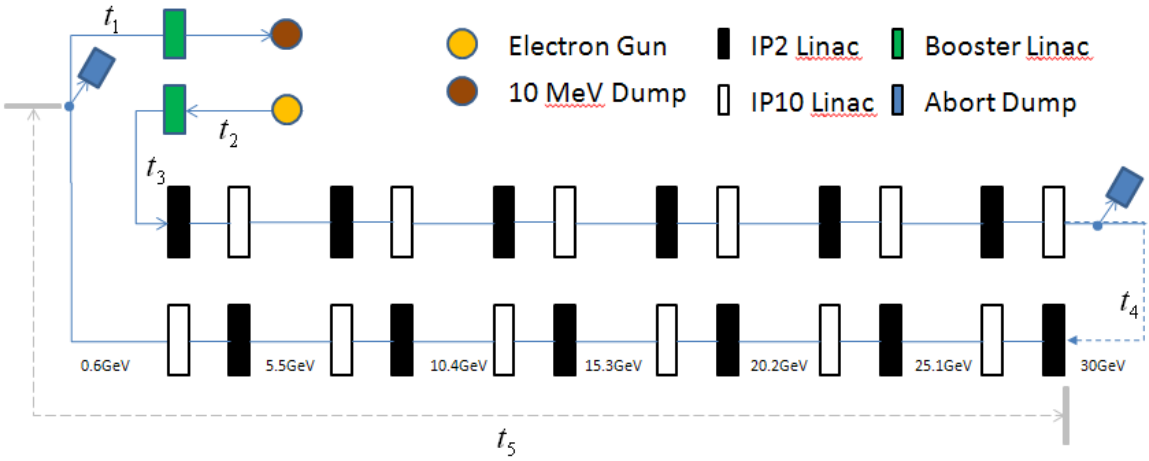

- Some relevant parameters required for the abort system are :

a) first stage with 5 GeV top energy

	Deposited Energy (KJ)	Deposited Peak Power* (MW)	RMS Size (mm)**	Energy spread	Pulse length (us)	Kick Angle	Kicker rise time (ns)	Full gap (mm)
0.1GeV Dump	0.38	4.9	0.97	50E-3	77		71	10
5 GeV Dump	19	246	0.45	3E-3	77		71	5

b) second stage with 20 GeV top energy

	Deposited Energy (KJ)	Deposited Peak Power* (MW)	RMS Size (mm)***	Energy spread	Pulse length (us)	Kick Angle	Kicker rise time (ns)	Full gap (mm)
0.4GeV Dump	1.5	20	0.77	50E-3	77		71	10
20GeV Dump	76	985	0.45	3E-3	77		71	5

c) third stage with 30 GeV top energy

	Deposited Energy (KJ)	Deposited Peak Power* (MW)	RMS Size (mm)	Energy spread	Pulse length (us)	Kick Angle	Kicker rise time (ns)	Full gap (mm)
0.6GeV Dump	0.58	7.6	0.77	50E-3	77		71	10
30GeV Dump	29	380	0.45	3E-3	77		71	5

.

- * The deposited peak power is calculated by averaging the power deposition over the 77us of beam abort. Assuming 0.2mm RMS bunch length, the peak power averaged over the RMS bunch length, i.e. from -0.2mm to 0.2mm, is about a factor of 3600 larger than the numbers shown in the tables.
- Beta function is assumed to be 300m at top energy dump (around splitter) and 10m at low energy dump (The more precise value should be determined from the returning path lattice design.).
- Due to beam-beam disruption, the electron beam emittance is assumed to increase from 0.68nm to 1.9 nm after collision for the 5GeV stage and to 1.2 nm for the 20 GeV and 30 GeV top energy stages.

- The kick angle of abort kickers are determined by the geometry, i.e. the space available in the beam line for the abort system. The relation among required field strenth, total required beamline space and kicker length is shown in the

following diagram:

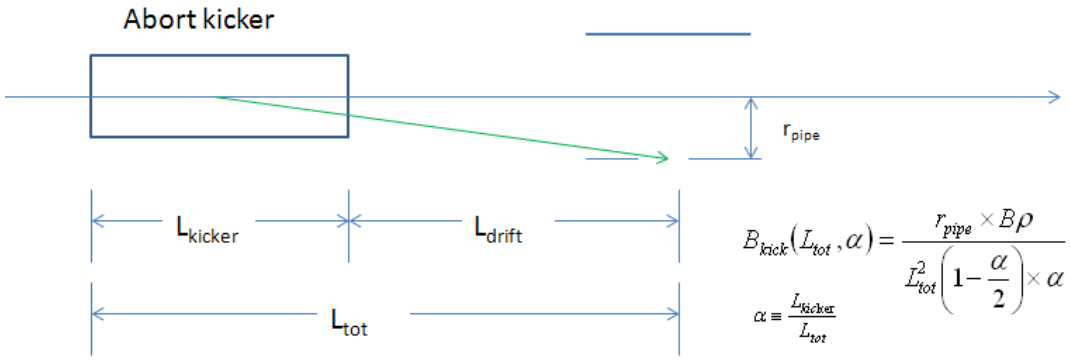

- The following plots show the required field strength as a function of required beamline space for various kicker length to total length ratio(i.e. α in previous diagram.). The full gap of beam pipe is assumed to be 5mm in the plots.

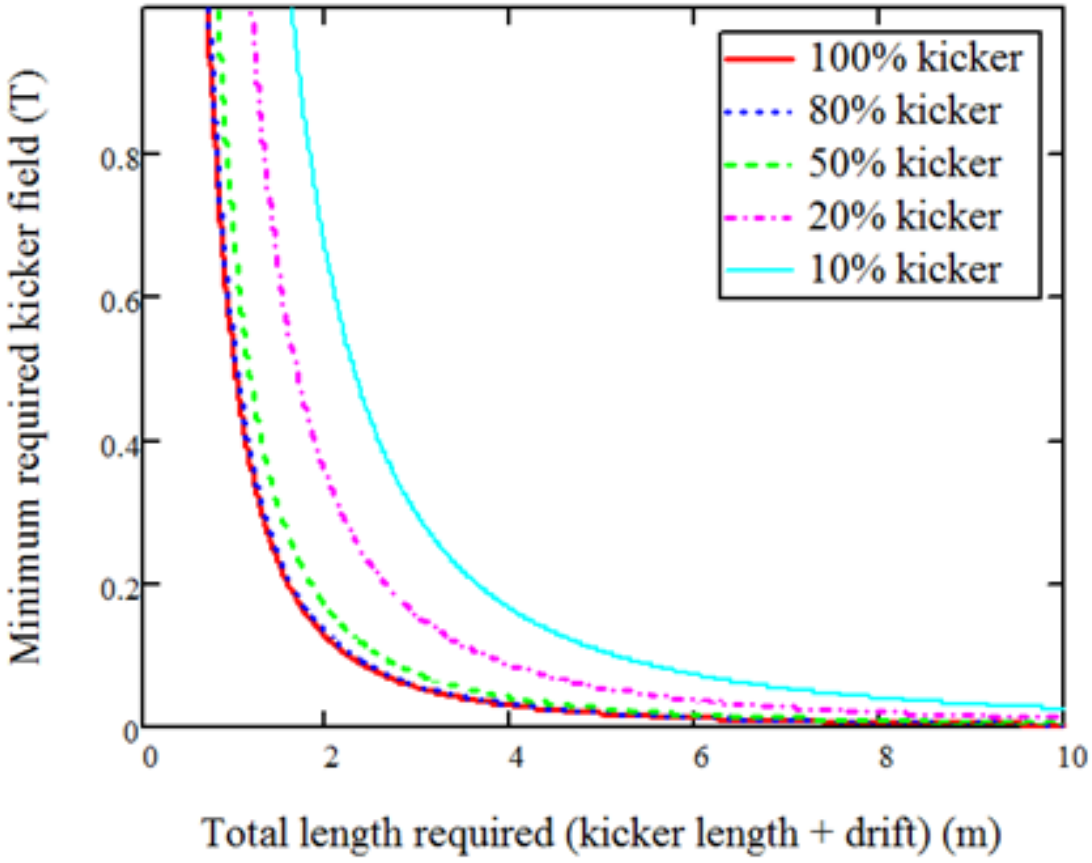

- The following tables show a few numerical examples of beam-kicking schemes, which could be used as a starting point of the abort kicker design.

L_{total} (m)	L_{kicker} (m)	L_{drift} (m)	$\Theta_{minimal}$ (mrad)	$B_{minimal}$ (T)
3	1.5	1.5	1.1	0.074
3	0.5	2.5	0.9	0.182
2	1	1	1.7	0.167
2	0.5	1.5	1.4	0.286

Note: the protection system should consider the protection from the potential damage by the synchrotron radiation (for instance, the tolerances on the beam orbit).

3 Ion Beam

Beam Parameters and Upgrades Overview

Overview

eRHIC will use all present capabilities of RHIC accelerator complex, which have been operating with heavy ions (up to 100 GeV Au ions) as well as with polarized protons (up to 250 GeV). However, in order to reach highest possible luminosities of electron-hadron collisions and extend the center-of-mass energy range, several modifications would be done in RHIC:

- Electron-hadron interaction region, which is not compatible with present RHIC interaction region (see Interaction Region chapter)
- Coherent Electron Cooling system to achieve small longitudinal and transverse emittances of hadrons
- Increased bunch repetition rate: 14.1 MHz (up from present 9.4 MHz)
- Increased highest energy of hadrons. Up to 325 GeV for protons, and up to 130 GeV/u for Au ions
- Added capability of polarized He^3 beam
- Added 704 MHz RF system (6 MV voltage), to provide required momentum spread (against microwave instability).
- Copper coating of the hadron beam pipe to reduce heat load due to resistive wall beam pipe heating
- Added transverse bunch feedback system

Beam Parameters

Beam parameter ranges for proton beam:

Proton for polarized e-p	max	Energy, GeV	min	Energy, Gev
Bunch intensity, 10^{11}	2	$E_p \geq 250$	0.08	$E_p=50$
Bunch charge, nC	32	$E_p \geq 250$	1.3	$E_p=50$
Beam current, mA	416	$E_p \geq 250$	17	$E_p=50$
Rms normalized emittance, 1e-6 m	0.18		0.18	
Rms emittance, 1e-9 m	3.4	$E_p=50$	0.52	$E_p=325$
Beam-beam parameter	0.015	$E_e \leq 20$	0.003	$E_e=30$
Beam size at IP, mum	13	$E_p=50$	5.1	$E_p=325$
Angular spread at IP, murad	260	$E_p=50$	102	$E_p=325$
rms bunch length, cm	8.3	$E_p \leq 250$	4.9	$E_p=325$
Peak current, A	78	$E_p=325$	1.8	$E_p=50$

Coherent Electron Cooling

The benefits of using the coherent electron cooling (CeC) include:

- increasing the peak luminosity by reducing β* from 25 cm down to 5 cm (*due to longitudinal CeC*)
- keeping the average luminosity from decreasing by counteracting the Intra-Beam Scattering diffusion (*due to both longitudinal and transverse CeC*).
- reducing the requirement on the polarized beam current down to 50 mA (*due to transverse CeC*)

According to the analytical calculations at eRHIC it would take about 12min with CeC to reach stationary proton beam values of the transverse emittance and momentum spread:

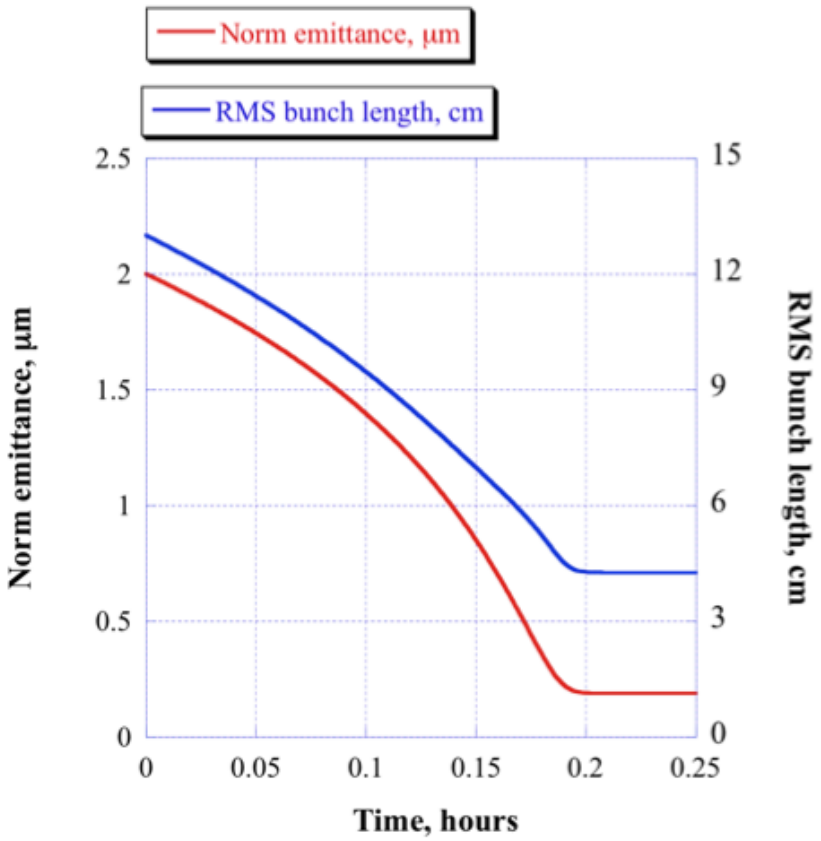

CeC proof-of-principle experiment is planned on RHIC at 2014-2015. More information concerning R&D on coherent electron cooling can be found at http://www.bnl.gov/cad/ecooling/CoherentEcooling.asp

Beam Dynamics

Coherent Instabilities

The instabilities studies have been done using the TRANFT code simulations and the present best knowledge of the RHIC impedances.

Longitudinal Microwave Instability

- The threshold for longitudinal microwave instability from the simulations is $\sigma_p > 2.2 \times 10^{-4}$, which agree with Keil-Schnell criteria within 10%.
- For 197 MHz rf cavity, in order to avoid longitudinal microwave instability, the rf voltage should be larger than 19MV.

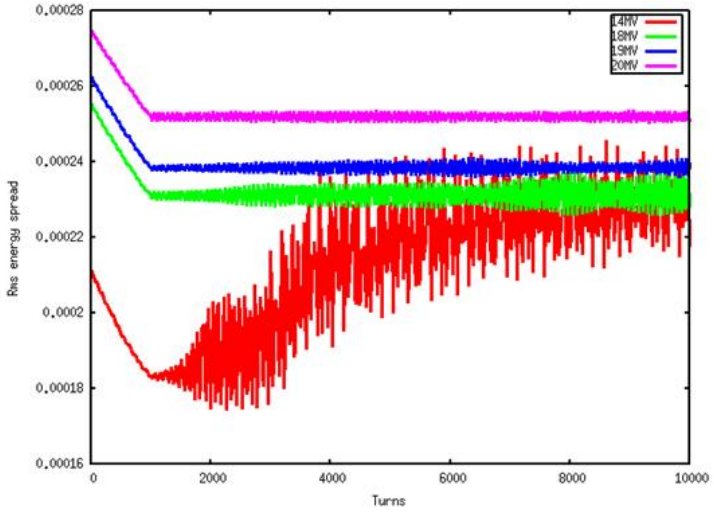

- For 704 MHz rf cavity, in order to avoid longitudinal microwave instability, the rf voltage should be larger than 6MV.

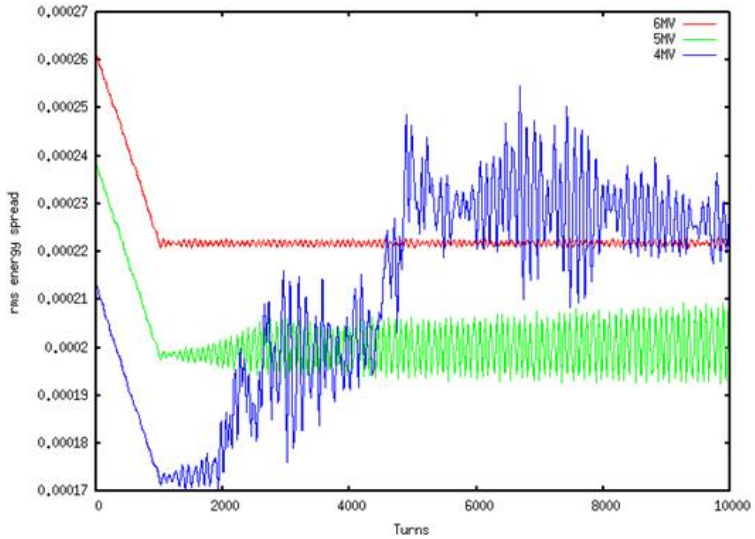

Transverse Coupled Bunch Instability

- Transverse coupled bunch instability is observed from simulation for evenly distributed 166 bunches with 2e11 protons per bunch.

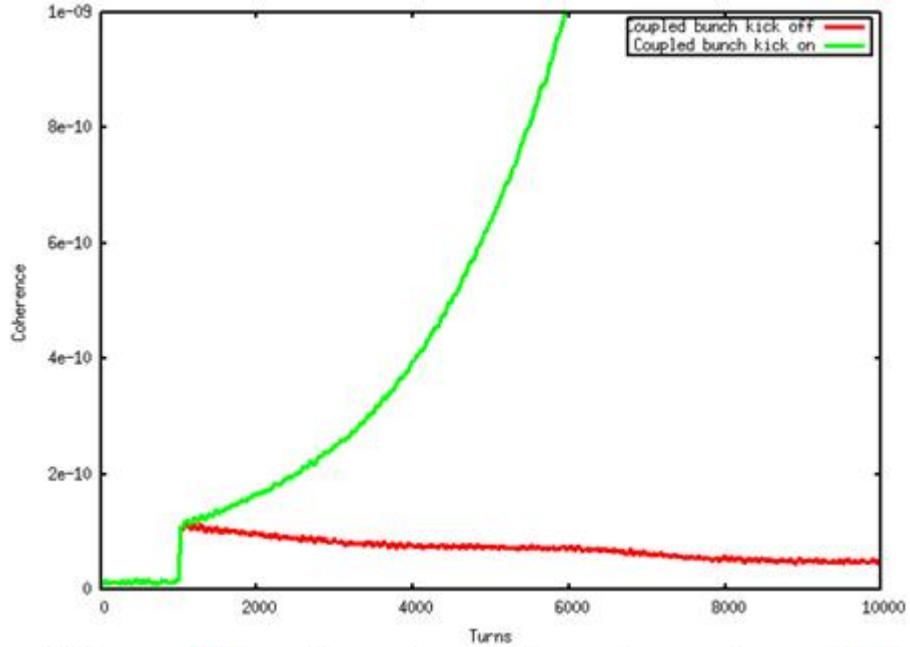

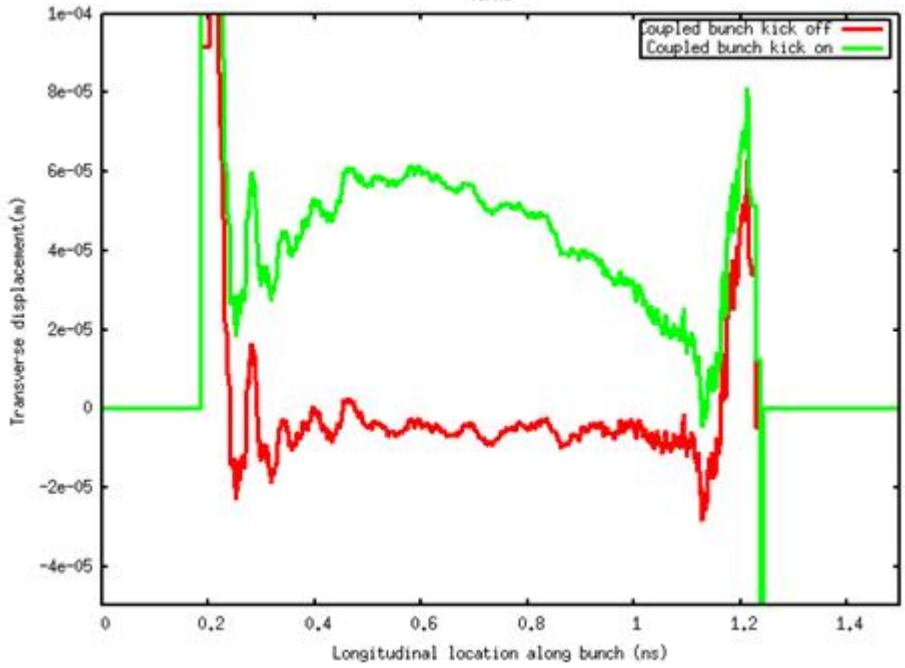

- Landau damping with linear chromaticity.

The following plot shows that 10 units of chromaticity is required to damp the coupled bunch mode instability:

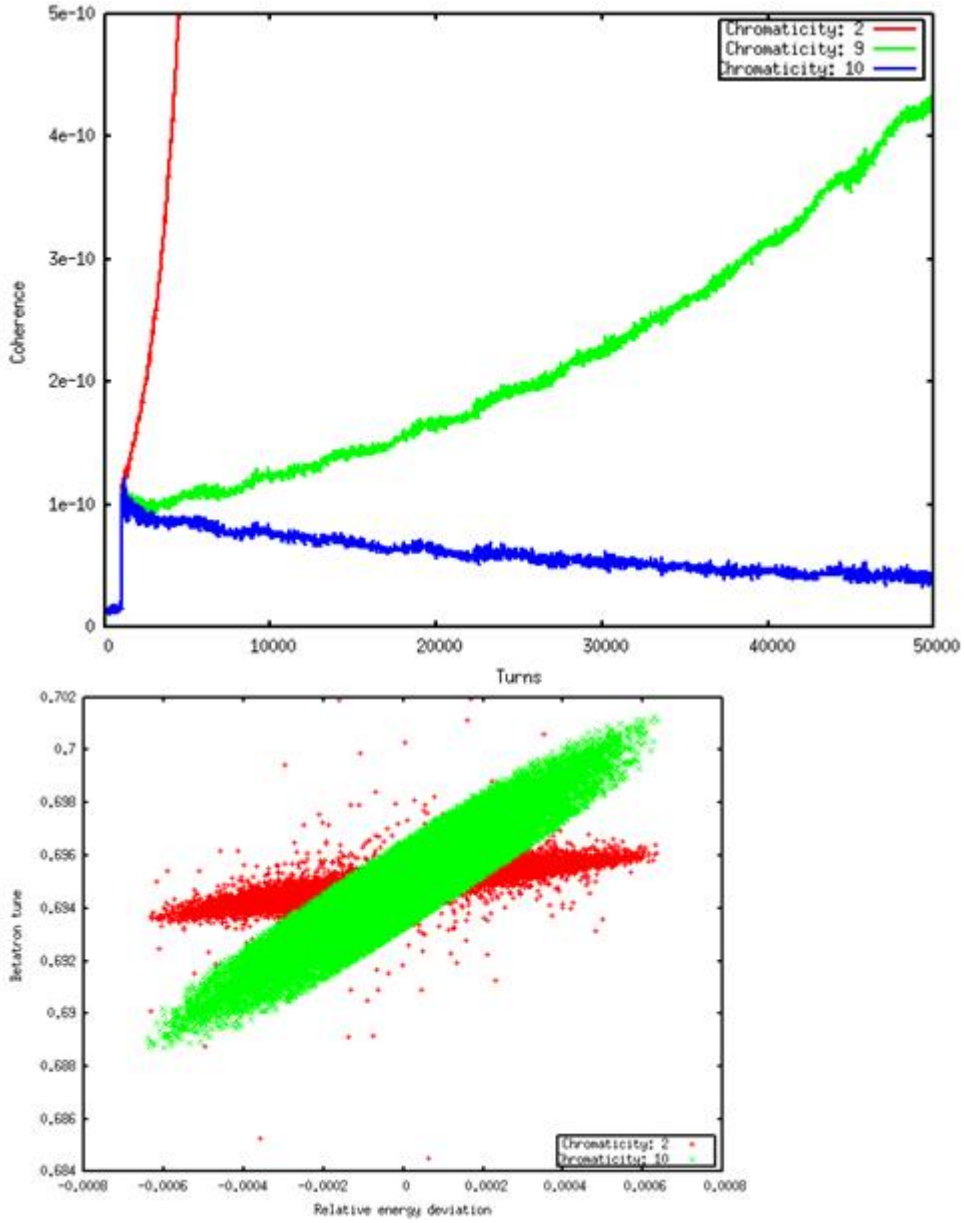

- Landau damping with amplitude dependant tune shift introduced by octupole.

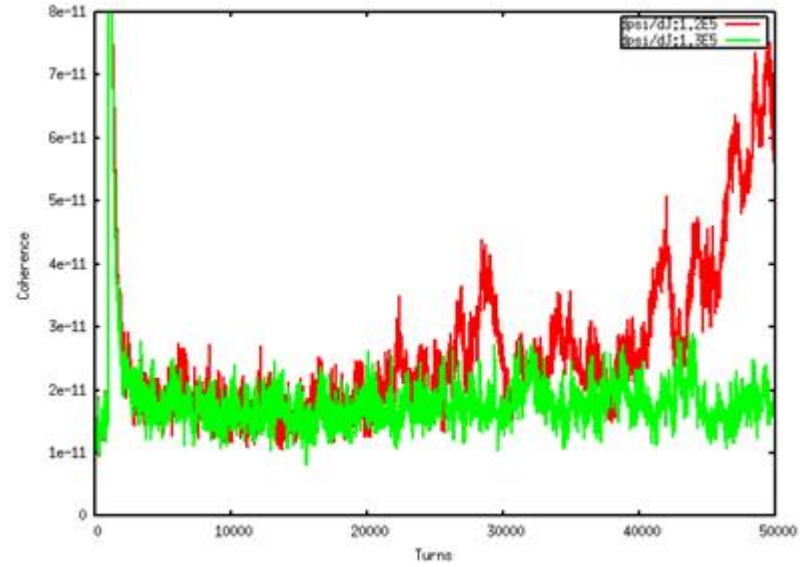

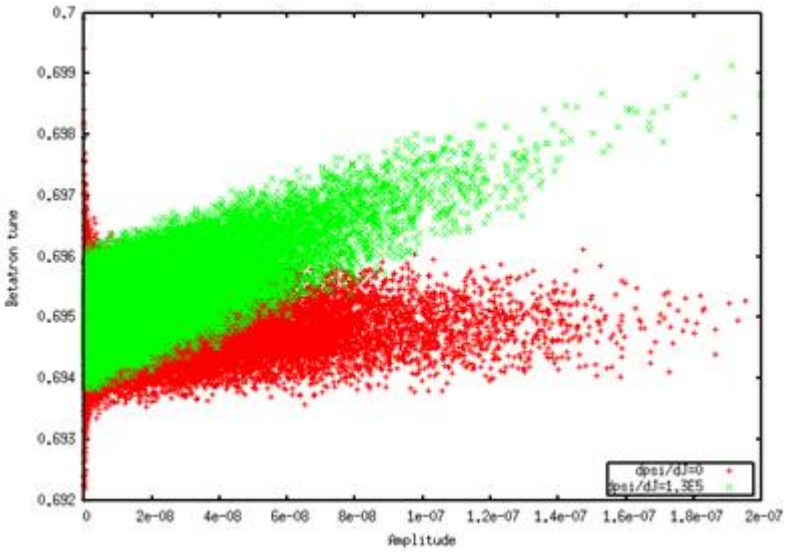

Beam-Beam Effects

Beam-Beam effects for the ion beam in ERL based EIC has the following concerns:

- The beam-beam tune shift limit (ξ_p<0.015)
- The kink instability limit
- The random electron beam properties variation issue.
- The interplay of the beam-beam force and the space charge force.

Kink Instability

Kink instability presents one of the limiting factors from achieving higher luminosity in ERL based electron ion collider (EIC). The beam-beam interaction between the ion beam and the opposing electron beam transports the imperfection in the head part of the ion beam to its tail, as if the ion beam experiences a wake field. This interaction may excite a head-tail type instability in the ion beam, which is named kink instability.

Threshold

Using a two-particle model, we can calculate the threshold of strong head-tail (SHT) instability due to the beam-beam interaction as: $\xi_p de < 4\nu_s / \pi$ where ξ_p is the beam-beam parameter for proton beam and ν_s is the synchrotron tune of the proton ring. A multi-particle linear model using circulant matrix [1] method confirms this threshold at low disruption parameter and show discrepancy at high de, as shown in Figure 1.

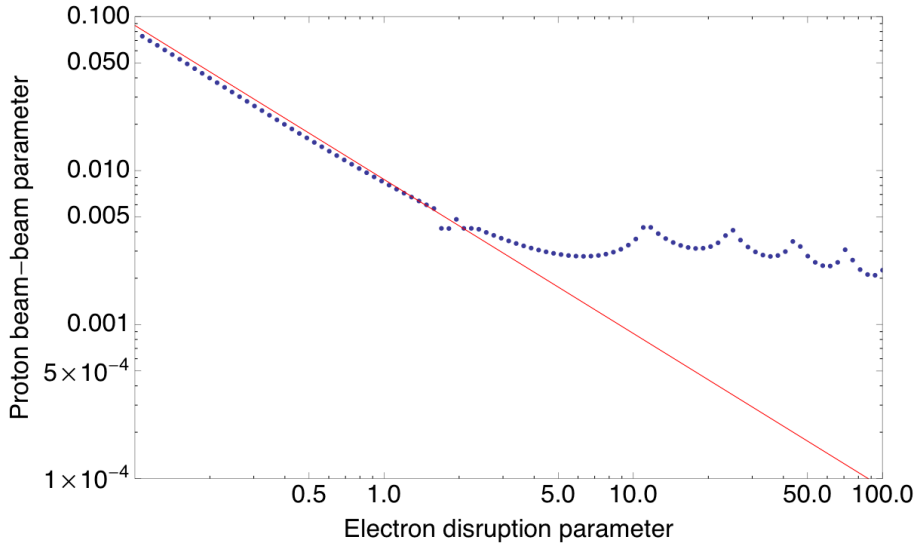

Figure 1: Kink Instability Threshold with the synchrotron tune 0.0069

The parameter of the RF system in the ion ring is:

Voltage	6 MV
Frequency	704

	MHz
Harmonic Number	9000

Since the disruption parameter is limited by the kink instability, we can express the luminosity for limited disruption parameter as well as the space charge tune shift and electron bunch intensity.

where the function is the geometric factor due to the hourglass effect.

Mitigation with Chromaticity

The typical design parameters of the proposed ERL based EIC exceed the threshold. Therefore the instability develops and the countermeasures are necessary to mitigate the emittance growth and luminosity loss.The classical way of the instability suppression is by means of Landau damping with introduced transverse tune spread with chromaticity or nonlinear field magnets. Figure 2 shows that a chromaticity of 20 is required to mitigate the emittance growth of the proton beam at the electron beam disruption parameter of 18.

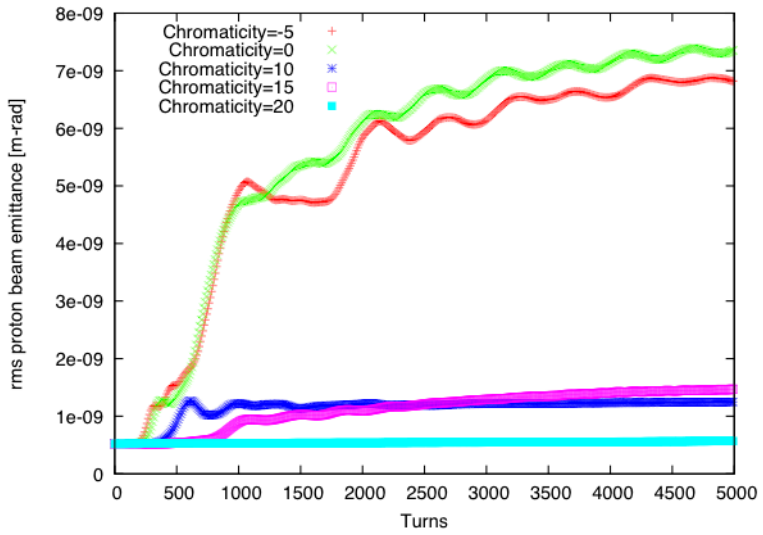

Figure 2: The proton beam emittance growth as function of turns. d_e = 18 and ξ_p = 0.015

However, the chromaticity also introduces unpleasant nonlinearity. The transverse tune spread is inevitably large for large chromaticity so that the nonlinear resonance will deteriorate the proton beam quality. Simulation results shows that the disruption parameter larger than 18 requires too high chromaticity so that the nonlinear resonance will severely affect the proton beam quality.

Mitigation with Active Feedback System

To avoid unpleasant nonlinearity to the system due to large chromaticity or strong

nonlinear magnet, by taking advantage of the flexibility of the linac-ring scheme, we can introduce a feedback system by reading the electron beam centroid position and angle after collision and feeding forward to the kick of the next fresh bunch that interacting with the same proton bunch, as shown in Figure 3. The scheme reads, here, M is the map that representing the algorithm of the feedback system, subscripts i and f denote the electron beam centroid phase space coordinates before turn and after nth turn respectively.

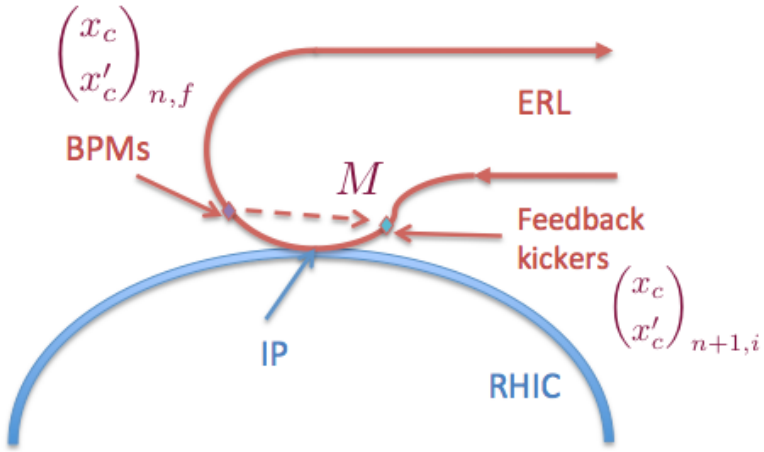

Figure 3: Kink instability feedback scheme.

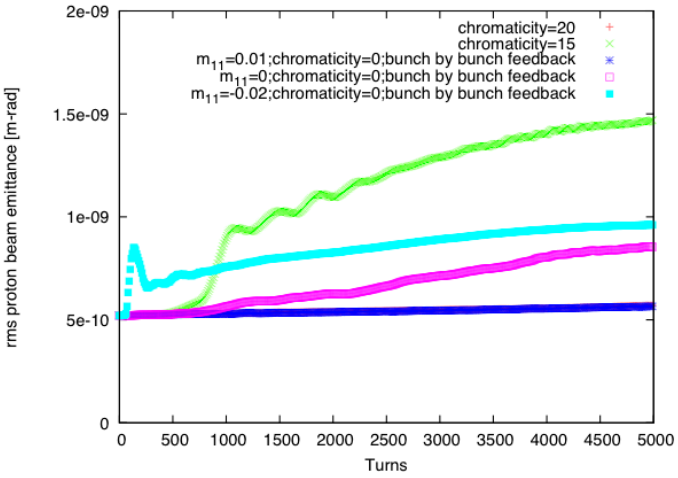

Figure 4: Emittance growth mitigation with the kink feedback system. de = 18 and ξ_p = 0.015

The advantage of this feedback system includes:

- The system is linear. The strength of nonlinear mitigation (chromaticity or nonlinear magnets) can be reduced or unloaded.
- The feedback system is applied turn by turn or even slower. The bandwidth requirement is low.

This feedback system also has its limitation:

- The system will introduce noise to the proton/ion beam. The noise must be small

enough to be cooled by the cooling system.

- The electron beam motion inside the proton/ion beam is not controllable. The efficiency of the feedback is function of the disruption parameter.

The extension of this system to higher disruption case is being developed.

Electron Parameter Fluctuations

Since the ion beam always collide with fresh electron bunches, the electron beam parameter fluctuation will affect the ion beam through the beam-beam interaction. The fluctuations can be classified as two types:

- Dipole errors for the ion beam: Electron beam transverse position offset.
- Quadrupole error for the ion beam: Electron beam intensity fluctuation, transverse beam size fluctuation.

White Noise Assumption

If the noise of the electron beam is considered as white noise, i.e. uniform spectrum in frequency domain, the effect of both dipole error and quadrupole errors can be evaluated.

For the quadrupole errors, the rms beam size of the ion beam is expected to grow exponentially, with the rising time where ξ_i is the beam-beam parameter of the ion beam, T is the revolution period and $\delta f / f$ is the rms error of the beam-beam focal length. For eRHIC parameters, to get slow rising time (~10 hours), the relative error of electron beam parameter should be better than .

For the dipole errors, the ion beam is kicked turn by turn due to the electron beam random offset. By following the well-known random walk formulas, the ion beam displacement gives and where dn is the electron beam displacement at nth turn. If we assume the transverse displacement dn has rms value of 1% of the beam size, the time for the ion displacement to reach 10% of the design beam size is 0.07 seconds.

Non-uniform frequency spectrum.

For a more realistic case, a Lorentz frequency spectrum is considered in ref[1], i.e. , where α is a parameter and ω_0 is the angular revolution frequency of RHIC. A frequency related factor $R(\alpha)$ can be found for the dipole and quadrupole errors respectively. In both cases the rising time τ is lengthened to $\tau / R(\alpha)$, where $0 < R < 1$.

For dipole error case,

For quadrupole error case,

where ν is the transverse tune, in eRHIC, which has value of 0.675/0.685.

Summary

The fluctuation of the electron beam is an important factor on the stability of the ion/proton beam. The white noise assumption of the fluctuation gives the strictest requirement on both error types. In reality the amplitude of high frequency noises are much lower than that of low frequency components. For a rough estimation of , the requirement of the relative quadrupole-related error of the electron beam (intensity and beam size) increases by factor of 40 (from 1e-4 to 4e-3). Therefore the precise requirement must be evaluated with the detail study of the noise source, including the laser and the power supplies of the magnets.

And for the same α, the time for displacement error accumulation to damage the luminosity increases by factor of , which is 100 seconds. For both noise models, the effect of the displacement error must be mitigated to ensure the desire luminosity and lifetime. In eRHIC, both feedback and CEC(Coherent Electron Cooling) will be introduced and serve as efficient tool to mitigate the displacement error.

Space Charge and Beam-Beam Interplay

In a collider, maximum achievable luminosity is typically limited by beam-beam effects. For heavy ions significant luminosity degradation, driving bunch length and transverse emittance growth, comes from Intrabeam Scattering (IBS). If IBS were the only limitation, one could achieve small hadron beam emittance and bunch length with the help of cooling, resulting in a dramatic luminosity increase. However, as a result of low energies or as a result of strong cooling, direct space-charge force from the beam itself may become the dominant limitation. Also, the interplay of both beam-beam and space-charge effects may impose an additional limitation on achievable maximum luminosity. Thus, understanding at what values of space-charge tune shift one can operate in the presence of beam-beam effects in a collider is of great interest for all of the above projects.

Ultimate limits on maximum values of space-charge and beam-beam parameters are typically associated with beam instabilities. However, before such limits are reached beam lifetime is strongly influenced by beam response to high-order non-linear resonances.

In hadron colliders, the total achieved tune spread due to beam-beam interactions is much smaller than in electron machines, which is believed to be due to a negligible effect of strong damping mechanism through synchrotron radiation which counteracts beam-beam diffusions in electron machines. The largest total tune spread due to

several beam-beam interactions per turn which was achieved in Tevatron is only about 0.03.

Similarly, when space-charge tune spread becomes significant, the beam overlaps many machine imperfection resonances, leading to large beam losses and poor lifetime. For machines where beam spends only tens of msec in high space-charge regime, and machines where the resonances are compensated, the tolerable space-charge tune shift can be as large as $\Delta Qsc=0.2-0.5$. However the acceptable tune shifts are smaller for longer storage times, with beam lifetimes of several minutes achieved for space-charge tune shifts of about 0.1-0.2. For a collider when one is interested in even longer beam lifetimes, smaller acceptable space-charge tune spreads can be expected. In dedicated studies of IBS in RHIC, without beam-beam collisions beam lifetime of few hours was measured for space-charge tune spread of 0.02-0.03.

Starting in 2009 several experiments were performed in RHIC in order to understand what beam lifetime can be expected for different values of the space-charge tune shift with and without beam-beam effects. Our observations and initial analysis are summarized in Ref. [1]. Table 1 and 2 show typical beam lifetimes measured in different experiments. Incoherent space-charge tune shift values ΔQsc were calculated using measured beam parameters at the start of the measurement. Other effects which were different for the experiments at different energies are indicated under comments. Beam lifetime values reported in the Tables are the result of fitting the intensity decay for individual bunches. More details on measured beam lifetime can be foud in Ref. [2].

Table 1: Beam lifetime for low-energy gold ion beam for different space-charge tune shifts without collisions.

ΔQ_{sc} (x,y)	τ [s]	γ	Comments
0.03	2000	10	$5\sigma_x$ acceptance, Q_s=0.002
0.05, 0.04	1600	6.1	$3\sigma_x$ acceptance, Q_s=0.006
0.09, 0.07	700	6.1	$3\sigma_x$ acceptance, Q_s=0.006
0.1	70	4.1	$2.2\sigma_x$ acceptance, Q_s=0.013

Table 2: Beam lifetime for low-energy gold ion beam for different space-charge tune shifts with collisions (with total beam-beam parameter ξ).

ΔQ_{sc}	τ [s]	γ	Comments
0.03	600	10	$5\sigma_x$, Q_s=0.002, ξ=0.002 (1 IP)
0.05	400	6.1	$3\sigma_x$, Q_s=0.006, ξ=0.0015 (1 IP)
0.09	260	6.1	$3\sigma_x$, Q_s=0.006, ξ=0.0027 (1 IP)
0.1	70	4.1	$2.2\sigma_x$, Q_s=0.013, ξ=0.003 (2 IP)

It is expected that effect of beam-beam on beam lifetime can be minimized if one can avoid beam-beam resonances by an appropriate choice of the working point. The effect of working point was already demonstrated in the first experiments on this

subject [1]. Moving working point closer to an interger allows one to avoid beam-beam resonance to a high-order by limiting space-charge tune spread to a modest value. In 2011, such experiments with working point below tune of 0.1 were done with a very small beam-beam paramter using heavy ions. This experiment will be repeated next year with protons for which we have large beam-beam paramter, as for eRHIC.

For present baseline parameters of eRHIC, we have chosen modest value of the space-charge tune spread $\Delta Q_{sc}=0.035$, which should provide long beam lifetime at least in the absence of beam-beam effects. Together with beam-beam, the total tune spread by design is presently $\Delta Q=0.05$. The impact of beam-beam on beam lifetime with such space-charge tune spread is under study.

Number of bunches

Present RHIC operations with heavy ion or polarized proton beams uses 9.4 MHz bunch repetition rate. This repetition rate corresponds to 120 bunch pattern (i.e. 120 bunches can be fit on the RHIC circumference), but only 111 bunches are used because of the need to provide the abort gap. In eRHIC 14.1 MHz bunch repetition is intended, which corresponds to a 180 bunch pattern, with 166 bunches actually in use. The distance between the bunches in eRHIC will be ~71 ns.

In order to work with 180 bunch pattern in RHIC an upgrade of the injection system is needed. The injection requirements are given as an integrated kick of 1 mrad that is obtained with 1 kA in a ferrite kicker with the aperture of w 4.84 × h 5.12 cm. The present injection kicker has the rise-time ~95 ns which is too long compared with the 71 ns bunch distance. The injection systems must be upgraded to fit into the less than 56 ns of a beam free bucket length. R&D studies directed at pulser and magnet designs are underway in order to establish the pathway for the injection kicker upgrade. A prototype solid state fast pulse generator has been acquired to evaluate its possibility for the system rise-time reduction [1]. A pulsar rise time of <15 neck at 50 kV has been demonstrated with this unit into a matched load, leaving 40 ns for the kicker rise time. The kicker deflector design, to reduce the rise-time, is also under investigation. Retaining the present kicker construction method would require replacing four 114 cm long by six 76 cm long magnets. Alternatively, the development of “plate kickers” with a characteristic impedance of 50 or 25 Ω and voltage holding of 60 and 30 kV respectively is a promising option. The impedance choice determines filling time and consequently also the number, 4 or 6, of kicker units and the system cost.

Resistive Wall Heating

RHIC hadron beam pipe is made of stainless steel, and has the diameter 7.2 cm at the most of the ring circumference, except the Interaction Region sections where the stainless steel pipes of larger diameters are used. In eRHIC the bunch length of the hadron beam will be much shorter than used presently in RHIC operation, and the proton beam current in eRHIC will be somewhat larger than presently used. This will lead to increased beam pipe heating due to the pipe material resistivity. Figure 1 demonstrates dependence of the power dissipated in the walls of the present RHIC beam pipe of the proton bunch length at eRHIC bunch intensity 2×10^{11}. **With 166 bunches the power loss in the pipe walls exceeds presently accepted RHIC cryogenic load limit of 0.5 W/m at the bunch length shorter than 17cm**.

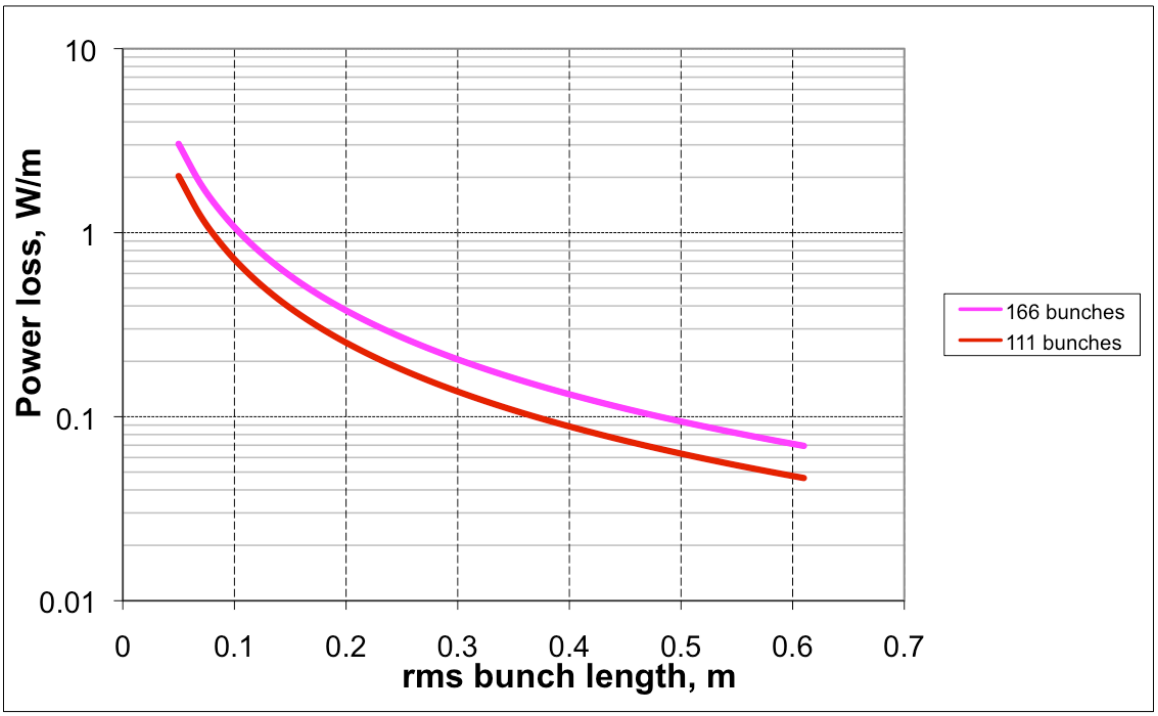

Figure 1: The dependence of the resistive wall losses per meter on the eRHIC proton bunch length for the present stainless steel RHIC beam pipe.

In order to operate with the bunch length of 5 cm, the copper beam pipe has to be used. The anomalous skin effect has to be included into the consideration for the copper pipe at the cryogenic temperature, since the electron mean free path length becomes greater than the skin depth in the frequency range of interest. The results of such consideration are shown in Figure 2, where power load per unit frequency is shown for two different resistivities of copper at cryogenic conditions (RRR denotes the ratio of the resistivity at room temperature to the resistivity at 4.2 K) [1]. The integration over the frequency leads to **the dissipated power load 0.064 W/m for RRR = 50, and 0.079 W/m for RRR = 25**. Those numbers are well within acceptable cryo-load.

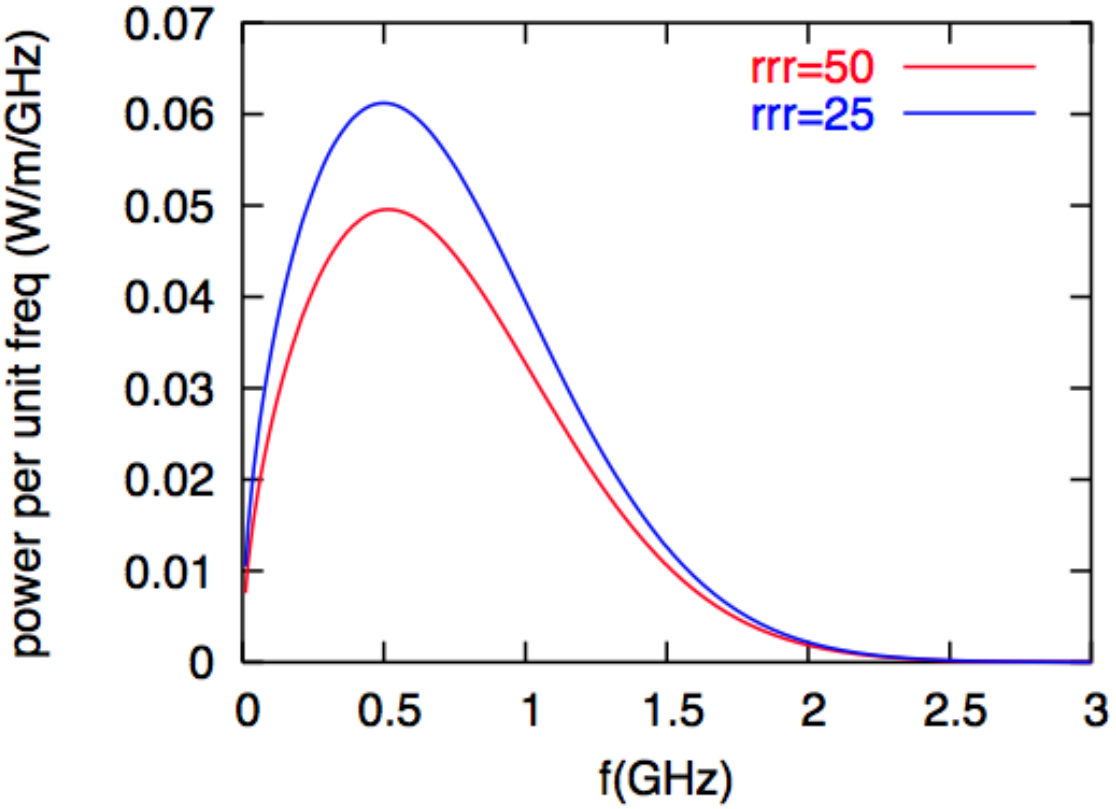

Figure 2: Ohmic loss per unit length per unit frequency for copper pipes of two different resistivities.

To reduce the resistivity of the present stainless steel pipe the high purity copper layer of 10 μm thickness can be sputtered on the inner pipe surface. A method to realize this in-situ coating of the beam pipe using robotic plasma deposition technique has been under consideration [3].

4 Interaction Region

Overview

The main features of eRHIC IR:

- Low beta* = 5 cm
- 10 mrad crossing angle and crab-crossing
- First magnet (combined function, hadron line) is 4.5 m from the collision point, providing the sufficient space for the detector.
- High gradient (200 T/m) large aperture Nb_3Sn focusing magnets
- Arranged free-field electron pass through the hadron triplet magnets
- Integration with the detector: efficient separation and registration of low angle collision products
- Gentle bending of the electrons to avoid SR impact in the detector
- The design is not compatible with parallel operation with p-p (ot ion-ion) collisions

The general layout of the IR is shown on the plot below. The electron beam enters the detector along its axis.

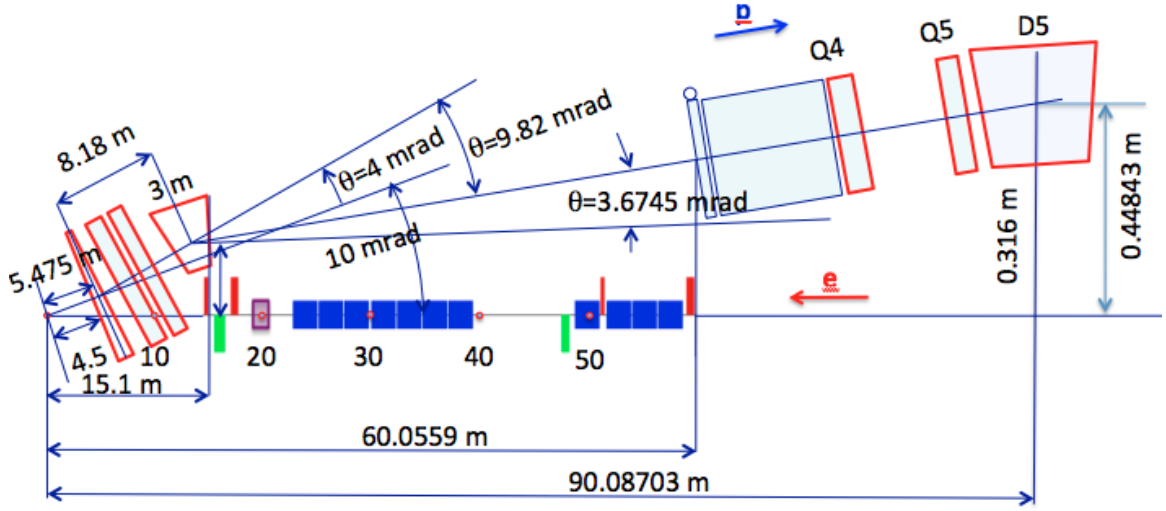

These plots presents the layout of IR in the region near detector:

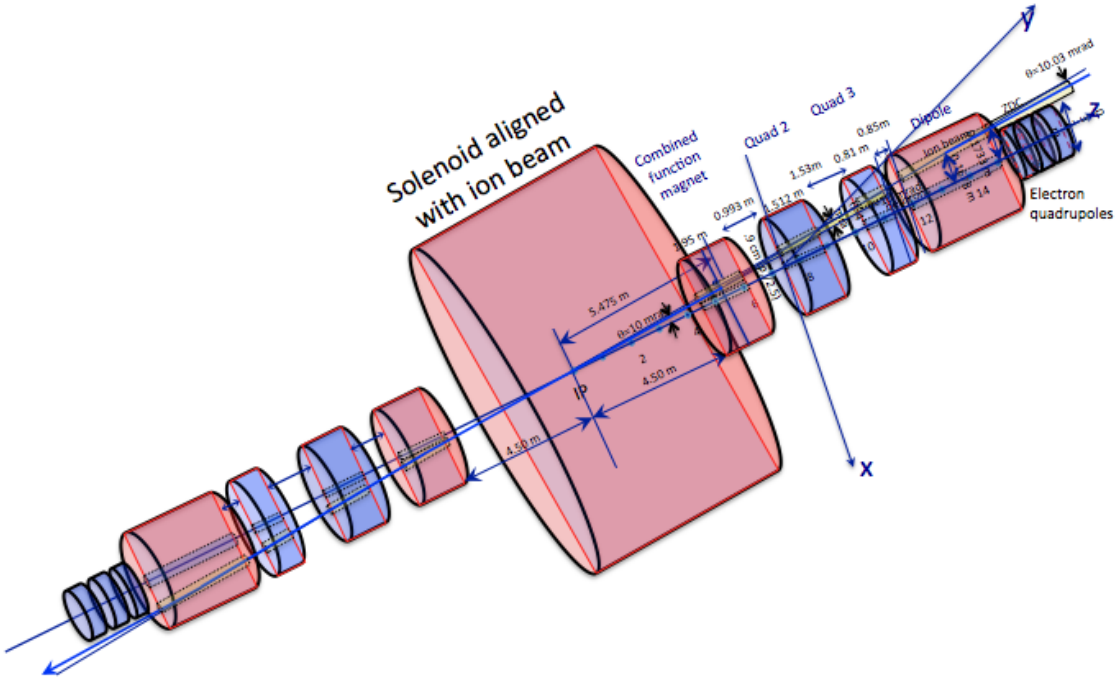

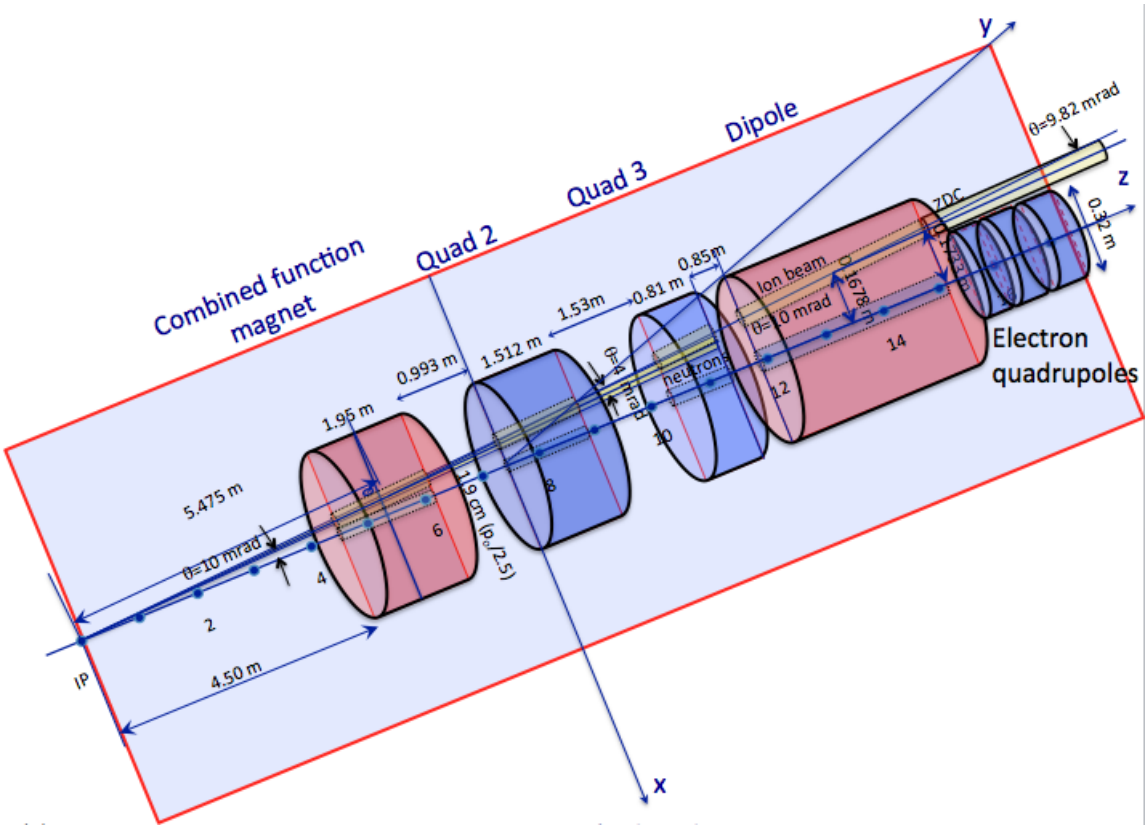

Detector Integration

The dedicated eRHIC detector can be considered as a cylinder with external diameter of 4 meters or less, filling the length between two final focusing triplets. Thus, the electron beamlines, which bypass the detector can be placed at about 2 m from the detector axis.

The IR design integrates the demands from experiments:

- Along the hadron direction:
  - Detection of forward protons from DVCS process
  - Forward neutron detection (ZDC) with the angle of +- 8 mrad
  - Detection of low energy protons (momentum p_0/2.5) from heavy ion fragmentation (this is low priority demand)
- Along the electron direction: forward electrons

- This plot demonstrates the passage of the protons with the momentum deviation through the hadron triplet.

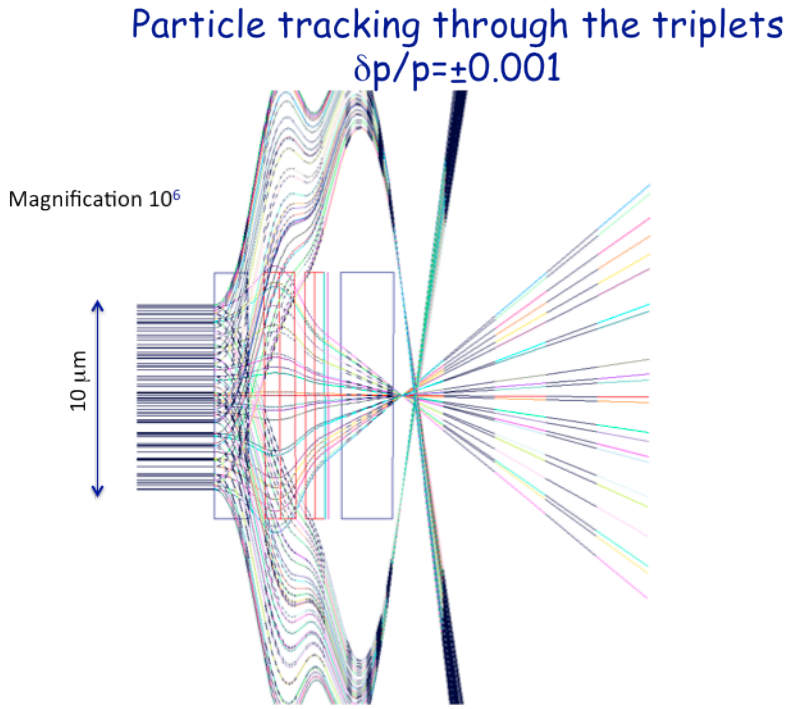

Hadron IR Beamline

Hadron Lattice

- β* = 5 cm design keeps the maximum of β functions in triplets of the order of the existing in the RHIC lattice ($\beta_{max} < 2500$ m)
- Large and flat horizontal β-function through the interval where the crab-cavity system is installed.

Horizontal (red) and vertical (green) beta-functions and horizontal dispersion function in the interaction region are shown in the figure below:

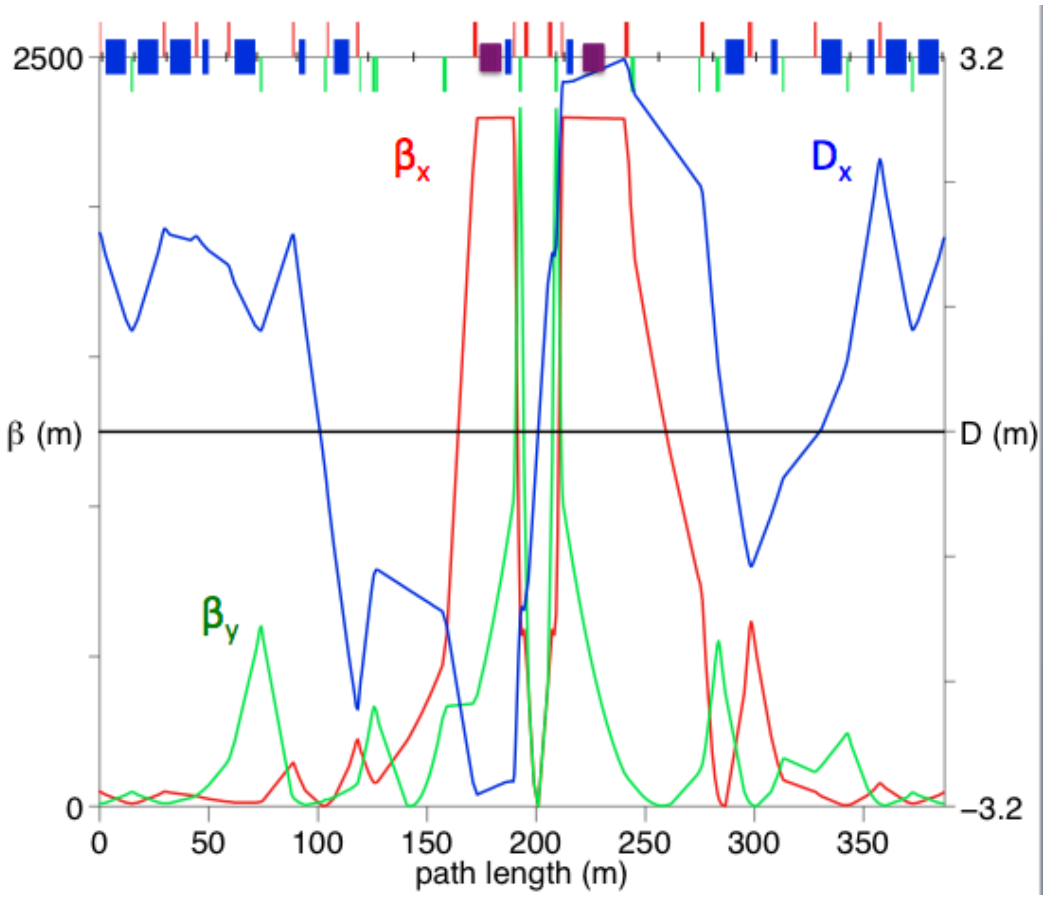

Figure 1: IR Hadron lattice functions

Chromatic Correction

- Natural chromaticity introduced by high-beta IR triplets is -110 (horizontal) and -133 (vertical)
- Chromatic correction of the interaction region combines sextupoles in the IR triplet

and the sextupoles at the beginning of the arc.
The sextupole locations are indicated by black lines:

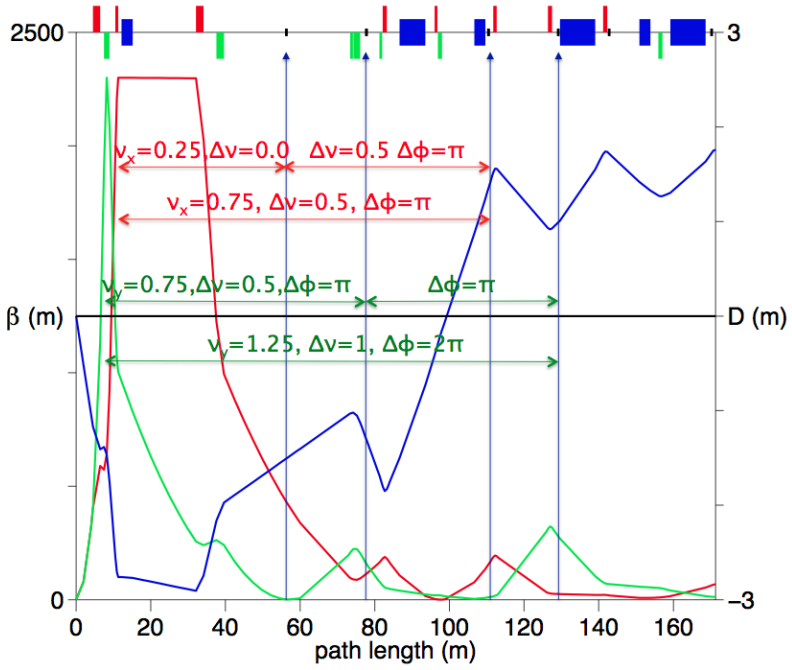

Figure 2: Hadron lattice functions of left side of the IR (reversed pathlength coordinate).

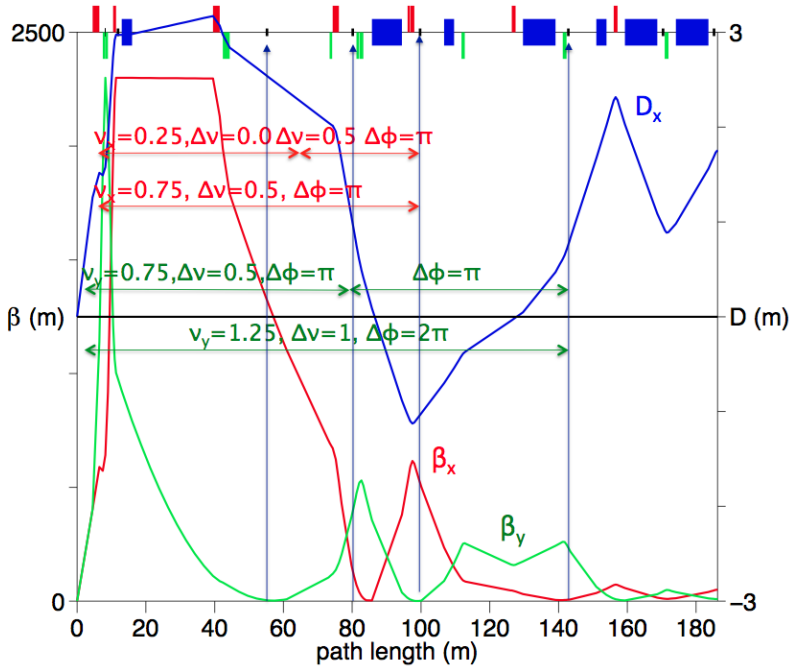

Figure 3: . Hadron lattice functions of right side of the IR.

Hadron Magnet Parameters

IR quadrupole parameters:

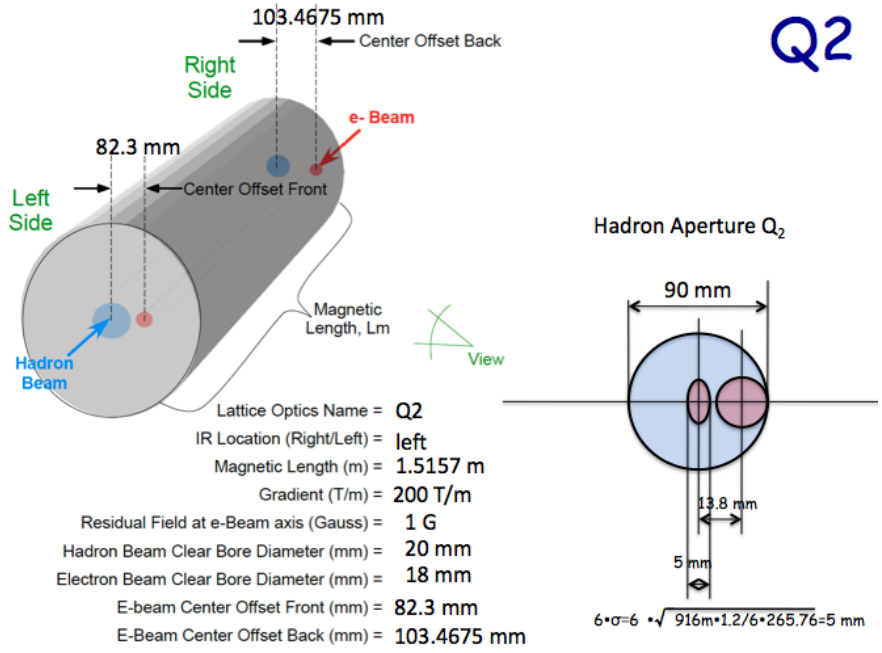

Figure 4: Parameters of hadron quadrupole magnet Q2

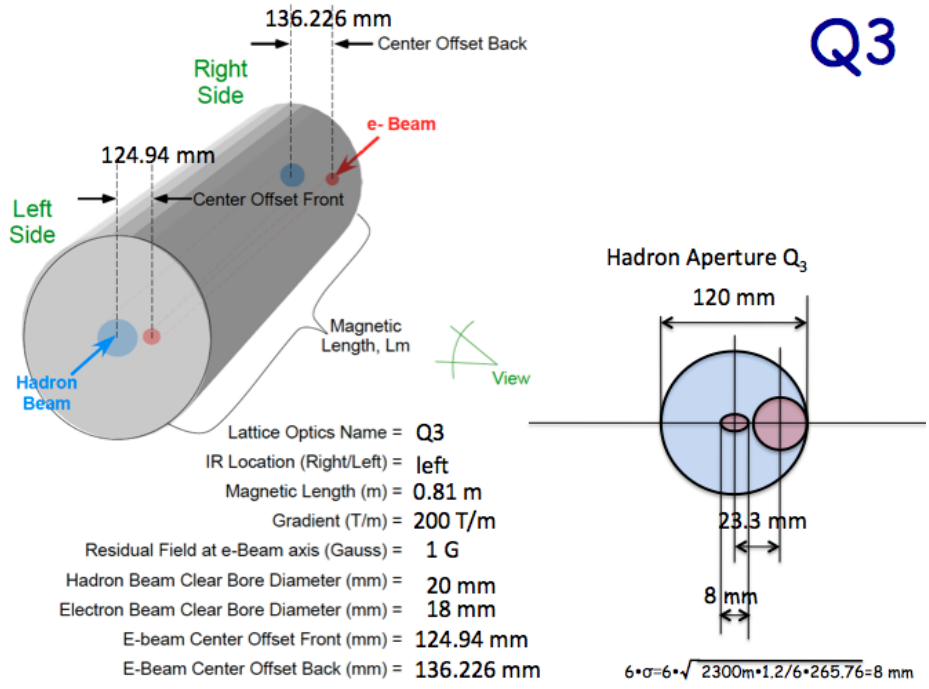

Figure 5: Parameters of hadron quadrupole magnet Q2

Electron Line

Layout and parameters

The top energy electron IR beamline has to bring electrons from recirculating pass location on outside part of the RHIC tunnel, direct the electron beam along the axis of the experimental detector and provide small β* at the collision point. The IR beamlines upstream and downstream of the detector have the same magnet and lattice structure.

The IR beamline can be divided in two parts, by their functions.

- The vertical shift beamline transports the top energy electron beam above the RHIC ion beam magnet cryostats and makes ~60 cm shift down, almost to the level of the detector center axis. The beamline is ~55m long and the bending is done with sufficiently strong magnetic field (0.122 T at 30 GeV). The lattice structure of the vertical shift beamline consists of 4 basic lattice cells used in the recirculating arcs, with two of those cells bending down and other two bending up.

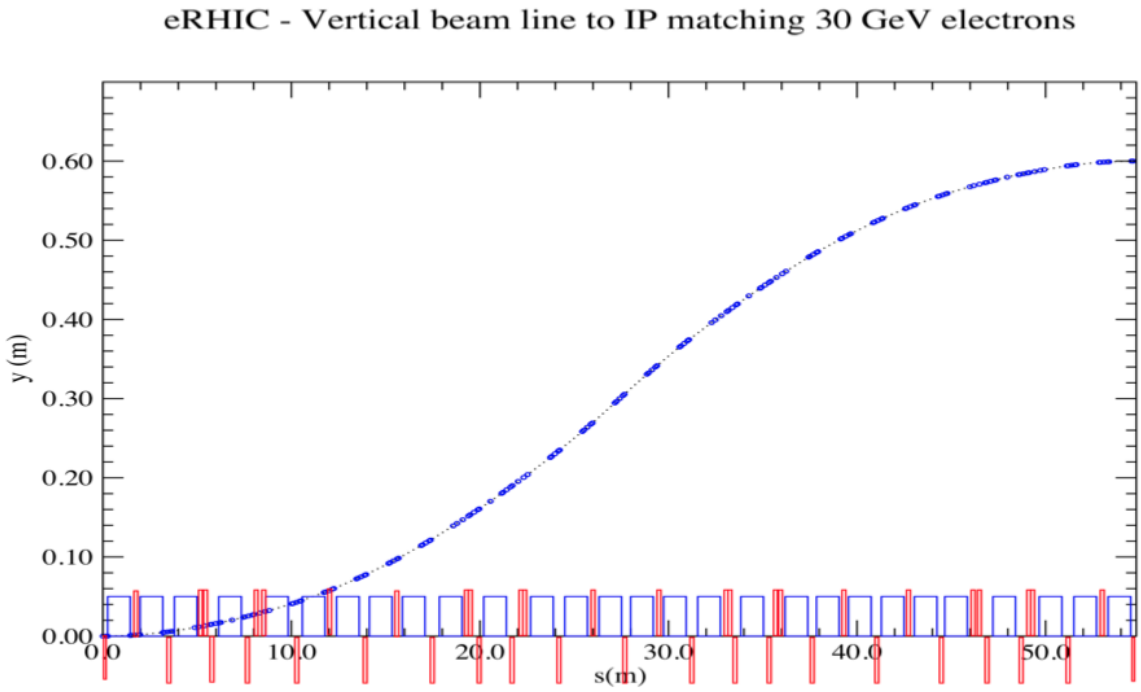

- After the vertical shift line, the inner IR beamline, also ~60m long, provides the final weak bending to put the electron beam exactly on the detector axis. The focusing magnets, including the final focusing triplet, provide β*=5 cm at the collision point. This beamline contains the bending magnets with the field from 160 to 24 Gs at 30 GeV beam energy. Using the 24 Gs dipole magnets for the final bending produces the very low intensity soft synchrotron radiation which does not create problems at the detector. The optical functions of the inner IR beamline are shown

here:

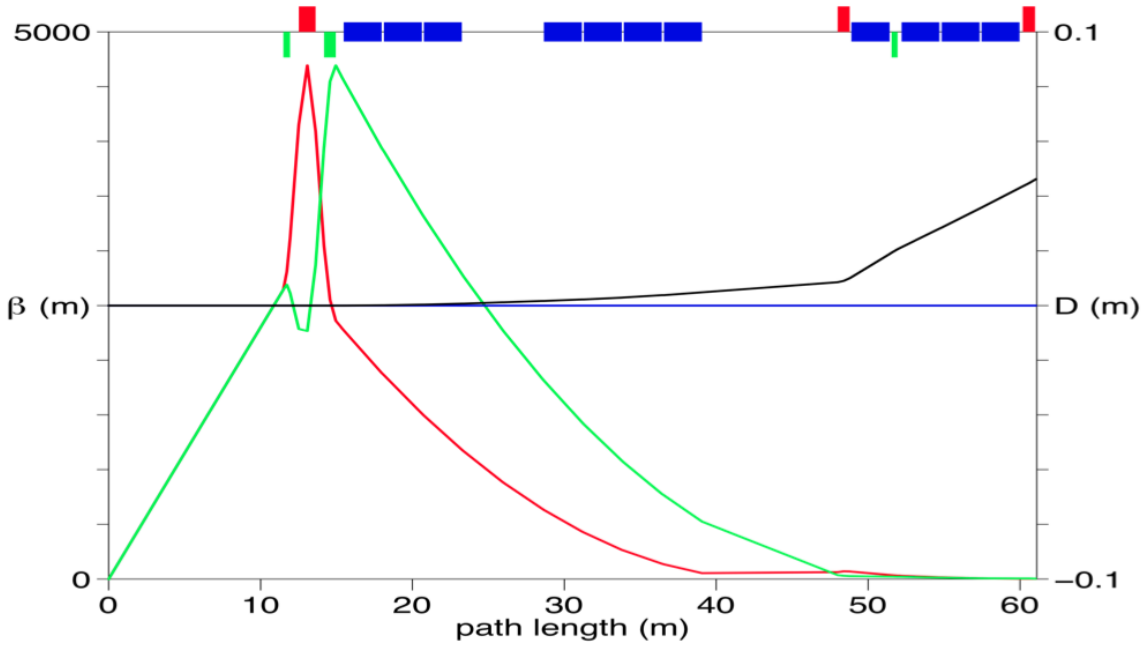

Maximum electron beam rms transverse size at the IR triplet varies:

- from ~1.5 mm when colliding with 325 GeV protons
- to ~3.8 mm when colliding with 50 GeV protons

Beam angular divergence at the straight section between collision point and the triplet varies:

- from ~0.1 mrad when colliding with 325 GeV protons
- to ~0.26 mrad when colliding with 50 GeV protons

Integration with detector components

- In the detector the electron beam passes along the axis of the experimental solenoid.
- On the electron outgoing side of the detector both electron and ion beam pipes will be surrounded by the calorimeter to detect small angle scattered electrons.
- For the luminosity measurement the bremsstrahlung monitors can be placed downstream of the detector in some location after the electron beam is bent up.

Synchrotron Radiation

The main features of dealing with SR, produced in the interaction region electron beamline, are following:

- There are no strong bending magnets within 60m from eRHIC detector in the current eRHIC interaction region design. It ensures that there are no radiation sources near the detector.
- The forward radiation from the up stream hard bend is completely masked. No hard radiation passes through the detector;
- Soft bend on both side of the detector. The forward radiation from the up stream soft bend pass through the detector.
- The secondary backward radiation induced by the forward radiation generated in down stream bends is largely masked from the detector;

- The synchrotron radiation photon spectra produced different IR electron beamline dipole magnets are shown for 30 GeV electron beam energy:

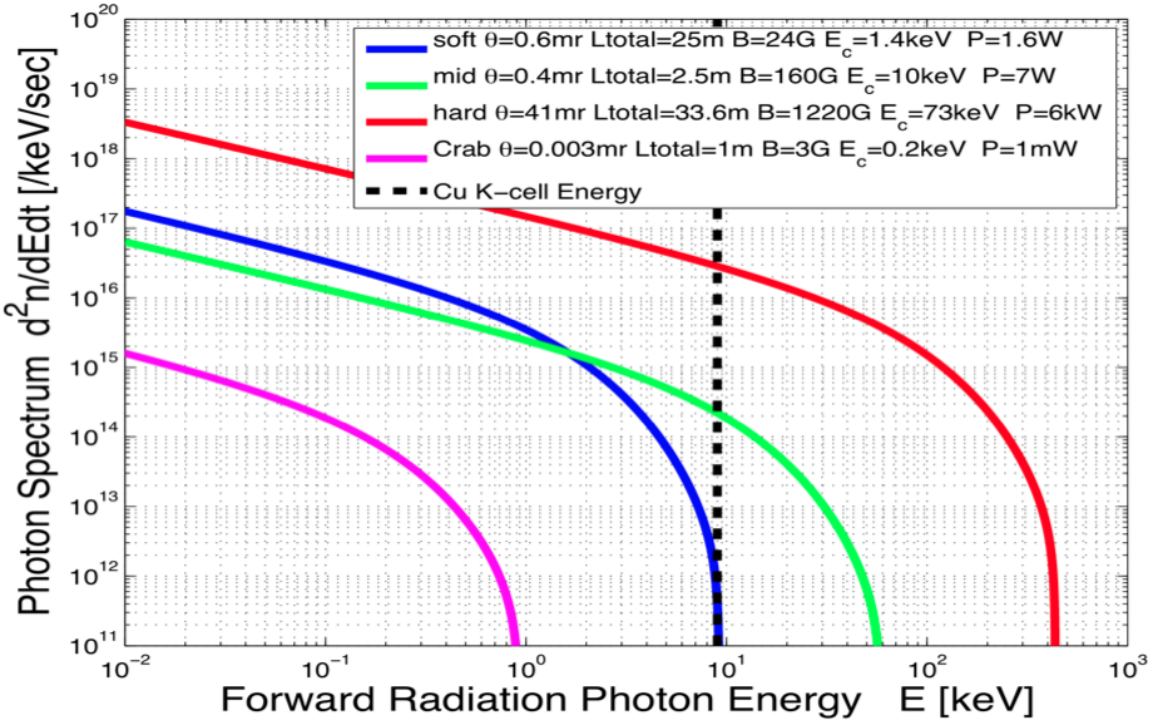

The synchrotron light only from soft bends passes through the detector but it can not penetrate through the beam pipe.

- The SR power load in the IR vertical shift beamline is shown below along the beam pipe. This plot considers 2cm distance between the beam orbit and the pipe antechamber wall. The distributed copper absorber can be placed along the

antechamber to accommodate this SR power load. The plot shows also a location (at ~32 m) when the orientation of the antechamber has to be switched from the top side of the beam pipe to the bottom side.

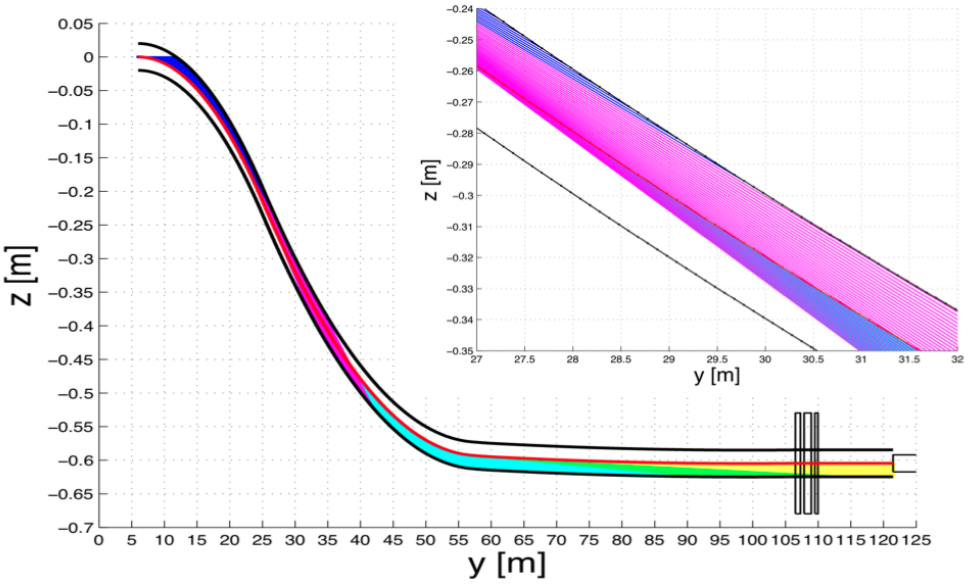

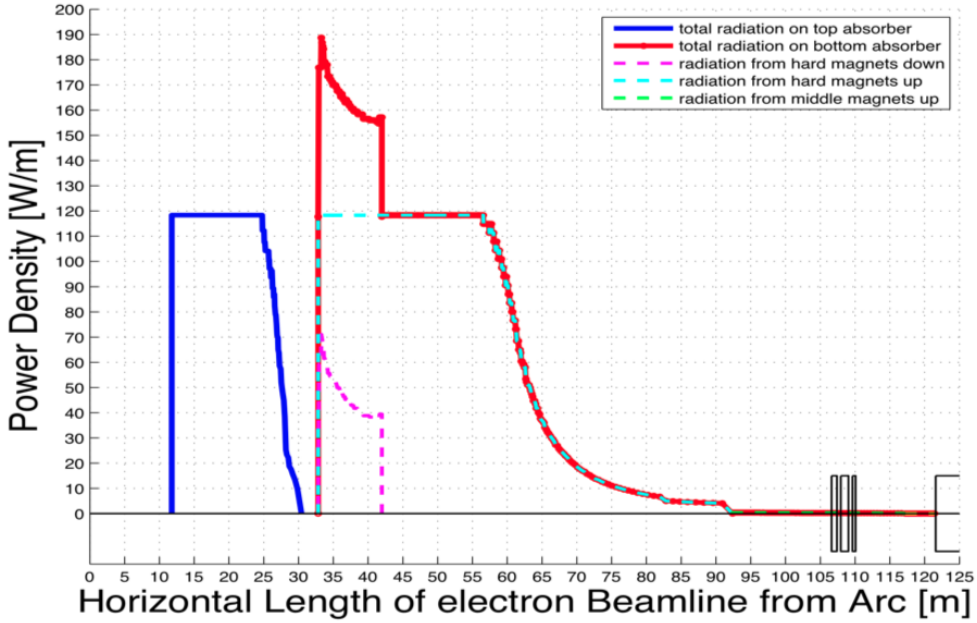

- The SR power load in the IR inner part beamline is shown on these plots. Only the radiation from very weak bends penetrates to the detector region. For now distributed copper absorber is assumed, also the lolac absorbers and mask have to be also considered.

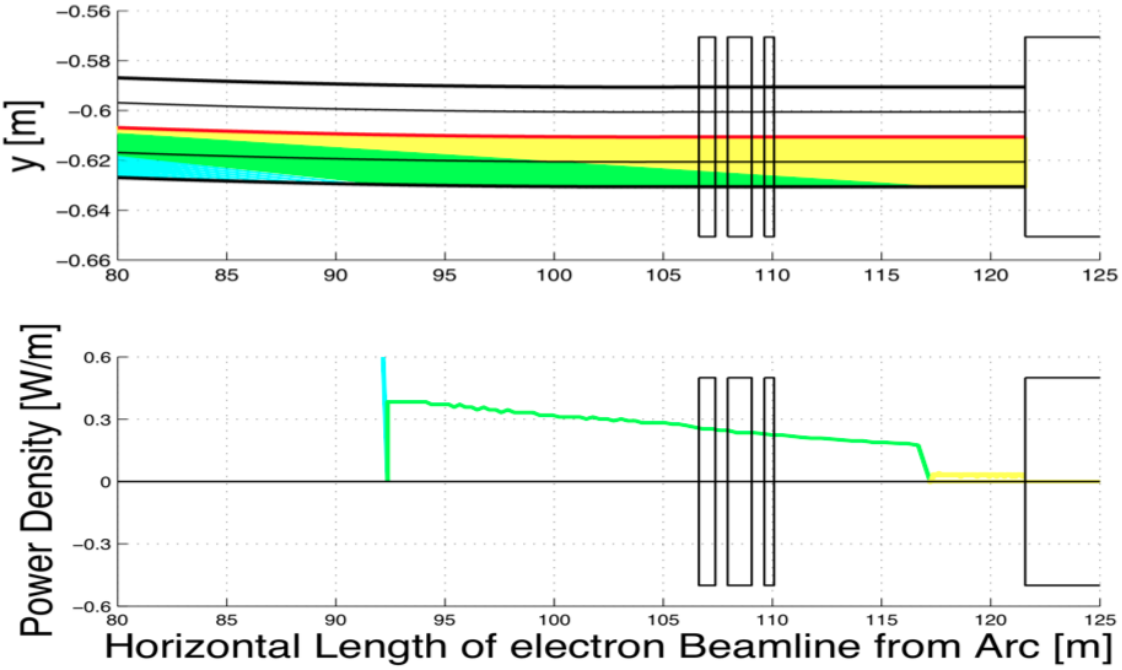
y [m]
−0.56
−0.58
−0.6
−0.62
−0.64
−0.66
80
85
90
95
100
105
110
115
120
125
Power Density [W/m]
0.6
0.3
0
−0.3
−0.6
Horizontal Length of electron Beamline from Arc [m]

Crab-Crossing

Since the IR uses 10 mrad crossing angle between electron and hadron beams, the crab-crossing is required to avoid the more than order of magnitude of the luminosity loss. The schematic of the crab-crossing is shown in the plot below. Both electron and hadron beams come to the collisions rotated by 5 mrad in the horizontal plane. The beam rotation is realized by the crab cavities. The beam crabbing scheme of both electrons and hadrons is local, so that the beam rotation does not propagate to outside of the interaction region area.

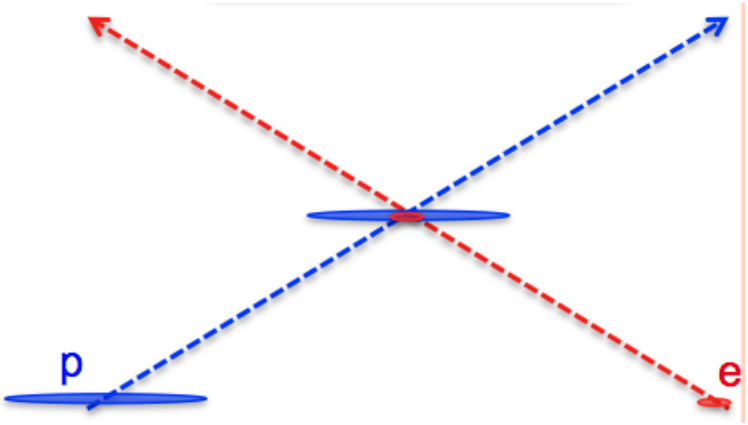

Hadron beam

Hadron crab cavities are located at 9.5m from the IR dipole magnets. At their locations the R_22 element of the horizontal transfer matrix between the crab cavity and the collision point is about 0. The R_12 element was enhanced by proper lattice design and is equal to 16.7m in the present lattice.

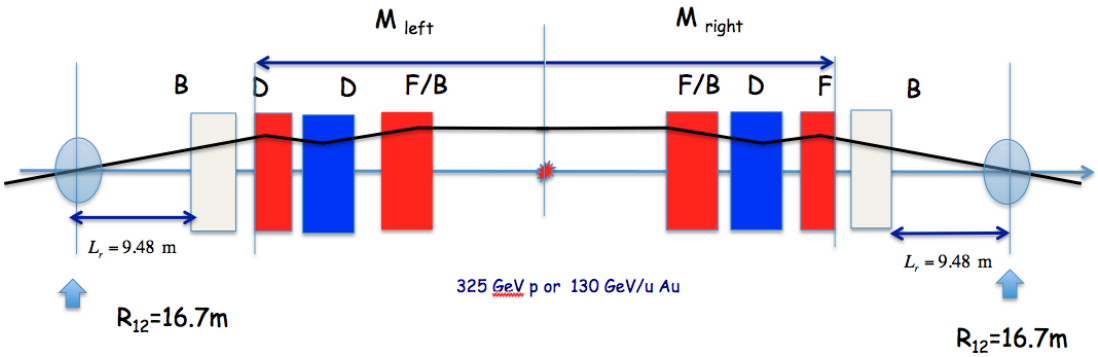

The required voltage of the hadron crab cavities can be calculated using the formula:

$$V_{\perp}[MV] \approx 11.9 \frac{E_p[GeV]}{325} \lambda_{rf}[m]$$

Sinusoidal form of the crab-cavity voltage leads to the transverse deviation of particle at the head and tail of the bunch from the perfect linear x-s correlation shape. On the basis of the experience with 10 Hz orbit oscillations at the collision points in RHIC, the criteria for the transverse deviation from the linear shape to be less than 1/10 of the transverse beam size in the longitudinal range of was accepted. The study showed that to satisfy this criteria with reasonable voltages of crab-cavities the system with two or more harmonics has to be used. The table below shows two possible variants of crab-cavity system:

System	Fundamental frequency	Cavity voltages
Fundamental + 2nd harmonic	< 142 MHz	V_{fund} = 34 MV, V_{2nd} =4.2 MV
Fundamental +3rd + 5th harmonics	< 181 MHz	V_{fund} = 23 MV, V_{2nd} =2.1 MV, V_{fund} = 0.15 MV

Electron beam

For the electrons the crab-cavities with 1.008 GHz frequency and 1.9 MV voltage are required.

Magnet Design

Combined function magnet

- The main features of the IR superconducting magnets, forming the hadron IR triplet, include the large aperture, required to pass through the forward momentum collision products, and the electron beam passage thorugh the field free region. Below the drawings shows the half of the combined function magnet with the field distribution throughout the magnet.

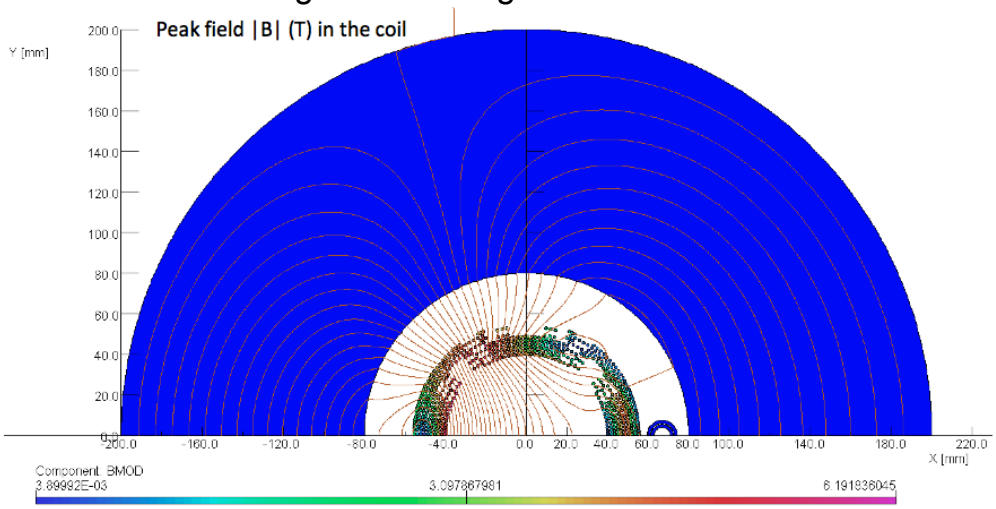

- At this plot the area around the electron free-field pass through the combined function magnet is shown:

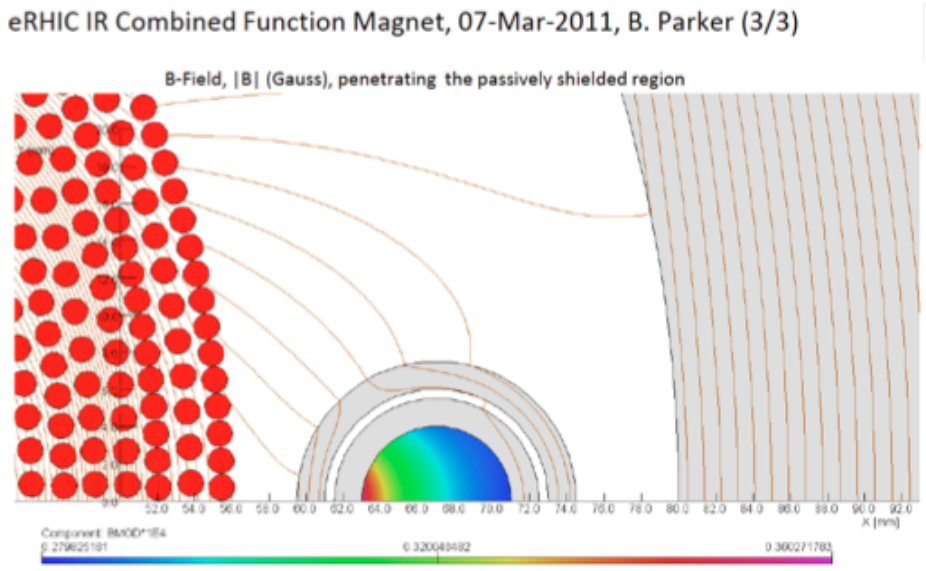

- The plot shows the on axis field, seen by the incoming hadron beam X = (22. to -0.67 mm) so that for an initial 10 mrad angle (w.r.t. electron beam) the exit angle

is 14 mrad.

B_0=2.701 T, the field gradient = -87.74 T/m, L_{mag} = 1.95 m.

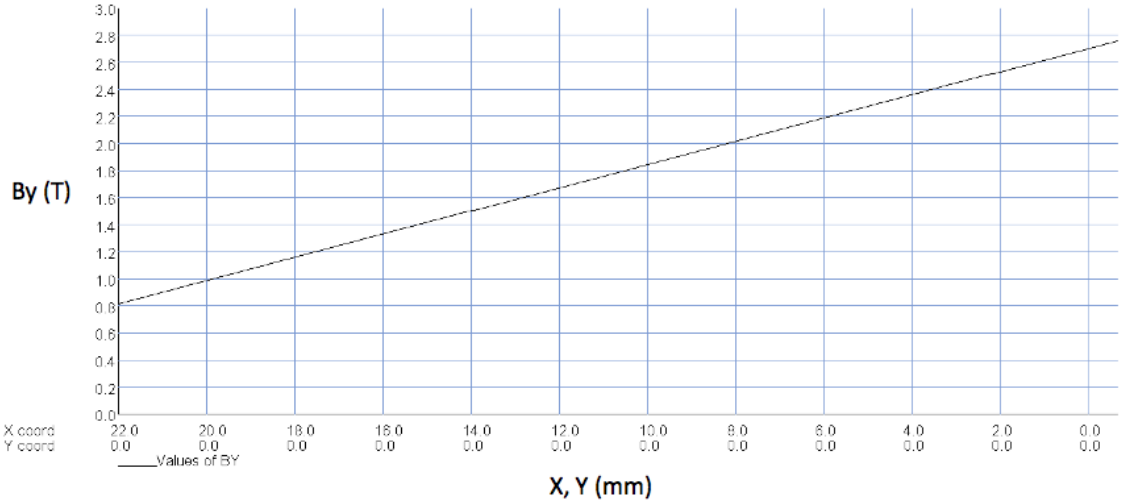

Spin Rotators

Since the stable proton spin direction in the RHIC arcs is vertical, the spin rotators have to be used in the interaction region areas in order to create the longitudinal spin orientation in the collision points. The spin rotators have been used in RHIC to realize a desired proton polarization direction in proton-proton collisions in STAR and PHENIX detectors (IP6 and IP8 regions). Every RHIC spin rotator presents the sequence of four helical magnets, each of them consisting of one helical period. The same rotator design can be used for eRHIC, so one can re-use the existing rotators and, if needed, provide easy switch from the e-p operation to the p-p operation in the same interaction region.

The proton spin rotator location in the eRHIC IR will be the same as in present RHIC, in the warm section just near Q4 magnet (see the IR layout figure in the IR Overview section). Two rotators are used, one on each side of the interaction region. Upstream rotator converts the vertical spin into the some direction (defined by the proton beam energy) in the horizontal plane. After the proton beam passes the collision point the spin rotator downstream of the IR converts the proton polarization back to vertical direction. The second rotator produces the spin transformation exactly inverse to the first one.

The spin rotator scheme is shown in Figure 1. It consists of four helical magnets, each magnet is 2.4 m long and presents one full helical twist. The magnets have different helicities, as shown in the Figure 1, and horizontally oriented field at the magnet entrance (and exit). Although the beam orbit makes excursion inside the rotator, the magnet field relations, shown in the Figure 1, provide the orbit restoration at the rotator exit, so that the beam orbit remains undisturbed (in the first approximation) outside the rotator. The example of the spin transformation through the rotator is shown in the Figure 2.

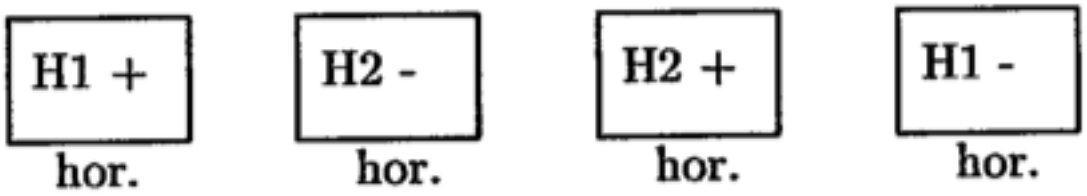

Figure 1: The spin rotator scheme, consisting of four helical magnet. The sign demonstrates the magnet helicity ("+" is right-handed,

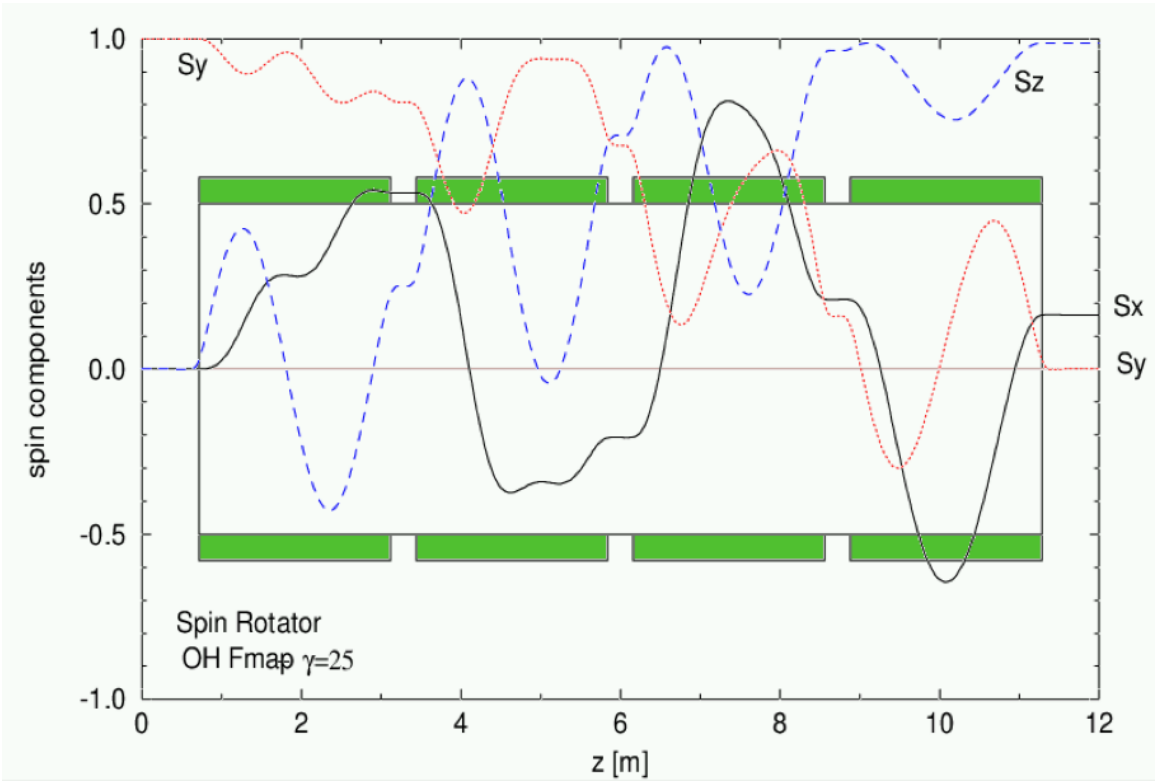

Figure 2: The example of the spin component evolution through the rotator. (Courtesy of W. MacKay)

The upstream rotator transforms the vertical spin into the horizontal plane. Since between the rotator location and the collision point the beam trajectory is bent by 6.325 mrad by the dipole and combined function magnets (see the IR Overview section), the spin orientation after the spin rotator is selected to lead to the longitudinal orientation in the collision point. This spin orientation depends on the beam energy. To work in the energy range from 50 to 325 GeV, the rotator has to be able to produce the spin orientation angle (counted from the longitudinal direction) in the range from 35 to 225 degrees. This spin orientation angle range is considerably larger than the range required for the present RHIC operation (from 10 to 100 degrees). Nevertheless it can be realized at reasonable magnet field. Figure 3 shows the magnet field of outer rotator helicies required for the longitudinal polarization at the collision point. Figure 4 shows the corresponding field of inner helicies. As comparison the magnet fields required for the present RHIC operation are also shown.

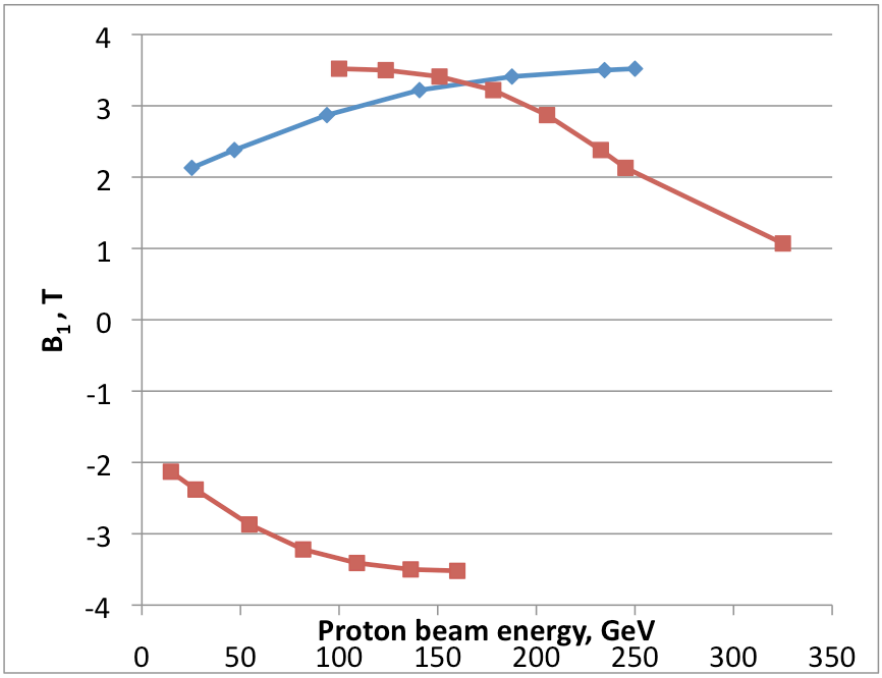

Figure 3: The magnet field of outer magnets, required for the longitudinal polarization in the IP, versus the beam energy]. Red squares - eRHIC, Blue diamonds - RHIC.

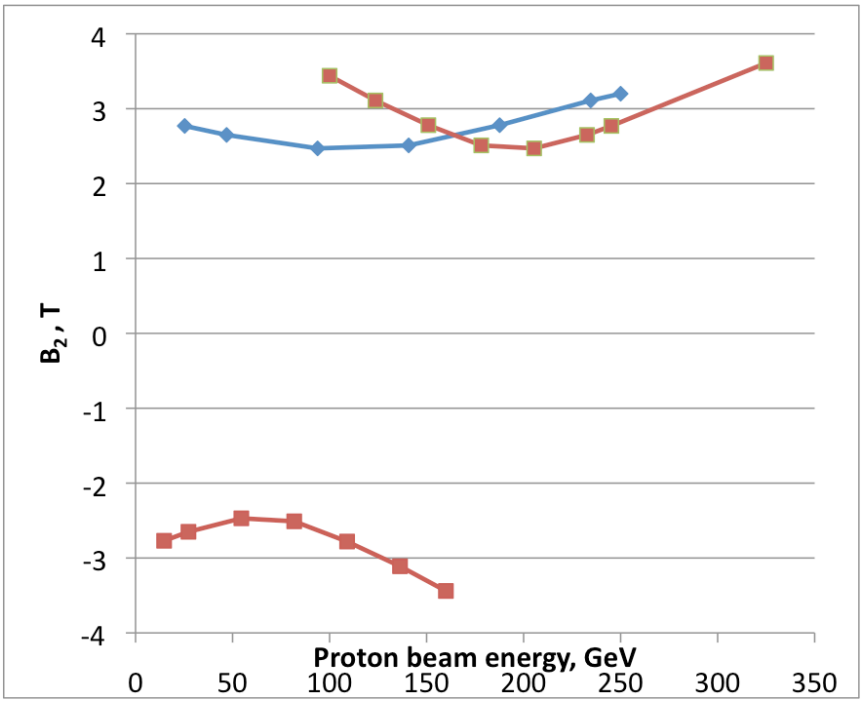

Figure 4: The magnet field of inner magnets, required for the longitudinal polarization in the IP, versus the beam energy. Red squares - eRHIC, Blue diamonds - RHIC.

The maximum required field is 3.6 T. In order to operate with the longitudinal polarization below 100 GeV proton energy the sign of the magnet field in all rotator magnets has to be switched.